AD-A043 917 COLUMBIA UNIV NEW YORK LUBRICATION RESEARCH LAB F/G 13/9
EXPERIMENTAL INVESTIGATION OF GAS BEARINGS WITH ULTRA-THIN FILM--ETC(U)
JUN 77 A SERENY, V CASTELLI N00014-75-C-0552
UNCLASSIFIED 26 NL

1 OF 2
AD A043917

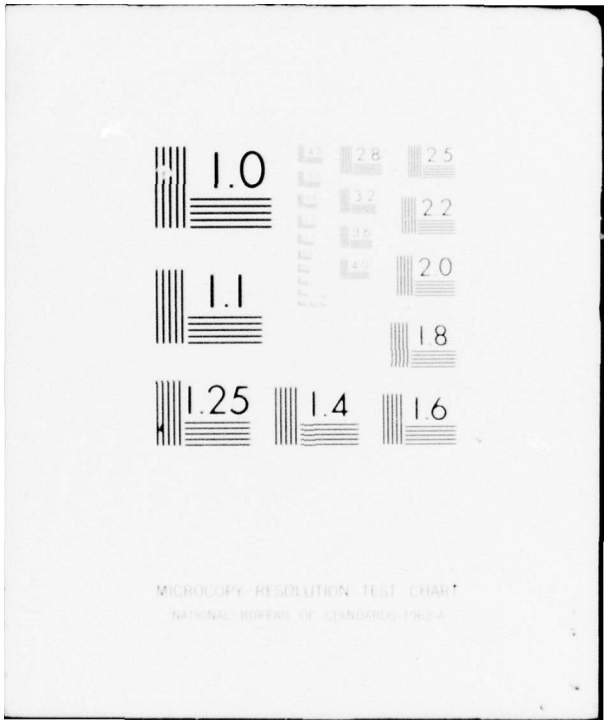
1.0
1.1
1.25
1.4
1.6
2.8
2.5
3.2
2.2
2.0
1.8
MICROCOPY RESOLUTION TEST CHART
NATIONAL BUREAU OF STANDARDS 1963-A

Report No. 26

Columbia University
in the City of New York

EXPERIMENTAL INVESTIGATION OF GAS BEARINGS WITH ULTRA-THIN FILMS

by

Aron Sereny

Vittorio Castelli

June, 1977

LUBRICATION RESEARCH LABORATORY
SCHOOL OF ENGINEERING AND APPLIED SCIENCE
DEPARTMENT OF MECHANICAL AND NUCLEAR ENGINEERING
COLUMBIA UNIVERSITY
NEW YORK, NY 10027

EXPERIMENTAL INVESTIGATION OF GAS BEARINGS WITH ULTRA-THIN FILMS

by

Aron Sereny

Vittorio Castelli

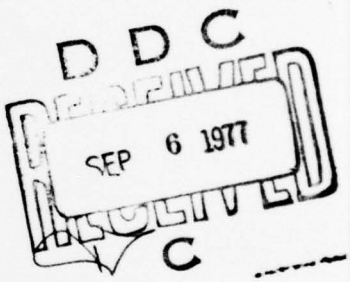

June, 1977

Report No. 26

Lubrication Research Laboratory
School of Engineering and Applied Science
Department of Mechanical and Nuclear Engineering
Columbia University
in the City of New York

Prepared under
Office of Naval Research
Department of the Navy
Task NR 062-491
Contract No. N00014-75-C-0552
Supported by Informations Systems Branch
and Fluid Dynamics Branch

ACKNOWLEDGMENT

Thanks are owed to the following individuals whose assistance made this thesis possible:

* to Professor V. Castelli for suggesting the topic and for serving as thesis adviser;
* to Professors H.G. Elrod, D.D. Fuller, and G.A. Domoto, and to Mr. G.K. Rightmire for their interest, suggestions and for the numerous, contributing discussions;
* to S. Chai of Xerox Corporation for providing flying heads and some of the experimental equipment;
* to Dr. J. Pirvics of S.K.F. Lab. for the help with the scanning electron microscopy, and last, but not least,
* to the "guys in the lab" - Harold Thompson, Gerry Bay, and Joe Evanish.

This study was performed under the Contract N00014-75-C-0552 administered by Mr. Stan Doroff and sponsored by the Office of Naval Research.

This study was awarded a grant by the New York State Science and Technology Foundation.

Their sponsorship and financial support are sincerely acknowledged.

TABLE OF CONTENTS

FIGURES AND TABLES

FIGURES AND TABLES (cont.)

FIGURES AND TABLES (cont.)

FIGURES AND TABLES (cont.)

ABSTRACT

EXPERIMENTAL INVESTIGATION OF GAS BEARINGS
WITH ULTRA-THIN FILMS

ARON SERENY

The experimental investigation described here involves the highly accurate measurement of bearing clearances on the order of 10 microinches in self-acting, pivoted, narrow-slider gas bearings. The experimental measurements are based on light interferometry using a variable-wavelength pulsed dye laser and a CW HeNe laser as monochromatic sources. The light interference in the gas bearing is obtained by flying the slider on a very precise, optically flat quartz disk through which the light beam is transmitted.

The combined effect of high Knudsen numbers and surface irregularities on the flying height of narrow gas bearings is observed by varying the load on the bearing and the ambient molecular mean free path. The experimentally measured bearing clearances are compared quantitatively with rather accurate theoretical predictions obtained by numerical solution of Reynolds differential equation

for compressible fluids with slip boundary conditions.

The result of this study indicates that as clearances in narrow gas bearings get progressively smaller, while the Knudsen number increases to values beyong 0.1, the theoretical model fails to predict the bearing behavior. It is also argued that this failure is because of the weakness of the continuum model.

I. Introduction

An experimental apparatus to study the lubrication phenomena associated with very low clearances was designed and fabricated. It is now working as a slider bearing tester at the Columbia University Lubrication Research Laboratory. Fig. 1 shows the experimental setup in its present state.

The experimental portion of this investigation involves gas bearings operating at very low clearances such as those often encountered in gas bearing gyroscopes, flying heads for rotating magnetic memories, and in any gas bearing during start up and low speed operation. The slider bearing used for this research is a type of read-write flying head used in many conventional computer disk memory units (Winchester head). This head is supported by two self acting air bearings.

Utilization of an air bearing to support a magnetic recording head was first introduced through the I.B.M. Ramac disk file in 1956 [8]*. The experimental investigation by Brunner, Harker, Houghton and Osterlund [4], established the effects of various parameters on the performance of air lubricated slider bearings with

*Numbers in brackets designate references

relatively large minimum film thickness (400 microinches). This experimental work compared well with theoretical results obtained by digital computer solution of Reynolds equation, an equation derived from the Navier-Stokes equations [1], which applies to low Reynolds number flow phenomena, where viscous forces are predominant over inertia forces and where clearance variations are slow. At that time, because of the high clearances involved (on the order of 100 molecular mean free paths), no effects caused by rarefaction were considered.

The continuous efforts to achieve higher recording bit density in magnetic recording reduced the head to disk spacing from 300 microinches, reported by [4], to the nominal gap of today's flying heads (20 microinches) [2]. This reduction in the flying height along with some additional development in head design increased the recording bit density from 1000 bit/inch-50 track/inch to 6000 bit/inch-400 track/inch. The relation between recording bit density and head clearance is given in [11] and in [8].

The lower bearing clearances required the extension of the classical Reynolds equation into the slip flow regime, Burgdorfer [10]. The suggestion that the range of applicability of the Navier-Stokes equation can be extended somewhat by the retention of slip boundary

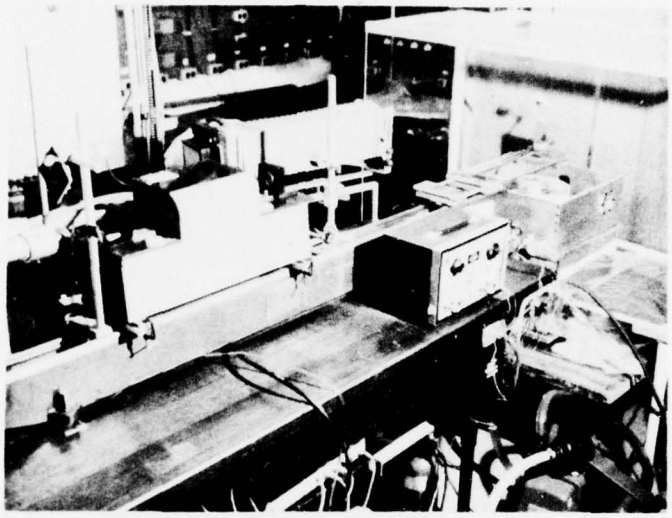

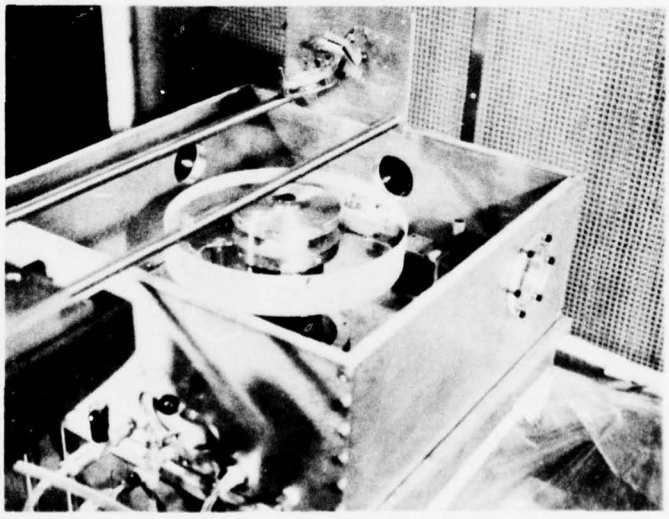

Figure 1 View of Experimental Apparatus

conditions was initiated by Schaaf [23]. With lower bearing clearances, the gas film thickness of bearings in use today is on the order of several mean free paths. This modified Reynolds equation is used for the design of gas bearings where the dimensionless ratio of the ambient molecular mean free path over the bearing trailing-edge-clearance, λ_a/h_1, (Knudsen number) is between 0.01 and 0.1. The effect of the mean free path being on the order of the clearance in a spiral grooved thrust bearing was studied by Hsing and Malinoski [19]. The results reported by [19] reveal that the effect of slip boundary conditions could contribute a substantial reduction in performance.

Only very recently was the first experimental data provided by Tseng [13] who reports measurements of load versus spacing characteristics of gas bearings with clearances of twenty microinches. According to Tseng [13], experimental data are in better agreement with numerical solutions when the slip at the boundary is included. In the above mentioned report, consideration is not given to crown height, nor is it given to surface roughness effects. In Tseng's experimental work, mean free path effects could not be observed for Knudsen numbers on the order of 0.5 because of the wide slider bearings that were used. With a wide slider bearing,

the region of high pressure dominates and that, in turn, causes the load carried to be less sensitive to slip boundary conditions. The perturbation solution of Reynolds equation with slip boundary condition, as described in Appendix D, indicates the slip effect for a wide bearing to be of the order $1/\Lambda$, (Λ = bearing number). It is interesting to note that elementary theoretical studies performed by Christensen [22] and by Rhow and Elrod [15] predict an increase in slider load with increasing roughness, while Tseng's clearance measurements are systematically below the predicted values.

A review of the techniques for the measurement of air bearing separations is given by Lin [3]. These techniques can be listed as capacitive, inductive, and optical. With larger size bearings, such as the 3/4 in. dia. slider of Ref. [4], the capacitance probe technique was reported to be suitable. For slightly smaller slider bearings (.42" × .35"), the unshielded capacitance probe technique was used for determining slider flying characteristics and for measuring flying heights in the 40 to 200 microinch range [6].

The implanted capacitor microprobes used by Briggs and Herkart [6] were almost twice as large in diameter as the skates of the slider bearings used in today's flying heads.

The miniature size of today's recording heads make

the implantation of capacitance probes extremely difficult if not impossible. The optical light interference method is applicable to such small slider bearings. This method, as applied to air gap measurements between a moving magnetic tape and a static recording head, is described in references [16] and [17]. One advantage of the interferometric technique is that it results in a complete mapping of the gap distribution between the magnetic tape or disk and the recording head. A white light interferometric technique applied to the measurement of very thin films (10 microinches) was reported by Lin and Sullivan [5]. Today it is well accepted that the optical interference technique is the most accurate method for the measurement of ultrathin gas bearing separations [3].

In this experimental research, in order to eliminate the domination of the high pressure region and to allow for significant enough slip effects, a relatively narrow slider bearing is used (length/width = 11). No experimental studies of narrow slider bearings operating in the slip regime have been reported.

The experiments demonstrate the failure of the modified Reynolds equation to predict accurately the bearing behavior. The results indicate that as the clearances in narrow gas bearings get progressively smaller, while simultaneously the Knudsen number

increases to values beyond 0.1, the theoretical model fails to predict the bearing behavior. Also, accurate measurement of the crown of the so called "flat" slider and the effect of this crown height is given.

In addition to the experimental work, attention was given to improve, and get some further insight into, the analytical treatments of the governing lubrication equation. Various numerical methods were investigated and comparisons were made with exact solutions, developed here, for wide slider bearings. This has been the first time that the exact solution to Reynolds equation with the molecular mean free path effects included were carried through. Also, in order to study analytically the slip phenomena, an asymptotic solution was obtained and it indicates effects to be of the order $1/\Lambda$ for the wide bearing case.

II. Theoretical Background of Self-Acting Slider Bearing with Ultra-Thin Film

The theoretical treatment of self-acting gas lubricated slider bearings is well established. Thorough treatment of the fundamentals of gas lubricated films is given by Fuller [1] and by Gross [18]. The steady state Reynolds equation is given here in dimensionless form,

$$\frac{\partial}{\partial X}\left(H^3 P \frac{\partial P}{\partial X}\right) + \frac{\partial}{\partial Y}\left(H^3 P \frac{\partial P}{\partial Y}\right) = \Lambda \frac{\partial PH}{\partial X} \qquad (1)$$

where $P = p/p_a$, $H = h/h_{min}$, $X = x/\ell$, $Y = y/\ell$,

$\Lambda = 6\mu U\ell/ (p_a h^2_{min})$, bearing number

p_a = ambient pressure; h_{min} = minimum clearance

Its validity in predicting the behavior of hydrodynamic bearings with continuum laminar flow between two smooth surfaces has been proven repeatedly. Equation (1) describes the fluid dynamics of bearings with clearances much larger than the molecular mean free path and the size of surface asperities. Further analysis of gas bearings with thinner and thinner fluid films requires review of the concept of continuum in the description of fluid flow. The continuum hypothesis for the flow between two bearing surfaces weakens with clearances approaching the value of the molecular mean free path.

Gas dynamics is usually divided into the regions of continuum, transition and molecular flow. In order to extend the range of validity of the Reynolds equation to the transition region, Burgdofer [10] introduced the commonly used first approximation of slip at the wall. This consists of using the new boundary condition

$$U_{wall} = f(\lambda_a) \left.\frac{dU}{dY}\right)_{wall} \tag{2}$$

where $f(\lambda_a) = \frac{2 - \sigma}{\sigma} \lambda_a$

U = velocity tangent to the wall

y = coordinate normal to the wall

σ = reflection coefficient, [29]

With $\sigma = 1$ for diffuse reflection, this led to the following modified Reynolds equation

$$\frac{\partial}{\partial X}\left(H^3 P(1 + \frac{6k}{PH})\frac{\partial P}{\partial X}\right) + \frac{\partial}{\partial Y}\left(H^3 P(1 + \frac{6k}{PH})\frac{\partial P}{\partial Y}\right) = \Lambda \frac{\partial PH}{\partial X} \tag{3}$$

with the Knudsen number, k being defined as the ratio of the ambient mean free path λ_a over the bearing trailing-edge-clearance.

This modified Reynolds equation predicts a reduction in the slider load carrying capacity. This reduction is pronounced at low bearing numbers. Although this equation has been used for several years in actual design and

analysis of low-flying slider bearings, the first experimental study by Tseng [13] in the area of rarefaction came only recently (1975). Tseng suggests the introduction of a surface accommodation coefficient of less than unity in order to explain the lower load measured by his experiment in comparison to the numerically predicted one. The numerical solution of the modified Reynolds equation using various values of molecular mean free path gives the load versus clearance behavior described in Fig. 2. This figure shows a significant reduction in minimum clearance under constant load, due to slip at the boundary. In Fig. 2, the Knudsen number increases with decreasing values of trailing edge clearance; the Knudsen number increases from values less than 0.1 to values greater than 0.3. Therefore, since the Knudsen number is larger than 0.1, the designer should expect the validity of these design curves to weaken at clearances below 20 microinches.

In addition to the mean free path effects, the very small air gaps in recent usage stimulated the initiation of some basic studies of the effects on bearing performance due to the roughness of the stationary and moving parts. Tseng and Saibel [20], Christensen and Tonder [21], and Elrod [14], have shown using Reynolds equation, that surface roughness can considerably affect the

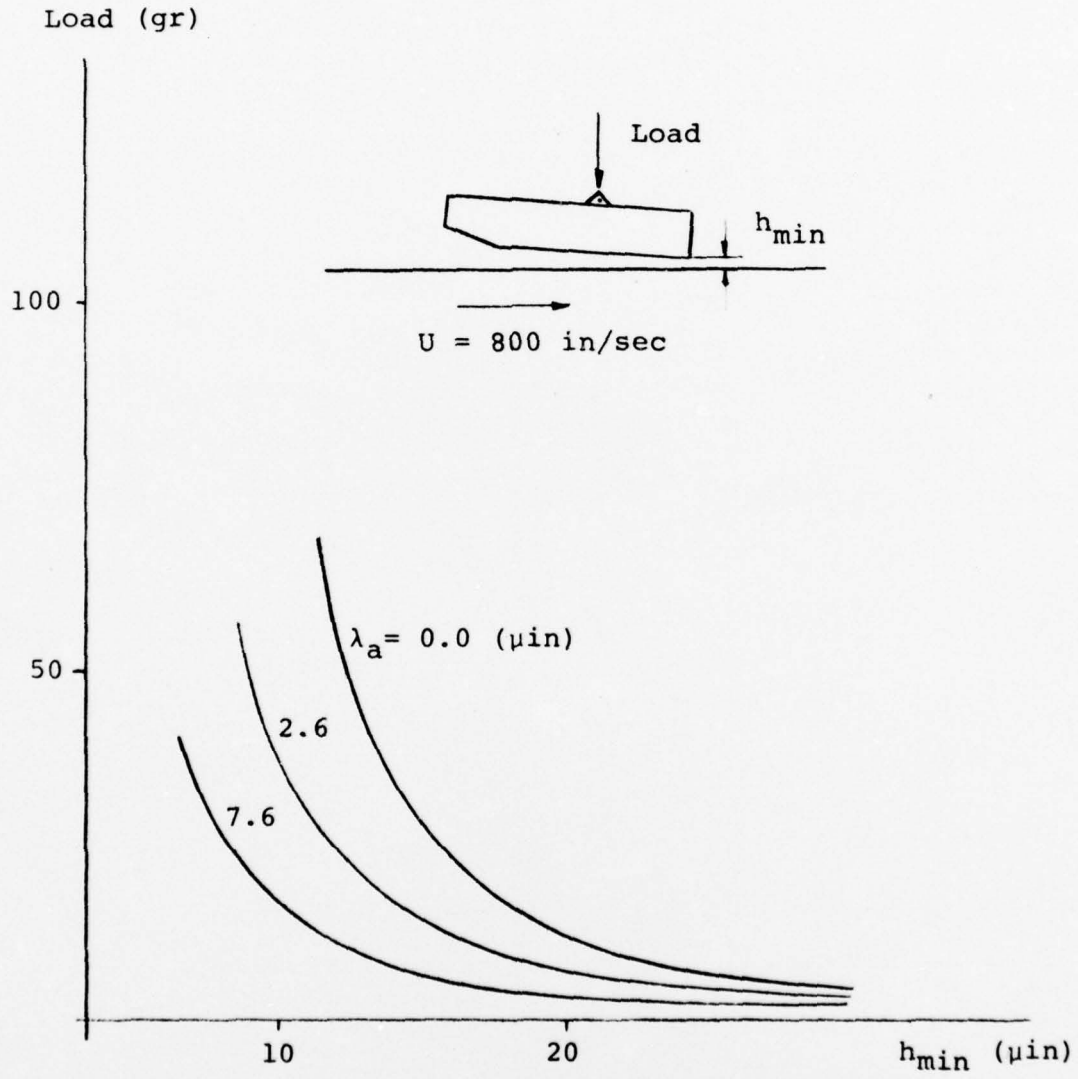

Figure 2 Results of Numerical Solution of Reynolds Equation with Slip Boundary Condition

bearing performance. More recently, Rhow and Elrod [15] showed that there is a general increase in load carrying capacity due to striated roughness when calculations are based on mean film thickness. They carefully distinguish between calculations based on mean film thickness and ridge film thickness, and their conclusion indicates that Stokes type grooving reduces the load capacity if it is calculated on the basis of ridge film thickness. If the roughness does not cause excessive rates of change of film thickness, they found the increase in load carrying capacity to be much larger for bearings with the roughness on the stationary surface than for the case of roughness of the moving surface (Fig. 3). No studies have yet attempted to apply theoretical predictions on roughness effects using some measured input from an actual bearing surface.

Consequently, for thin film bearings, under fixed load, there is a decrease in clerance due to approaching rarefacted conditions and an increase in clearance due to surface irregularities. Fig. 2 shows the predicted flying height without including surface roughness. Since all actual bearings have some surface irregularities, the curves in Fig. 2 should be moved toward the higher load - higher clearance region. Although some theoretical treatments have already been performed on certain roughness effects

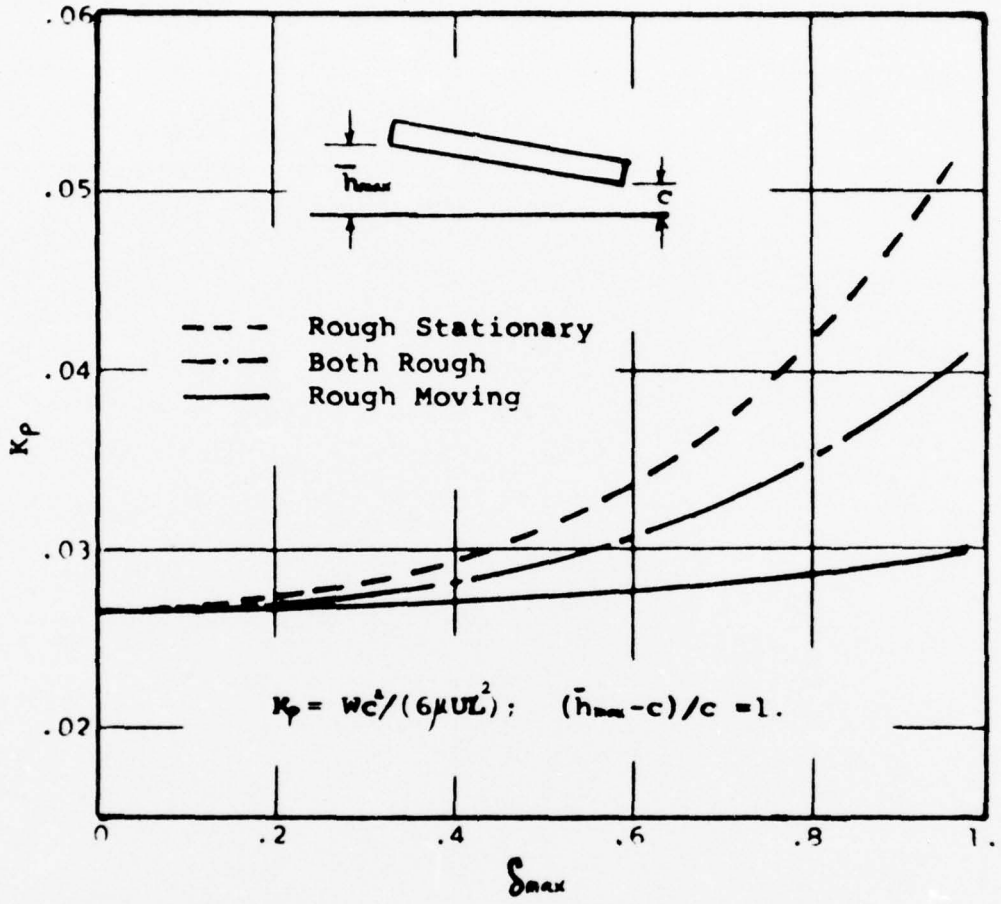

Figure 3 Load vs Roughness; Transverse Roughness

Adopted from Rhow and Elrod, ref. [15]

δ_{max} = maximum roughness height, dimensionless with respect to c

W' = bearing load

L = slider length

as well as on slip boundary conditions, as yet no theoretical studies have combined rarefaction and roughness effects or predicted the regions of domination for gas lubricated bearings. In this experimental study the observed behavior of a particular slider bearing with its surface roughness characteristics is given.

III. Experimental Apparatus

In order to test the performance of ultrathin film slider gas bearings with various mean free paths and flying heights, a testing setup with the ability of controlling these parameters is needed. Since the pressure is inversely proportional to the molecular mean free path, the ambient pressure in the testing chamber is to be held at sub-atmospheric values in order to achieve the desired increase in the mean free path. To control the flying height, a variable loading mechanism was constructed.

The testing setup was designed as follows:

* to have a vibration-free flat and very smooth running surface oposite the stationary slider;

* the ambient pressure to be controlled from 14.7 to 1.5 psia;

* the mean free path to be controlled from 2.6 to 26 microinches;

* to set the load on the slider bearing from 10 to 100 grams;

* to have the very clean environment needed for bearings with ultrathin films.

A. Description of Apparatus and Instruments

The experimental setup that was designed and built at the Columbia University Lubrication Research Laboratory is a highly versatile testing bench for small-size, self-acting gas lubricated slider bearings. The essential components of the apparatus are illustrated schematically in Fig. 4. The equipment consists of two major parts: one, the controlled environment chamber which encloses the running and stationary parts of the bearing; and the second, the optical bench which carries the interferometer optics and the image recording equipment for the measurement of bearing clearances.

The chamber itself is divided into two enclosures by a middle plate. This middle plate acts as a partition between the enclosure with the speed-controlled DC motor drive and the enclosure with the bearing being tested. By enclosing the electric motor and the belt drive in the environmental chamber, the difficult problem of sealing the high precision spindle is solved.

The bearing testing apparatus can be operated with or without the upper box depending on its functional

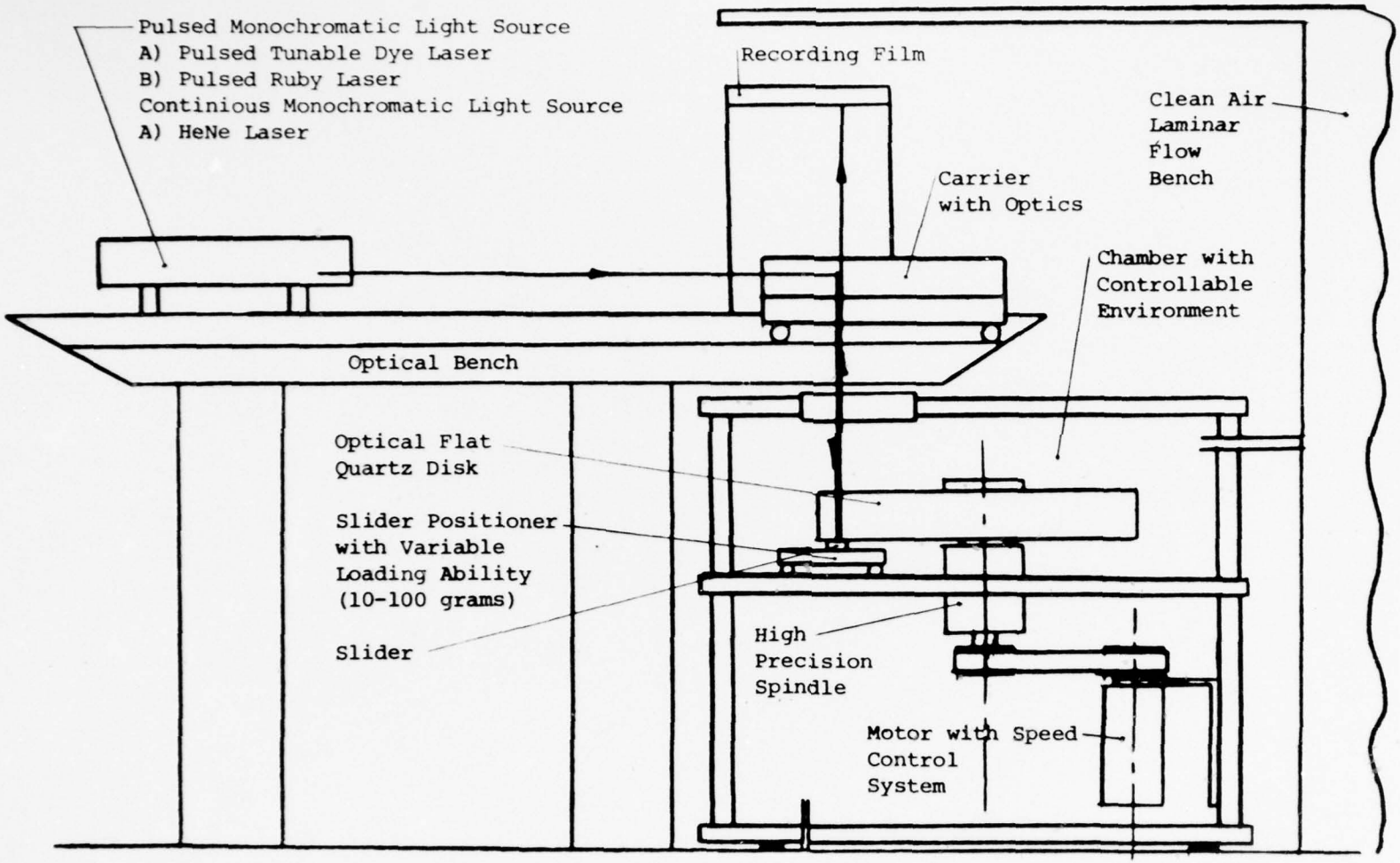

Figure 4 Schematic Diagram of Experimental Apparatus

requirements. For operation in atmospheric conditions, the experiment is performed without the upper cover, with the testing setup positioned in front of the laminar flow air bench. For operation under controlled ambient conditions, the upper box is positioned so that it covers the bearing. In this mode of operation, the necessary clean environment is provided, by letting the gas enter the upper chamber through a line of absolute filters and exit from the lower chamber through a vacuum pump. This cycle provides a continuous flow of gas from the upper to the lower chamber and thus prevents contaminants from the belt drive and the electric motor from entering the bearing test area.

In the sealed environmental chamber, the mean free path of the lubricant can be varied by simply changing the pressure and the lubricant gas. Because flight behavior at high Knudsen numbers is of interest, the chamber is designed for subambient operation only. In the upper chamber, a highly polished, double surface, optically flat disk with surface flatness of $\lambda/20$ is mounted on the spindle. The optical flat is made of quartz and has the dimensions of 1.75 inches thick, 10 inches O.D., 1.8 inches I.D., and it weighs 10 lbs. The disk has a peak to valley surface roughness of 0.5 microinches. In order to achieve the desired vibration-

free operation at velocities up to 6000 R.P.M., the spindle, with the optical flat at one end and the pulley at the other, was dynamically balanced to within less than 100 microinches peak to peak. Fig. 5 illustrates the balancing. The actual balancing was performed using 24 balancing screws in 3 different planes along the shaft of the spindle. The electric motor with the driving pulley was also balanced to within 100 microinches peak to peak vibration at the nominal operating speed.

While the moving part of the bearing is the quartz disk, the stationary part is a spring loaded two-rail, tapered-flat ferrite slider with nominal length of 0.22 inch and a width of 0.02 inch per skate. The arm holding the gimbal with the head is clamped to a precision stage with six degrees of freedom: three rotations and three linear displacements around the x, y, and z directions. The precision stage permits the alignment of roll and pitch angles during flying.

The variable loading mechanism applied to the slider consists of a pneumatic rubber diaphragm with a loading button. The load on the slider can be continuously adjusted by pressure variation under the diaphragm. The arm is made of Delrin* and is instrumented by means of

---

* Trade name of polyformaldehyde, Du Pont Co.

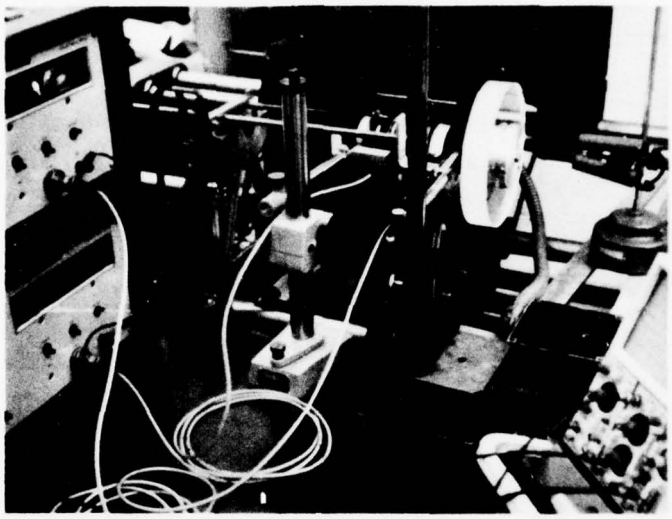

Figure 5 View of Disk Balancing

four strain gages, two on each side, which measure the load with a sensitivity of 10.5 microinches/inch strain per gram.

Hence, an addition of 5 grams to the load causes the strain reading to increase by 53 microinches/inch. The arm and the loading diaphragm have been calibrated by means of dead weights. The loading diaphragm and the calibrated arm are illustrated in Fig. 7.

In this experimental setup, the bearing film thickness is measured using optical interferometry. The usual application of interferometry requires a transparent and optically flat reference plane, a monochromatic light source, and a reflecting microfinish on the surface to be

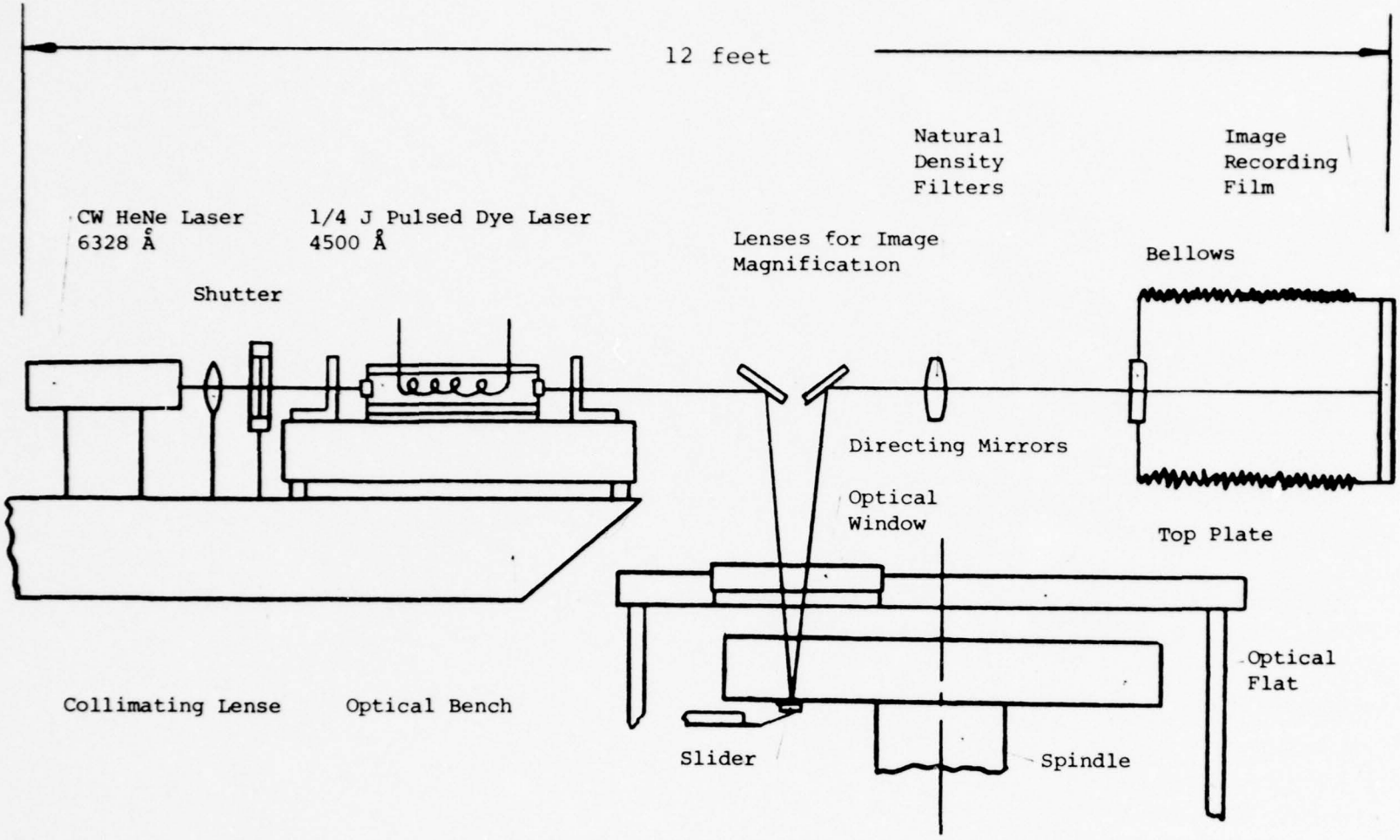

Figure 6 Schematic Diagram of Interferometric Setup

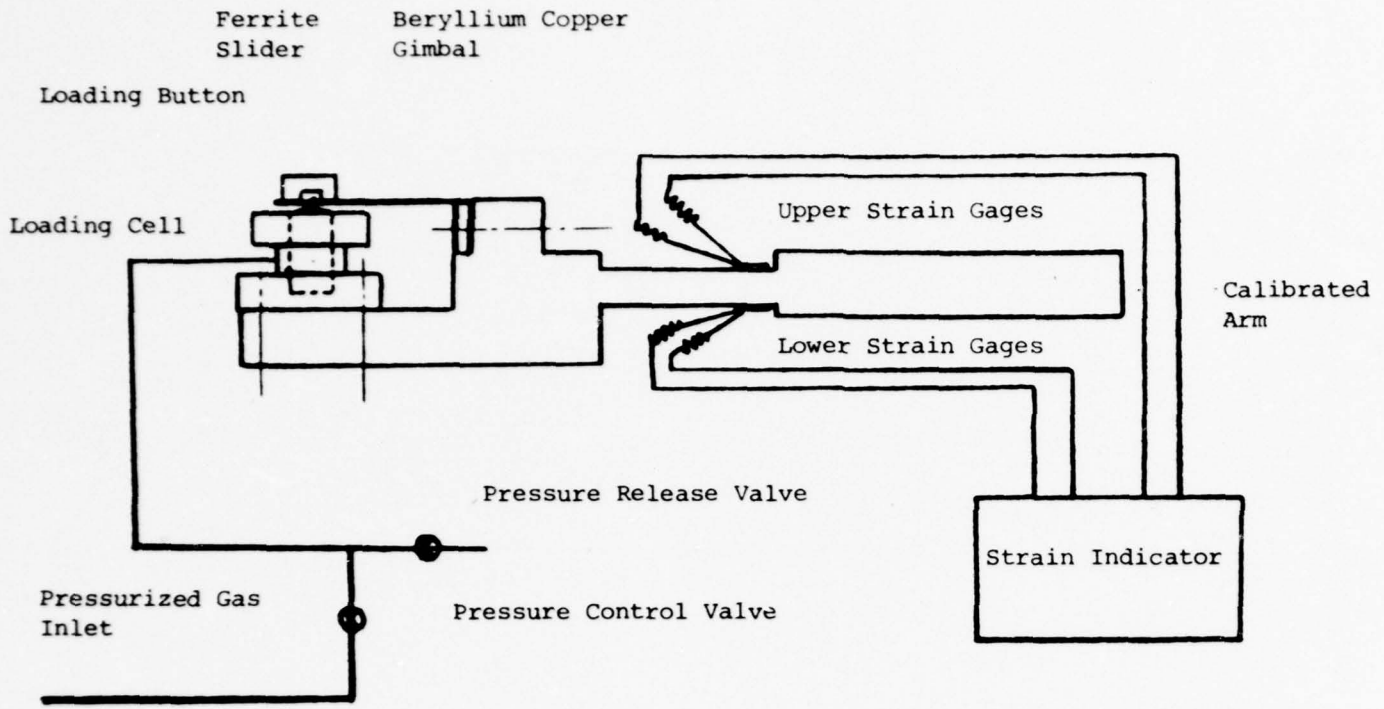

Figure 7 Calibrated Arm with Loading Cell

analyzed. By projecting the light from the monochromatic source through the flat reference plane and onto the reflective surface to be analyzed, interference "fringes" between the incident and refracted light may be observed. The position and number of fringes is a function of the distance and parallelism between the two surfaces. Knowing the wavelength of the monochromatic light, the observed surface can be mathematically described in numerical terms as a function of the number and type of observed fringes.

The actual interferometric setup is illustrated in Fig. 6. The .5 mwatt CW HeNe laser is located right behind and collinear with the pulsed tunable laser. By passing the continuous monochromatic source through the coaxial flash lamp of the dye laser, the CW collimated light beam is allowed to travel through the same path and to use the same recording setup as the pulsed laser. While the CW allows a continuous observation of the interference pattern, the pulsed laser records only the fringe pattern with its variation in a period of 0.5 microsecond. The blue, 4500 Å and the red, 6328 Å , wavelengths give the distinct difference in fringe pattern needed for the clearance measurements. Two such interference patterns are shown in Fig. 8.

B. Description of the Slider Bearing and its Preparation

The slider bearing used for this experimental study is a recording flying head of a conventional computer disk memory unit. A schematic description of the slider bearing and a drawing to actual size is given in Fig. 9. The design concept that permitted the adaptation of the two-rail tapered-flat ferrite slider to the low-load head was developed at I.B.M. [2]. The most significant design difference between the two-rail slider and its predecessor heads is in the suspended mass and load force. The head is made of high density sintered ferrite with excellent wear and surface finish characteristics, properties highly needed to accommodate for the bearing to start and stop in contact and to maintain a finite constant spacing between the head and the recording surface. The head dimensions were designed such that under 10 gram load the actual center of slider pitch and roll is at the recording gap that is located between the two skates at the trailing edge.

This narrow slider bearing with a relatively high length-to-width ratio allows a significant side leakage of lubricating air from beneath the slider. The slight pressure generated by the tapered portion of the bearing

HeNe

λ = 6328 A

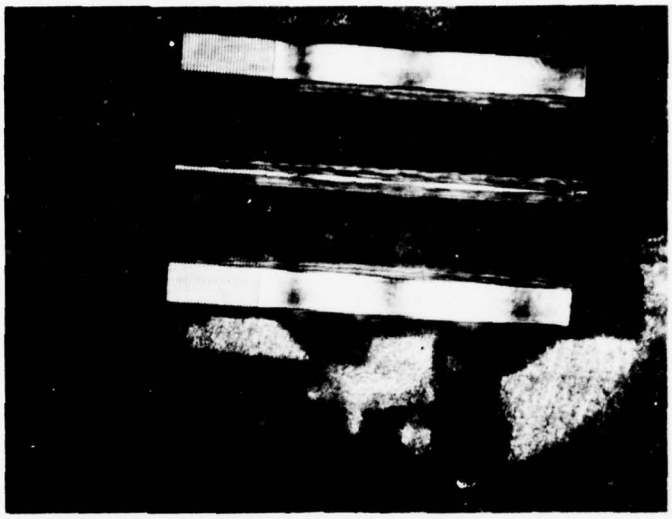

Coumarin Dye

λ = 4500 A

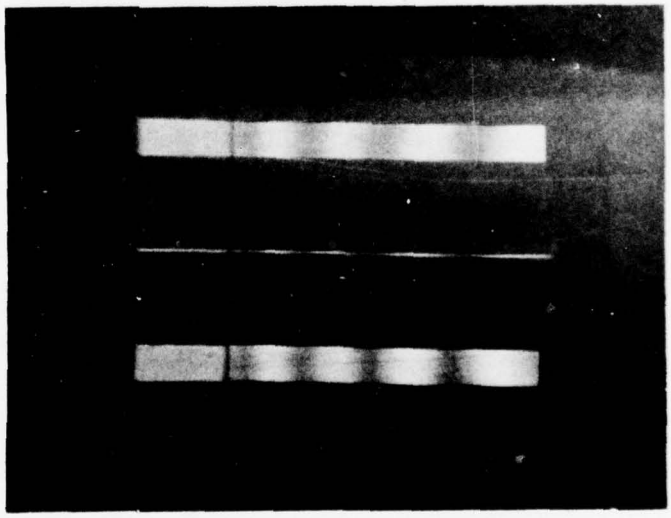

Figure 8 View of Typical Interference Patterns

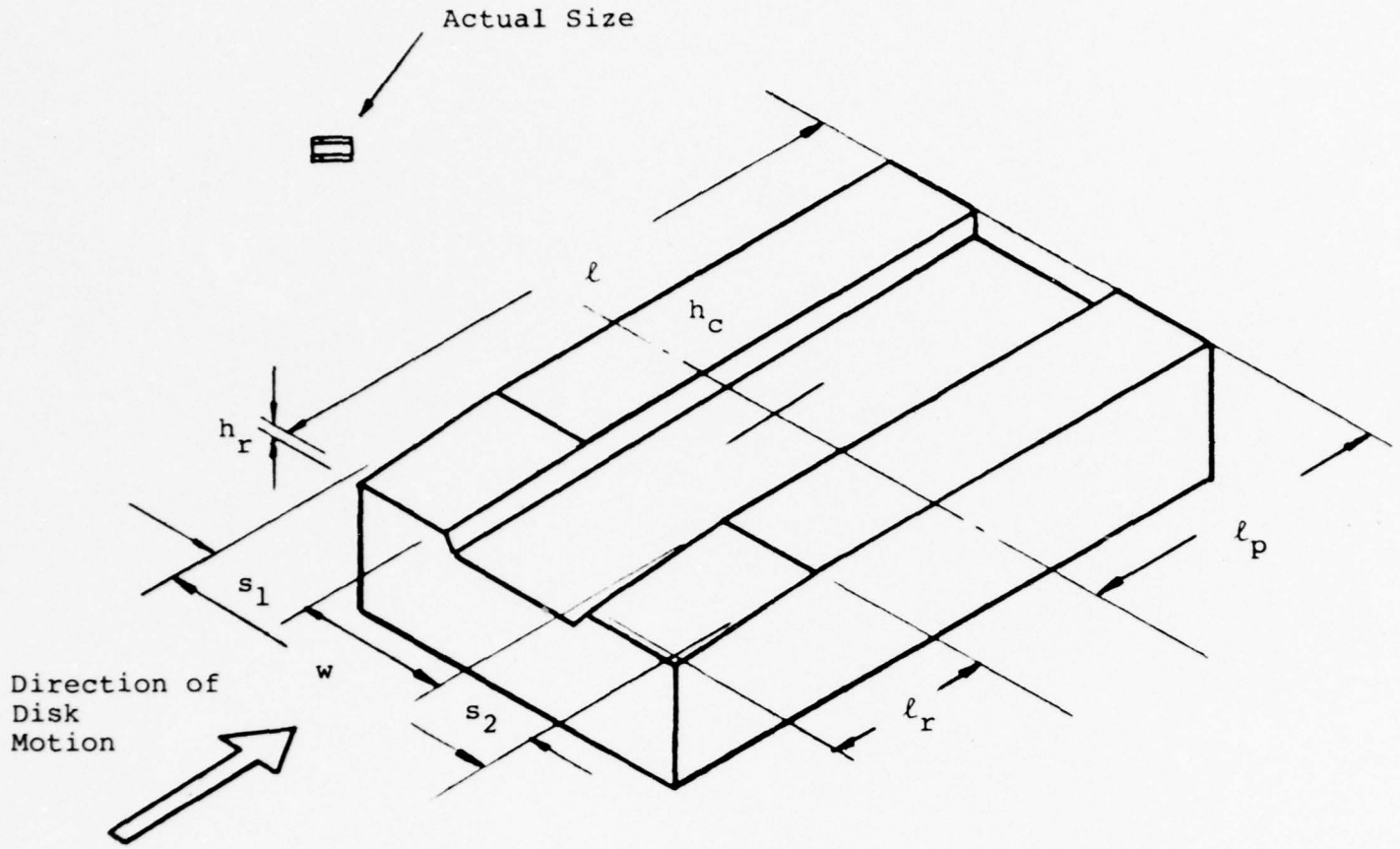

Figure 9 Dual Skate Tapered Flat Slider Bearing

is leaked to lower values before being compressed again by the trailing end of the flat portion of the skates. The integrated pressure profile under the skates results in a load of 10 grams with nominal trailing edge clearance of 20 microinches at speeds of 1500 in/sec.

To obtain a qualitative knowledge of the bearing surface roughness characteristics, a few of the bearing surfaces were studied, using Scanning Electron Microscopes. Some of the typical micrographs are given here in Figures 10-11.

Generally, the micrographs exhibit a surface with two types of irregularities: large ones at great intervals, and very fine ones closely spaced. The large grooves, possibly caused by crystal pullouts during lapping, are on the order of 5 - 20 microinches in depth and width, spaced at intervals of 200 microinches or larger. The irregularities spaced at small intervals were estimated to be on the order of one microinch in depth and width.

The electrical conductivity of the ferrite bearings is sufficient for the SEM application so that no conductive coating was necessary.

One of the major challenges in testing gas bearings is the demanding standards of cleanliness. A study of the levels of surface cleanliness needed when assembling

Figure 10 SEM Micrograph of Slider Surface

20000X

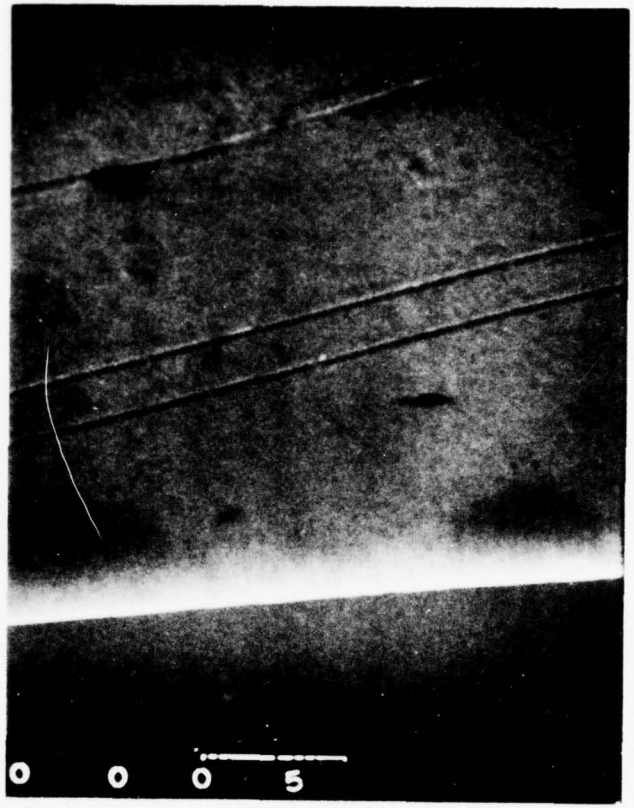

Figure 11 SEM Micrograph of Slider Surface

6000X

and testing gas lubricated bearings is given by Galvin, Monecraft and Patterson [7]. The methods applied in cleaning the skates of the flying head for the present experimental research are those described in Ref. [7]. The cleaning processes include organic solvent and deionized water washes of the surfaces. It was found necessary to repeat, in a trial and error fashion, this washing process while a flying attempt was performed between each wash. During a flying try, surface contamination could be observed on the projected pattern of interference. The appearance and accumulation of dirt between the initial cleaning processes could easily be observed during the flight. It should also be reported that if no dirt marks appeared between the bearing surfaces during the first few minutes after take-off, the heads flew with no dirt-caused disturbance for several hours.

C. Accuracy of Measurements and Calibration of Instruments

A description of the analytical formulation relevant to this experimental study has been given in Sections II and VI of this report. The knowledge of the following quantities is required for the correlation of the experimental and theoretical results:

(a) μ = viscosity of air

λ_a = molecular free path of air at atmospheric pressure

p_a = atmospheric pressure

λ_{red} = wave length of HeNe monochromatic light source

λ_{blue} = wave length of the Pulsed Dye Laser (coumarin)

(b) U = linear velocity of disk under the slider

ℓ = slider total length; (Fig. 9)

ℓ_t = tapered length; (Fig. 9)

ℓ_p = distance of pivot point from trailing edge

s_1, s_2 = width of skates; (Fig. 9)

h_c = crown height of the flat portion of the bearing skates; (Fig. 9)

h_r = ramp height; (Fig. 9)

The values of the quantities in list (a) were assumed to have constant values;* $\mu = 0.26 \times 10^{-8}$ lb×sec/in^2, $\lambda_a = 2.65 \times 10^{-6}$ inches, $p_a = 14.7$ psia, $\lambda_{red} =$ 6328 A, and $\lambda_{blue} = 4500$ A. All these values, with the exception of λ_{blue}, are believed to be accurate to within 1%. The wavelength of the blue monochromatic light source is reported by the supplier (Phase-R, New Durham, New Hampshire) to be within 4%.

The values of the physical quantities in list (b) of this section were determined experimentally. The linear velocity of the disk under the slider was monitored by a magnetic pick-up. The frequency of pulses generated in the magnetic coil were counted using an electronic counter. The estimated error in speed measurement was less than 1%. The transistorized closed-loop control system for the motor speed kept the set speed to within a range better than 1%. The geometrical dimensions of the slider bearing ℓ, ℓ_1, s_1, s_2 were measured with an accuracy of .0005 inch, which gives a maximum relative error of 3%. These estimates are based on applying, whenever possible, at least two methods of measurement. The ramp height was measured wiht an accuracy of $\lambda_{red}/2 =$ 12.4 (μin.), which gives a maximum relative error of 4%.

---

* Ambient temperatures were kept in the range of 70-74°F

The crown height determination suffered from the largest relative error because of its extremely small value; (3 microinches $\sim$ 1/10 of 1 wavelength of visible light) the measurements of this crown were not better than ± 1.0 microinches, which in relative error terms indicates a possible error of 30%.

The load on the slider bearing was determined by the read-out of the change in strain in the Delrin arm supporting the slider bearing. The arm was calibrated while loading it with dead weights. To minimize drift in the strain read-out caused by the slightest temperature variation related to the low thermal conductivity of Delrin, gages with the most suitable self-temperature-compensating backing material were chosen. With this proper choice of backing material, the drift in the read-out and the error in the calibration curve were reduced to a maximum relative error of less than 10% for the lowest load of 10 grams. The instrumented arm was tested for variation of strain because of air drag and forced convection, and these effects were included in the above error estimate.

The accuracy of the flying height measurements were of the order ± 1.5 microinches. For the larger flying heights this error is only of order 10% while at the lowest trailing edge clearance measurements the relative

error was about 30%. To minimize errors in fringe-order identification three methods were carefully followed. These methods are described in Section IV.

IV. Experimental Results

A. General Remarks

The slider bearing used for this experimental study is a recording flying head of a conventional computer disk memory unit. The heads for this experimentation were provided by the Advanced Development Laboratories of Xerox Corporation and C.D.C. A schematic description of the recording head and a drawing to actual size are given in Fig. 9. The head is mounted onto a beryllium-copper gimbal that permits the head to incline relatively freely in any direction. The gimbal is welded onto a leaf spring that loads the head with 10 grams through a so-called pivot point. This 10 gram load, provided by the spring, is the load under which all take-offs and landings were performed.

After the static measurements of the slider geometry (described in Sec. IV-B), the gimbal-spring load was measured. Attaching the gimbal-spring to the loading arm, the head was lowered against a weight measuring micro-balance and from the reading on the instrument, the stiffness and the load of the spring were established. Next, the loading cell and the instrumented supporting arm were calibrated against dead weigts. It was found

that, although the zero reading (no-load) of the strain in the arm varied somewhat, the slope of the load versus strain remained within tight limits. With this in mind, the zero for determination of the total applied load was determined by using the reading under the ten gram load of the gimbal-spring.

The variation in strain read-out between static and dynamic conditions both under atmospheric and sub-atmospheric bearing ambient pressure was investigated, and it revealed changes in strain of ±5 microinch/inch (equivalent to ±.5 gram). The strain gage instrumented arm was checked for performance in partial vaccum (up to 152 mmHg); no variation in strain read-out was observed due to the change in ambient pressure.

Several experimental steps were performed to study in general the bearing behavior in this setup. The interference pattern under static condition (disk not spinning) between the slider and the disk surface was studied for take-off clearance configuration. After a few initial starts and stops the head was allowed to land on the slowly coasting-down disk. The white, red and blue light interference patterns were applied to investigate the relative configuration between the slider and the disk. These measuremnets disclosed no visible contac fringes between the 10 gr. loaded slider and the quartz disk

after landing. The clearance at the leading edge of the slider was $\sim$ 10 microinches while at the trailing edge on the order of 2 microinches. This observation of no-contact take-off was confirmed by the fact that approximately 1000 take-offs and landings performed during this experimental work and no visible contact marks on the two sides of the bearing (slider and disk) were produced.

To observe stability of the bearing, the quartz disk and the air gap, a fast pulse (.45 microsecond) dye laser was used. The laser was triggered using a signal generated once every cycle by a magnetic probe. By delaying the triggering signal, pulsed interference patterns were taken at different points along the circumference of the disk. These recorded interference patterns revealed no change whatsoever in the bearing clearance topography. This indicated an insignificant level of vibration. The slider followed the disk with its waviness, if any, (flat to $\lambda/20$) extremely well.

In the load-vs-clearance measurements described in Figs. 17 and 19 , for $_{a}$ = 14.7 psia, two sets of measurements were included. In each of these figures one set of the measurements was done without the upper cover, while the other set was done with the cover in place. These measurements generally show no variation in performance betwwen the covered and uncovered testing.

B. Measurement of Slider Dimensions

The initial step taken for both the numerical solution and the experimental measurements of flying height is the measuring of the geometrical dimensions of the slider tested. The crown height in the direction along the skates, the pivot location and the ramp length and height were found to be especially important. The dimensions of the head used for the experimentation and given in Table 1 were measured using optical microscopes and interferometric techniques with a special 10X magnification. The head itself is described in Fig. 9.

Except for the ramp height, all given dimensions are the result of measurements made by these two methods. The dimensions obtained with the two methods were in agreement with each other within less than 4%. The dimensions given in Table 1 for the slider bearing tested are averages and round-offs of the measurements.

The ramp height, one of the most important dimensions for bearing performance prediction was measured by optical means. Leaning the slider against an optical flat while reflecting a monochromatic light at, and back from, the slider surface, brought about the highly dense interference pattern indicated in Fig. 12.

	ℓ	h_r	w	s_1	s_2	ℓ_r	ℓ_p	h_c
nominal	0.2200	0.000380	0.155	0.0200	0.020	0.050	0.100	---
head #1A	0.2185	0.000375	0.152	0.0204	.0204	.0495	0.098	$3x10^{-6}$

Table 1 Measured Dimensions of Slider

(all dimensions are in inches)

(Figure 9)

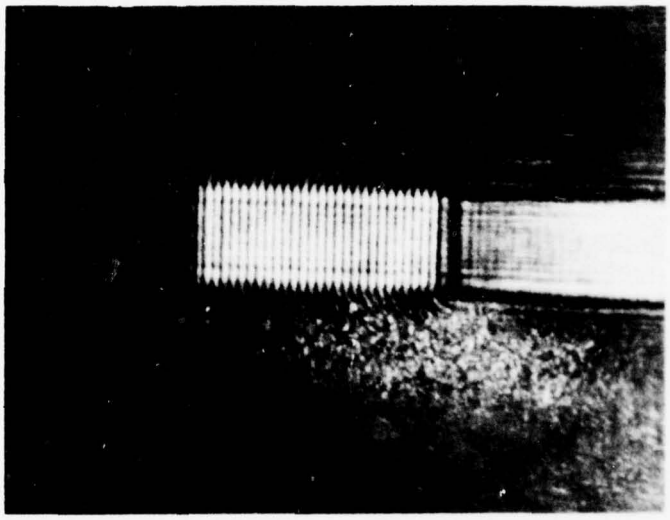

Figure 12 Interference Pattern for Ramp Height and Length Measurements

This interference pattern needed at least 10X magnification for fringe clarity.

The crown of the skates was measured using a projected interference pattern with 10X magnification obtained while flying the head at a speed of 1490 in./sec. loaded with 10 grams. Fig. 8 shows such an interference pattern. The gradual increase in spacing between consecutive fringes indicates presence of surface crown. At this point, the numerical solution for the pressure distribution for the appropriate speed and load was used to check for possible elastic deformation of the slider due to this load. The various calculations with specific assumption of beam shape and load distribution predicted maximum deflections on the order of 1/5 microinch. Additional calculations under even higher load indicated these deformations to be negligible.

In order to increase the number of interference fringes within the skates and, by that, increase the number of data points along the slider and the accuracy of crown height measurements, a monochromatic source with the shortest wavelength possible is needed. The optical alignment and image recording procedures limit the monochromatic sources to be in the visible range of light. In this interferometric setup a short-pulse tunable dye laser was used. A schematic description of crown height

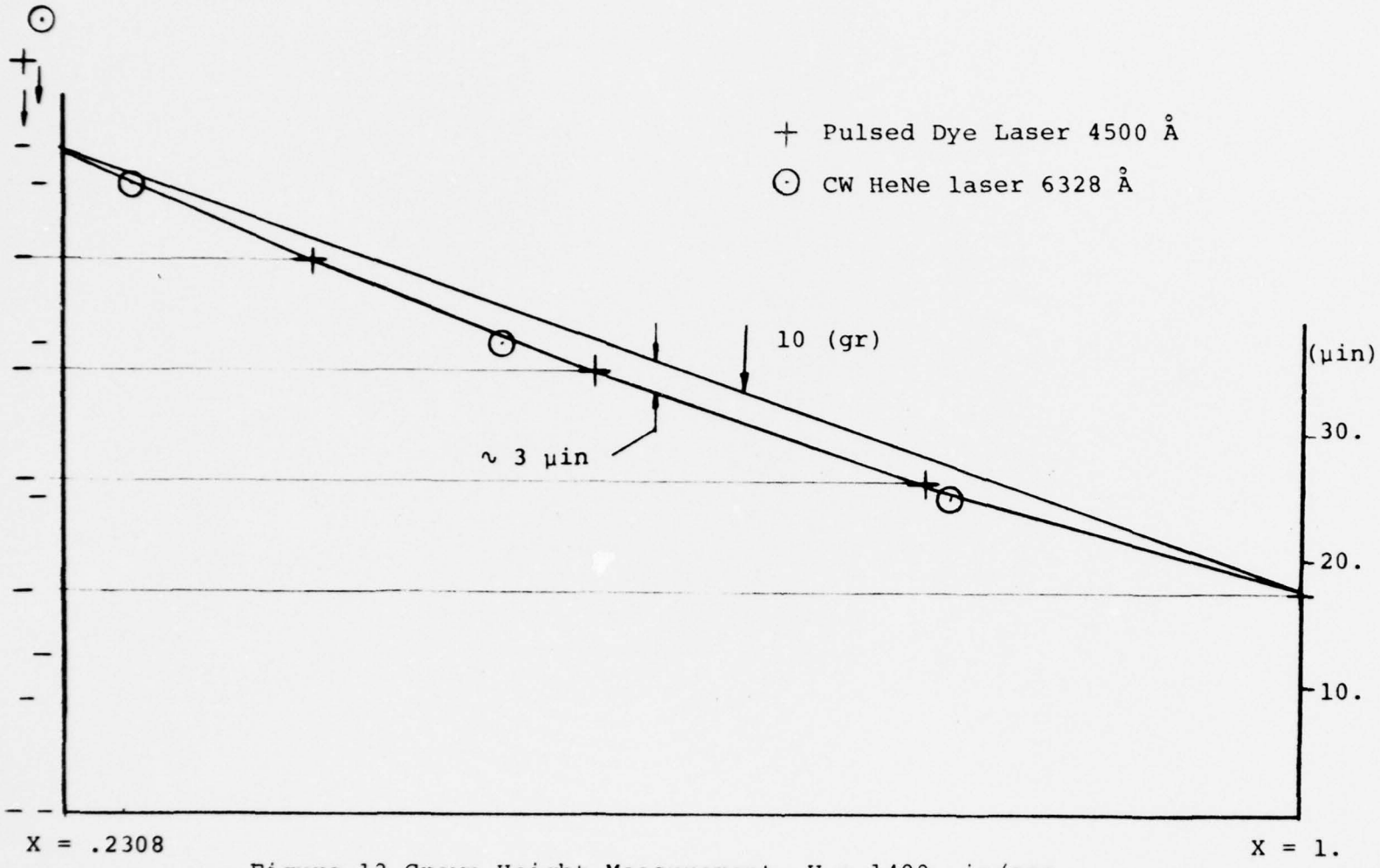

Figure 13 Crown Height Measurement, U = 1490. in/sec

measurement is given in Fig. 13.

Some crude attempts were made to estimate crown height across the bearing. Such attempts showed this crown, if any, to be on the order of 1 microinch. Numerical solutions including this 1 microinch crown across the bearing did not show significant differences in performance. From here on the skates were taken to be flat in the direction perpendicular to motion.

Finally, the lapped slider profile used for all the numerical calculations is given in Fig. 14.

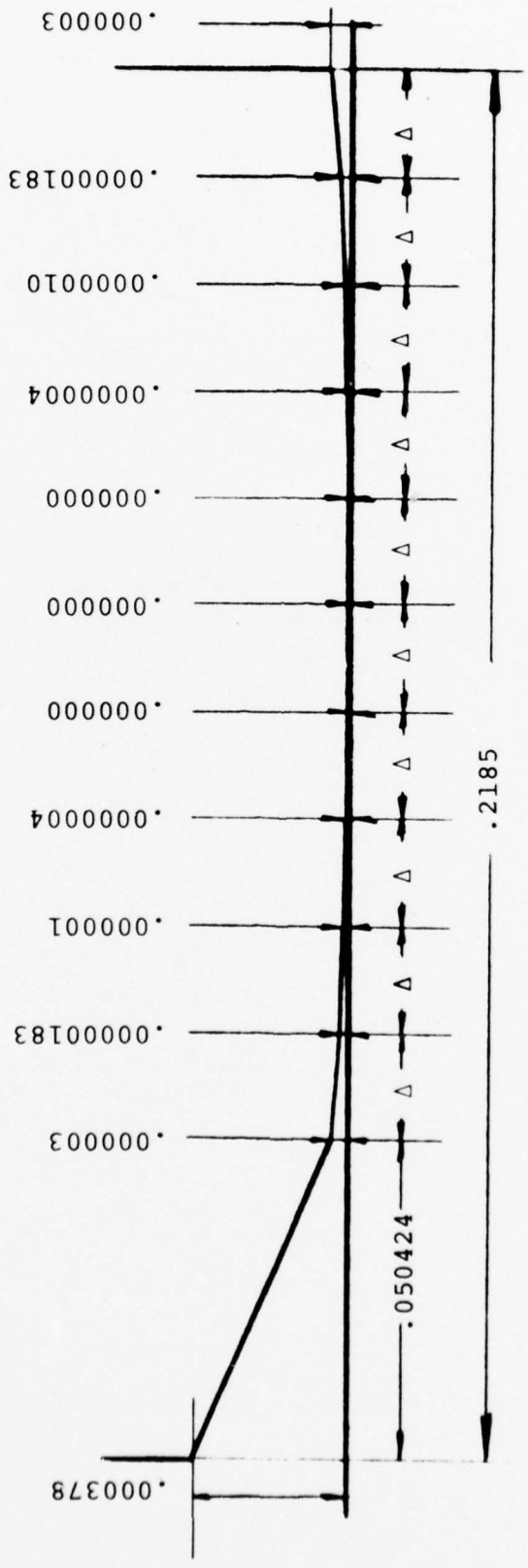

Figure 14 Surface Lapping Used for the Numerical Solution,
Head #A1, (all dimensions are in inches)

$\Delta = 0.016808$

C. Comparison with Numerical Results for Various Bearing and Knudsen Numbers

This section describes the numerical solution, and the experimental technique; a comparison between these results is given.

The numerical solution used to obtain the theoretical results is described in Appendix A. In order to compare the experimental results with the theoretical predicitons, an accurate solution of Reynolds equation with slip boundary conditions was needed. Two major difficulties were encountered in solving Reynolds equation numerically for this particular low-load low-clearance slider bearing. These problems resulted from numerical instabilities in solving Eq. (3) with large bearing numbers ($\Lambda \sim 1000$) and from inaccuracies in load predictions caused by the discontinuities in clearance slope.

To overcome the instabilities in the numerical solution, a careful distribution of the variable grid spacing was needed. The knowledge of the trailing edge boundary layer thickness being on the order of $1/\Lambda$ was the criterion applied for the positioning of the grid points. For half the symmetric bearing, a mesh grid 15×31 was used (15 spacings across and 31 spacings along the bearing).

To handle inaccuracies in pressure profile solutions caused by the large discontinuities in clearance slope, the integral descretization described in Appendix A was used. This algorithm, obtained by using the Gauss integral theorem, satisfies mass balance at each grid point as the column solution method is applied [9]. This discretization reduces the order of the partial differential equation by one. With this discretization, positioning of grid points at clearance discontinuities eliminates the need to approximate derivatives at lines of singularity.

The numerical solution was checked against the exact 1-D solution of Reynolds equation with slip boundary condition (Appendix B). The numerical program was also checked against results obtained by a high-Λ algorithm obtained by Elrod and Cheng [30].

Convergence checks using larger number of grid points were also performed.

These tests indicated accuracies of 2% and of 7% for bearing numbers of 1000 and 4000, respectively. Solutions are not known to be available in the literature for the modified Reynolds equation (3) for a narrow bearing configuration.

The computer program using IBM FORTRAN-G complier needs a core of 160K bytes and 40 seconds of computation

time for each solution of the Reynolds equation for the pivoted slider tested.

The objective of this experimental research was to compare measured bearing clearances with theoretically predicted values. A flow chart describing the procedure for the testing of a slider bearing is given in Fig. 15. After the cleaning of the bearing surfaces and the taking of the static measurements (steps which are described in Secs. III-B and IV-B) the head was flown at a high velocity and low load for the measurements of both slider crown and slider dimensions. The crown measurement is described in Sec. IV-B.

Next, after all the geometrical dimensions were determined, a parametric study of the slider performance was conducted. The pivoted slider bearing, whose dimensions are given in Table 1 and in Fig. 9, was tested under various ambient pressures and molecular mean free paths with loads of 10 to 30 grams and disk velocities of 800 to 2000 in./sec.

One of the most important steps in the flow chart given in Fig. 15 is the processing of a picture of the interference pattern. Knowing the order of the fringes appearing in a recorded pattern allows for clearance measurements with an accuracy of 2 microinches. If an error is made in the fringe order determination, the

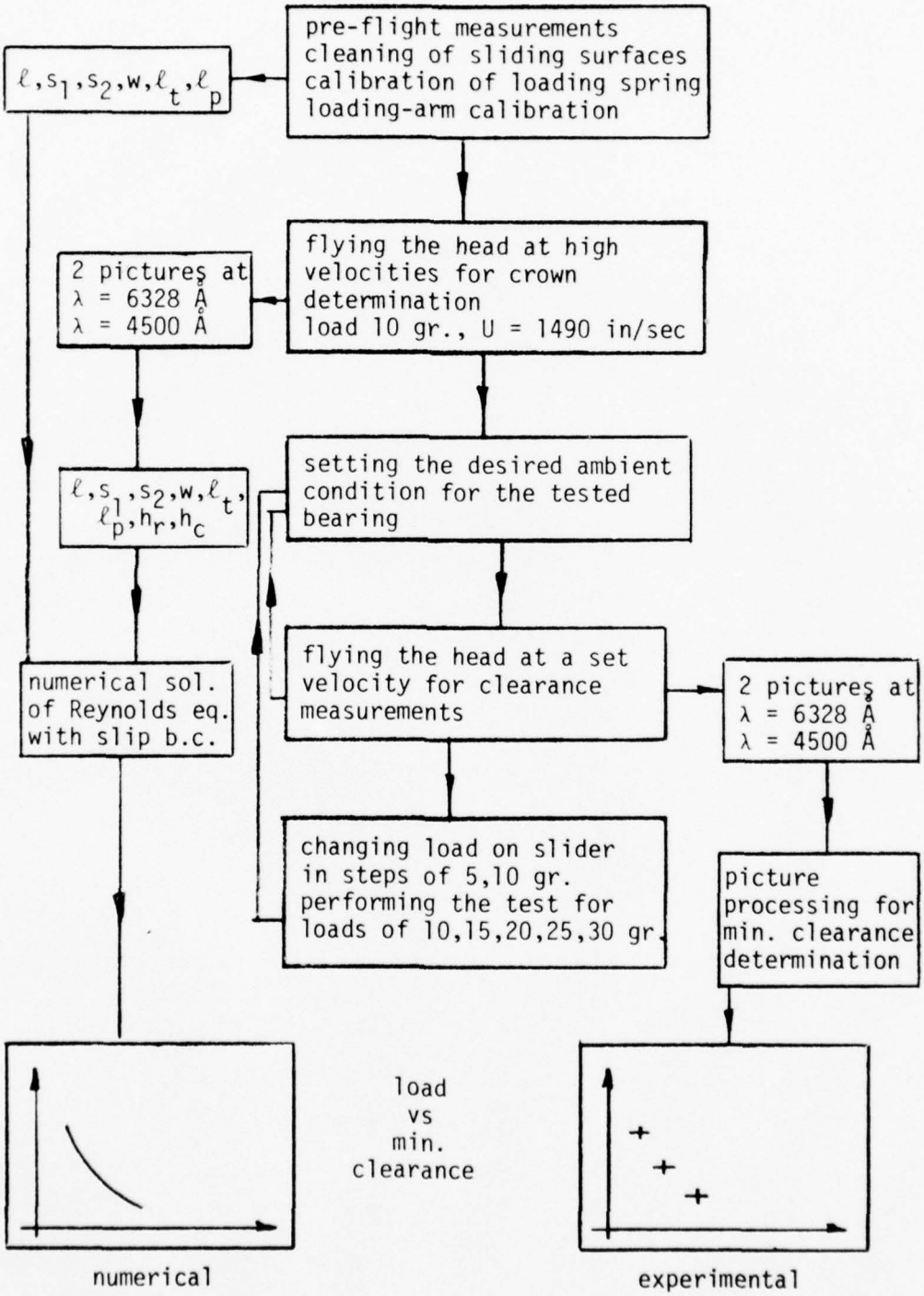

Figure 15 Flow Chart of Bearing Testing Procedure

inaccuracies in clearance measurements could go to values of 15 microinches. Therefore, determining the fringe order has major importance in the measurements of clearance topography.

Three independent methods were applied to eliminate any possible error in fringe order determination.

One of the best ways to determine the fringe order was to follow and count fringes during take-off, loading, pressure change and disk speed variation. Being able to follow the fringes during these transient steps was one of the benefits of the extremely stable and flat quartz disk. A typical stable fringe pattern is shown in Fig. 8. The top fringe pattern in this figure includes the effects of clearance variation with time, since the exposure time is on the order of a full disk rotation. In previous experimental studies by Lin and Sullivan [5] and by Tseng [13] on the performance of these bearings at very low clearances, due to the surface waviness of a large thin disk (14.0" dia., 1/4" thick), no such stability was achieved. The disk used by [5] and [13] represents more a functional surface than an optically flat one.

The second independent way to determine fringe order took advantage of the fact that two blue fringes (4th and 5th blue) will appear between the third and the

fourth red fringes. The order in which the blue and the red fringes line up is given in the left column of Fig. 16.

The third method applied to determining fringe order was by trial and error.* Assuming first the orders of of red fringes the skate profile was plotted and then a check of this profile was performed using the blue fringes. This trial and error was repeated two or three times until a fit similar to the one in Fig. 16 was achieved.

Experimental results versus numerical predictions are given here in Figs. 17-25. These figures describe the bearing load (in grams) versus the trailing edge clearance (in microinches) for various ambient pressures and bearing velocities. On the upper line of these plots the bearing numbers based on trailing edge clearance and the Knudsen numbers, $k = \lambda_a/h_1$ are given.

The ambient molecular mean free path of the bearing was set by lowering the ambient pressure. Assuming isothermal conditions, which can be shown to be valid, the molecular mean free path varies inversely with the pressure; the mean free path was set to values

---

* This method was not used after a while since the first two were found superior.

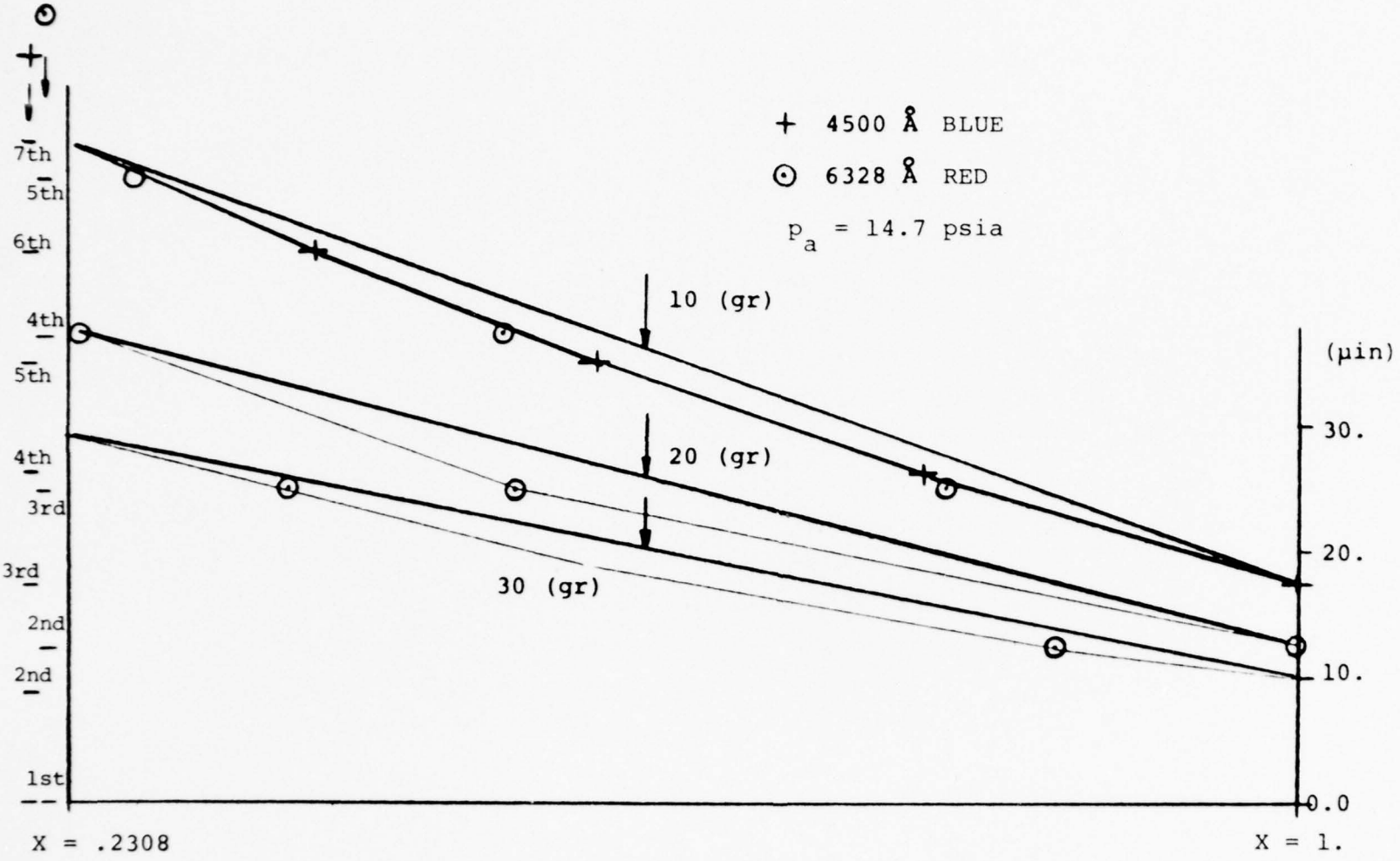

Figure 16 Processing of Interference Pattern, U = 1490. in/sec

of 2.6, 5.2, and 7.8 microinches. With trailing edges on the order of 5 to 12 microinches, the Knudsen number, k , was increased to values beyond one. This indicates that load versus clearance measurements were perfomed for bearings where the value of the trailing edge clearance was the same as the molecular mean free path of the ambient gas. One could already suspect that in low-load bearings the theoretical models, based on slip flow approximations, will not perform well, especially at the trailing edge region.

After careful observation and cross plotting of the theoretically predicted and experimentally measured results, several observations related to Figs. 17-25 can be made. First, examine Figs. 17 and 18, for results under a constant load of 10 grams. The results on these figures indicate significantly better agreement for the bearing with the 2000 in./sec. than for the 800 in./sec. velocity. Note that the bearing with the higher velocity runs with a clearance almost twice as large as the one with the lower speed. In Fig. 18, the measured flying height under the 10 gram load is in relatively good agreement with the predicted clearance. This measurement, which agrees the best with theoretical predictions already has a relatively high Knudsen number (k = .11). The experimental setup did not allow for bearing testing

with Knudsen numbers below .11.

At this stage, without even increasing the molecular mean free path, results indicate that as the clearances in this narrow gas bearing get smaller, while simultaneously the Knudsen number increases from .1 to .173, the theory progressively fails to predict bearing behavior. The progressive failure of the theory to provide the needed side leakage to lower the bearing load is seen in Fig. 18, where discrepancies go from 20% to 25% and to 40%, while the Knudsen numbers vary from .1 to .173 and to .210, respectively. Looking now at Fig. 17, where clearances change from about 12 to 5 microinches, this trend of progressively increasing disagreement stops at about 7 microinches and the general direction seems to reverse itself. Here, with clearances on the order of 5 microinches, the agreement seems to improve as the gap gets smaller and smaller. At this point of the analyis, thoughts related to increasing load because of surface roughness could come to mind.

In Fig. 18, an attempt was made to use the suggested surface accommodation coefficient by [13] but, as the figure indicates, it did not change the results significantly enough.

In Figs. 20-24 measurements with larger molecular mean free path are given. In Figs. 30-32, the

experimental results for pressures 14.7, 7.35, and 4.9 psia indicate that the discrepancy between experiment and theory increases when the ambient pressure is reduced (i.e., ambient mean free path is increased). In Fig. 24, the bearing reaches bearing and Knudsen numbers on the order of 27000 and 1.5, respectively. This discrepancy, under low load at a high Knudsen number, could also be observed in Fig. 5 of [13], where a wide slider bearing with a very low load was tested.

It is interesting to observe that slip effects are still important at such large bearing numbers ($\Lambda \sim 2000$). An asymptotic study on the slip effects at large bearing numbers is given in Appendix D. This analytical solution indicates, as previous researchers show, that slip effects diminish at large values of Λ. This statement immediately raises the question of how large is a large Λ. For a finite width bearing, the magnitude of Λ, an indicator for slip effects, should only be used after the pressure profile (or load) is compared with the solution for $\Lambda \to \infty$. Since, for the narrow slider bearing used here, the load carried is only a fraction of that of a $\Lambda \to \infty$ bearing, bearing numbers on the order of 2000 should still be considered small.

Finally, a cross plot of the experimental and theoretical results is given in Fig. 25. Curves of Fig.

25 represents the solution of Reynolds equation for various values of bearing and Knudsen numbers for a pivoted slider bearing. This figure indicates that, for better agreement with the experiment, the slide leakage in the bearing ought to be increased.

Figures 26 and 27 present the numerical solution and the experimentally measured pivot clearance versus the load on the slider. These two figures indicate a good agreement between theoretical predictions and the experiment for the pivot clearance.

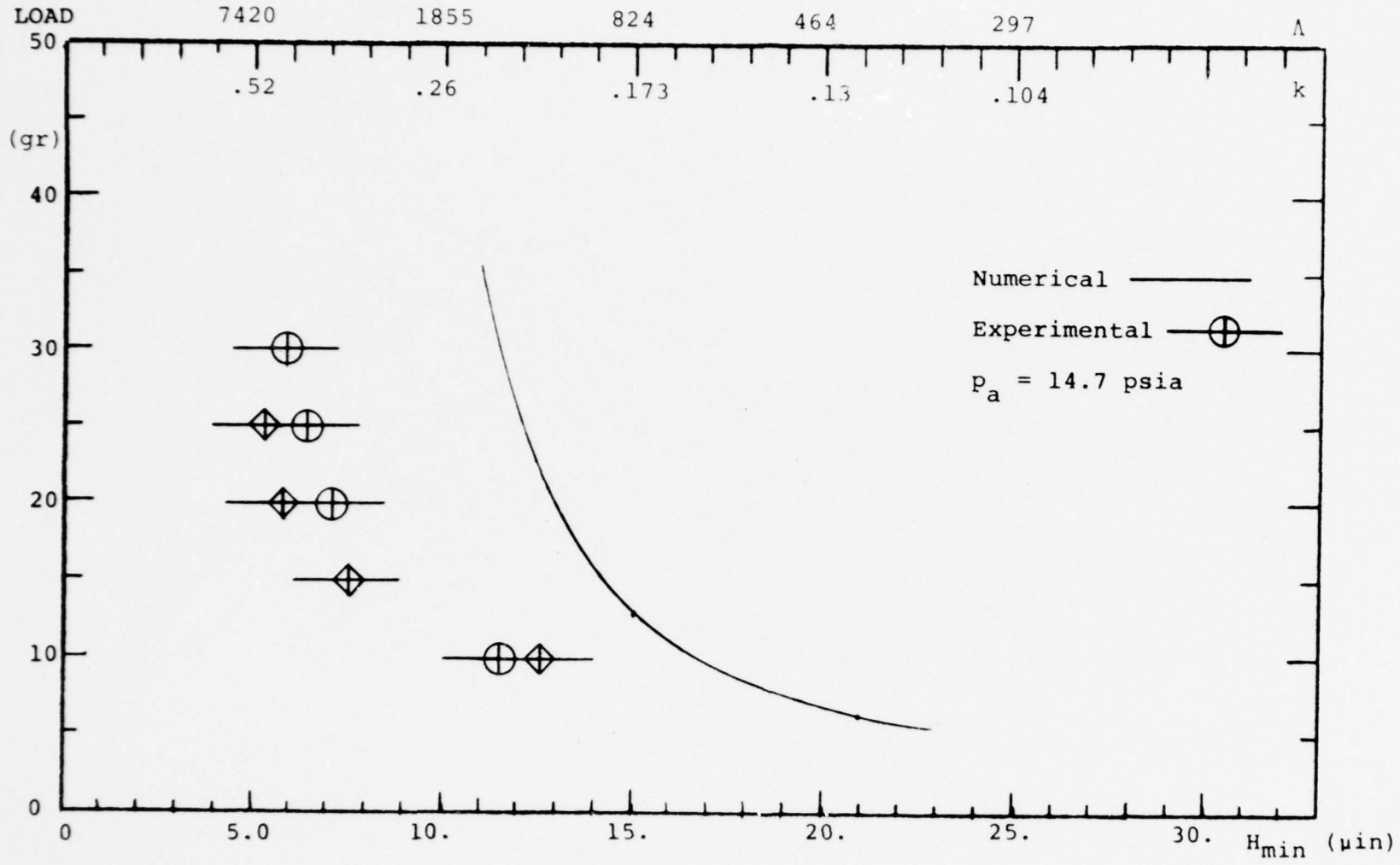

Figure 17 Load vs Minimum Clearance, U = 800 in/sec

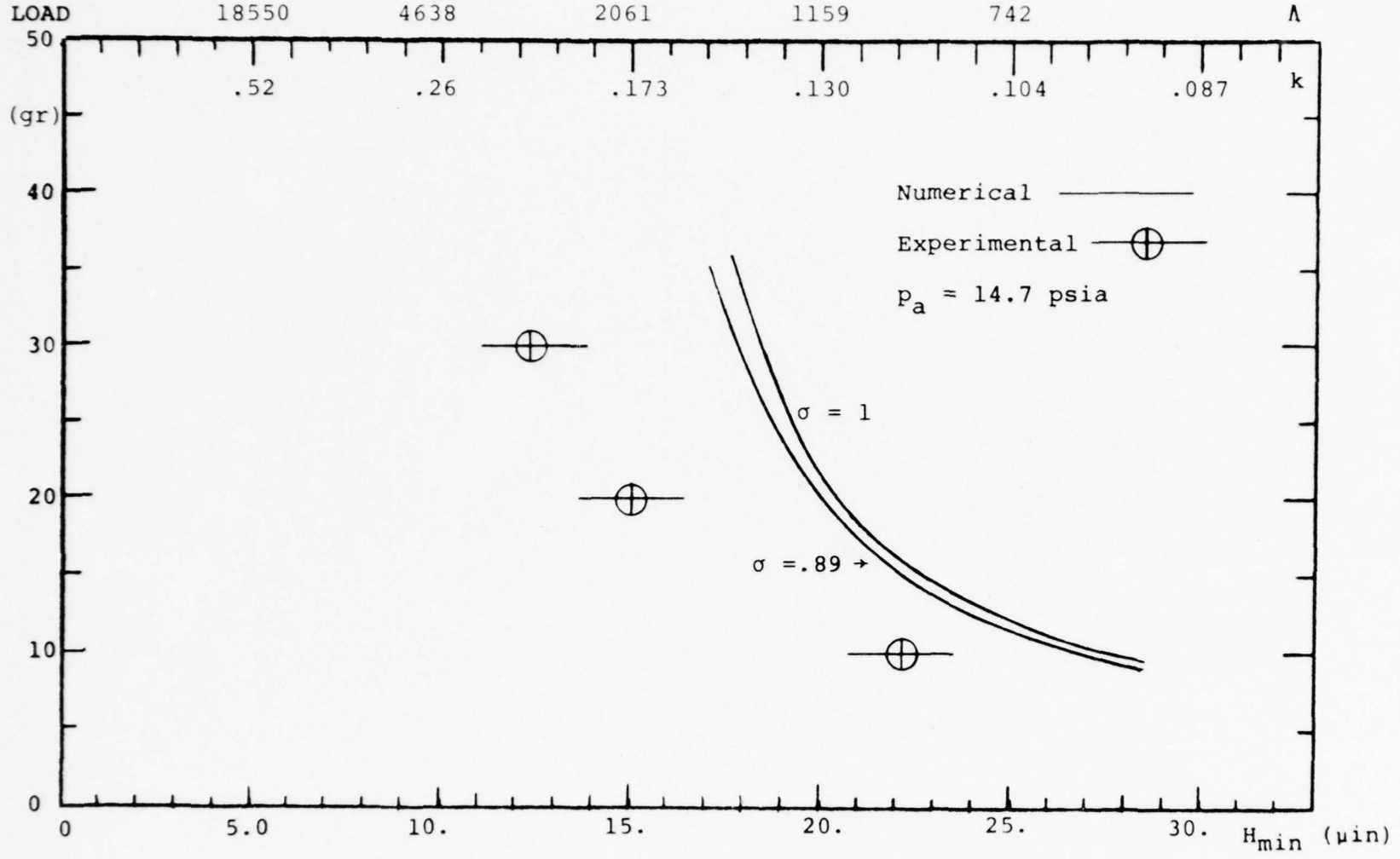

Figure 18 Load vs Minimum Clearance, U = 2000 in/sec

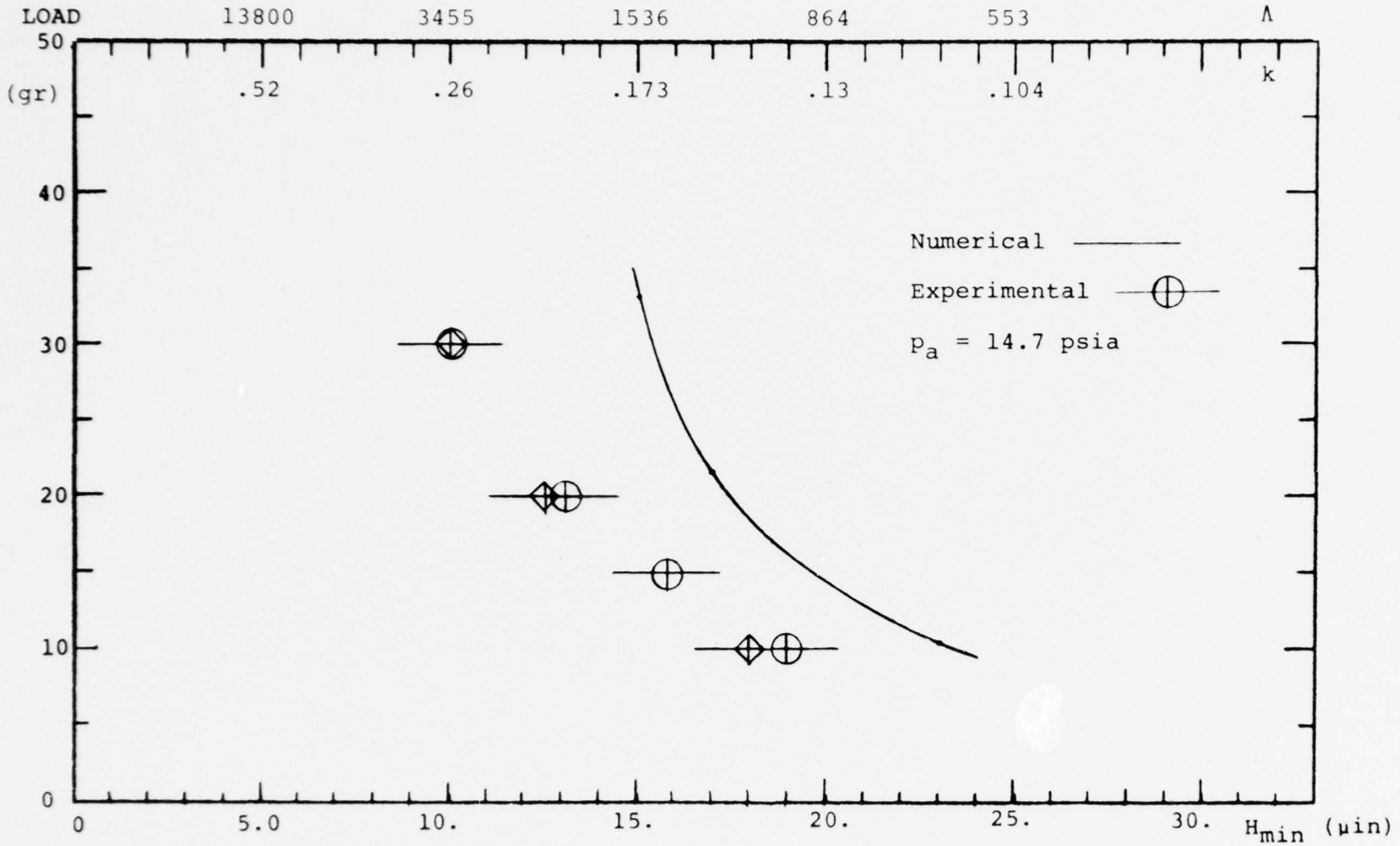

Figure 19 Load vs Minimum Clearance, U = 1490 in/sec

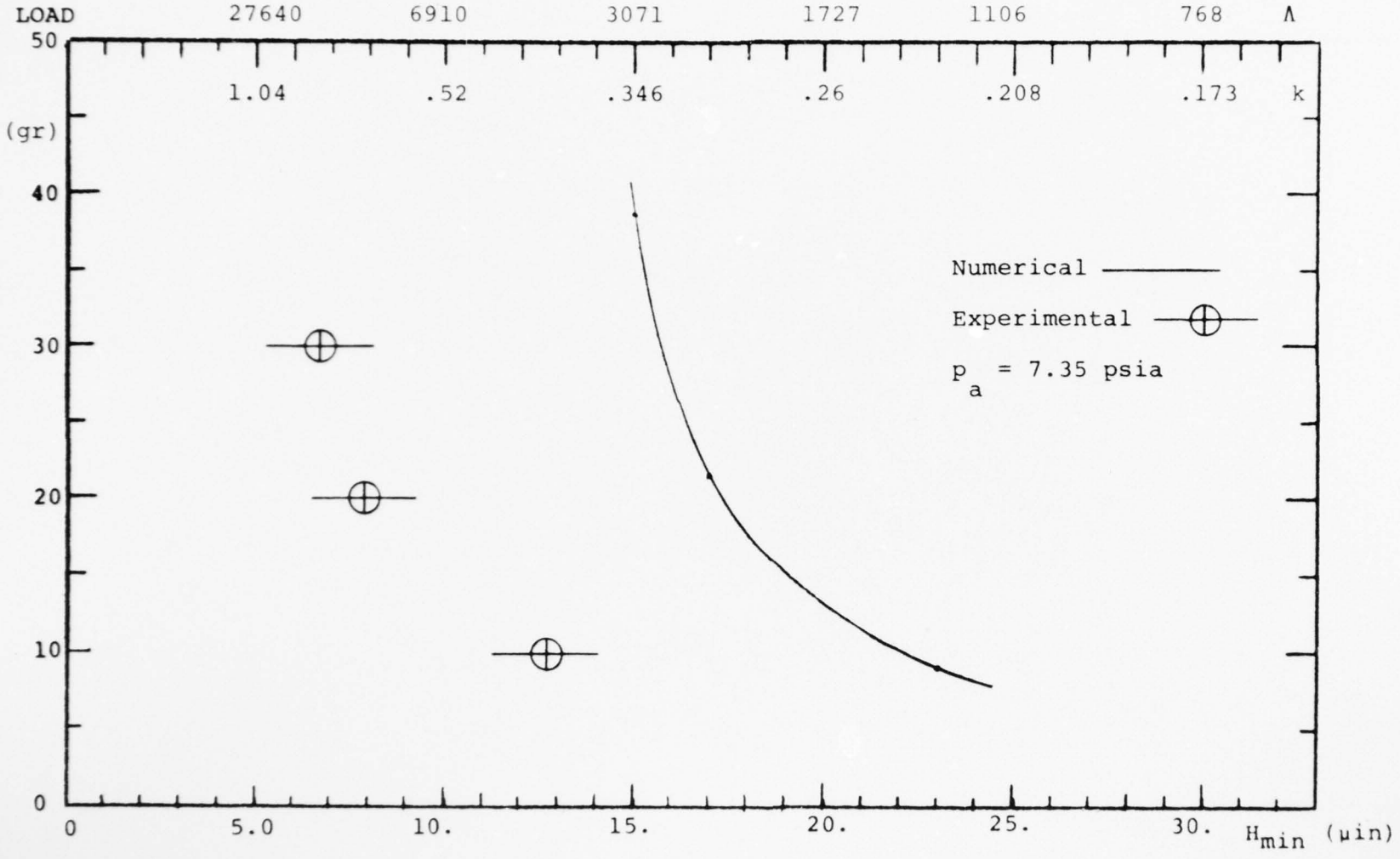

Figure 20 Load vs Minimum Clearance, U = 1490 in/sec

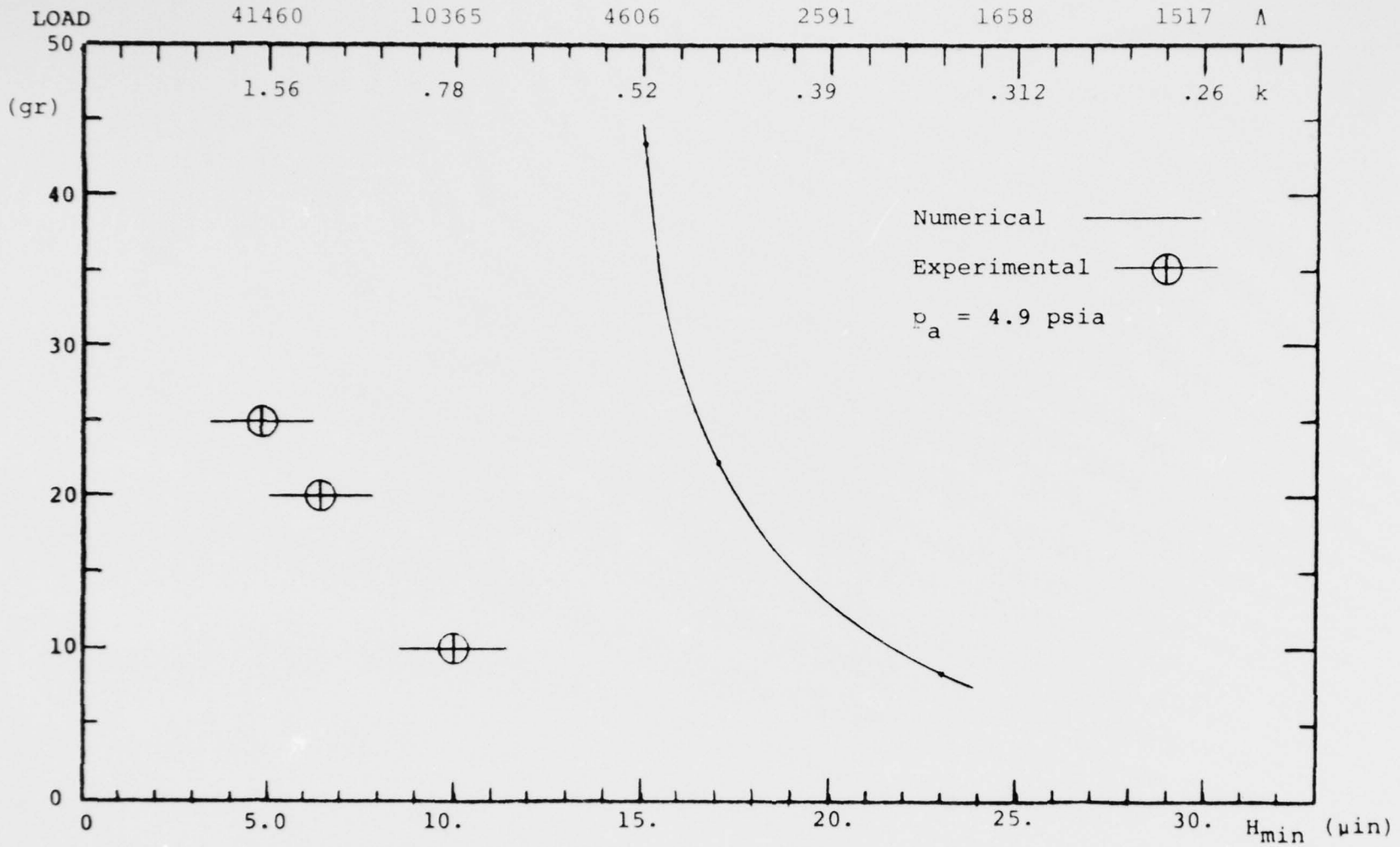

Figure 21 Load vs Minimum Clearance, U = 1490 in/sec

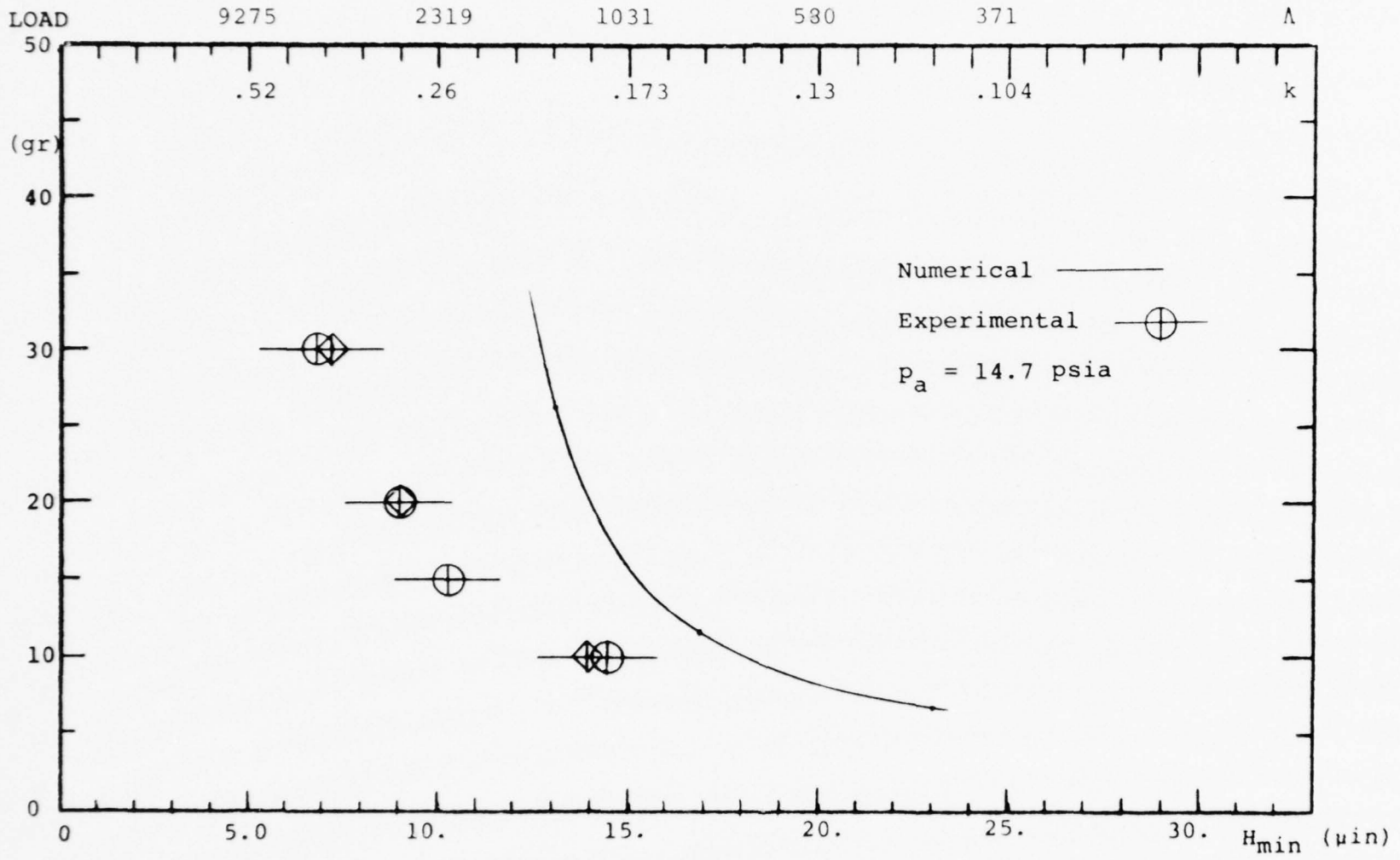

Figure 22 Load vs Minimum Clearance, U = 1000 in/sec

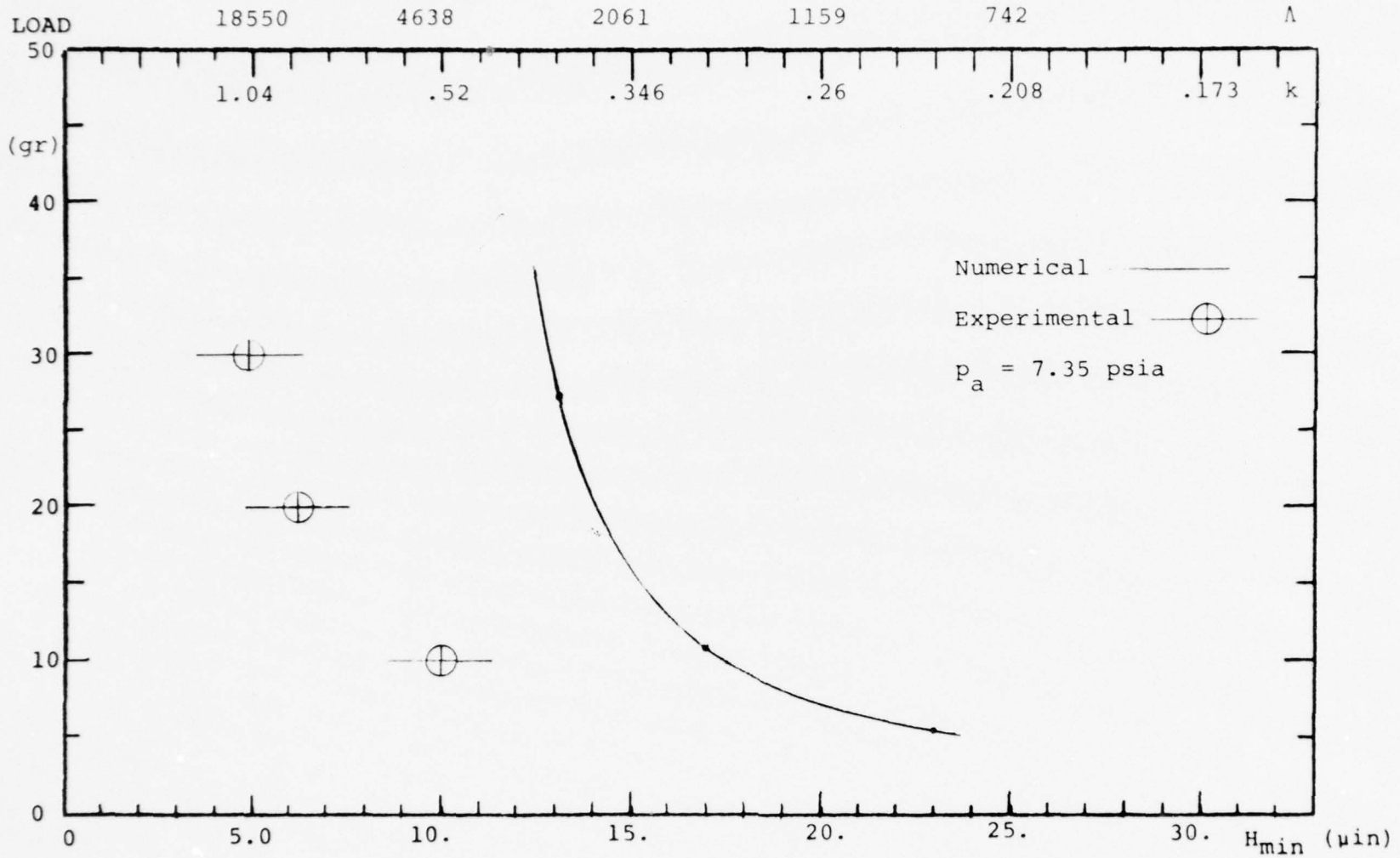

Figure 23 Load vs Minimum Clearance, U = 1000 in/sec

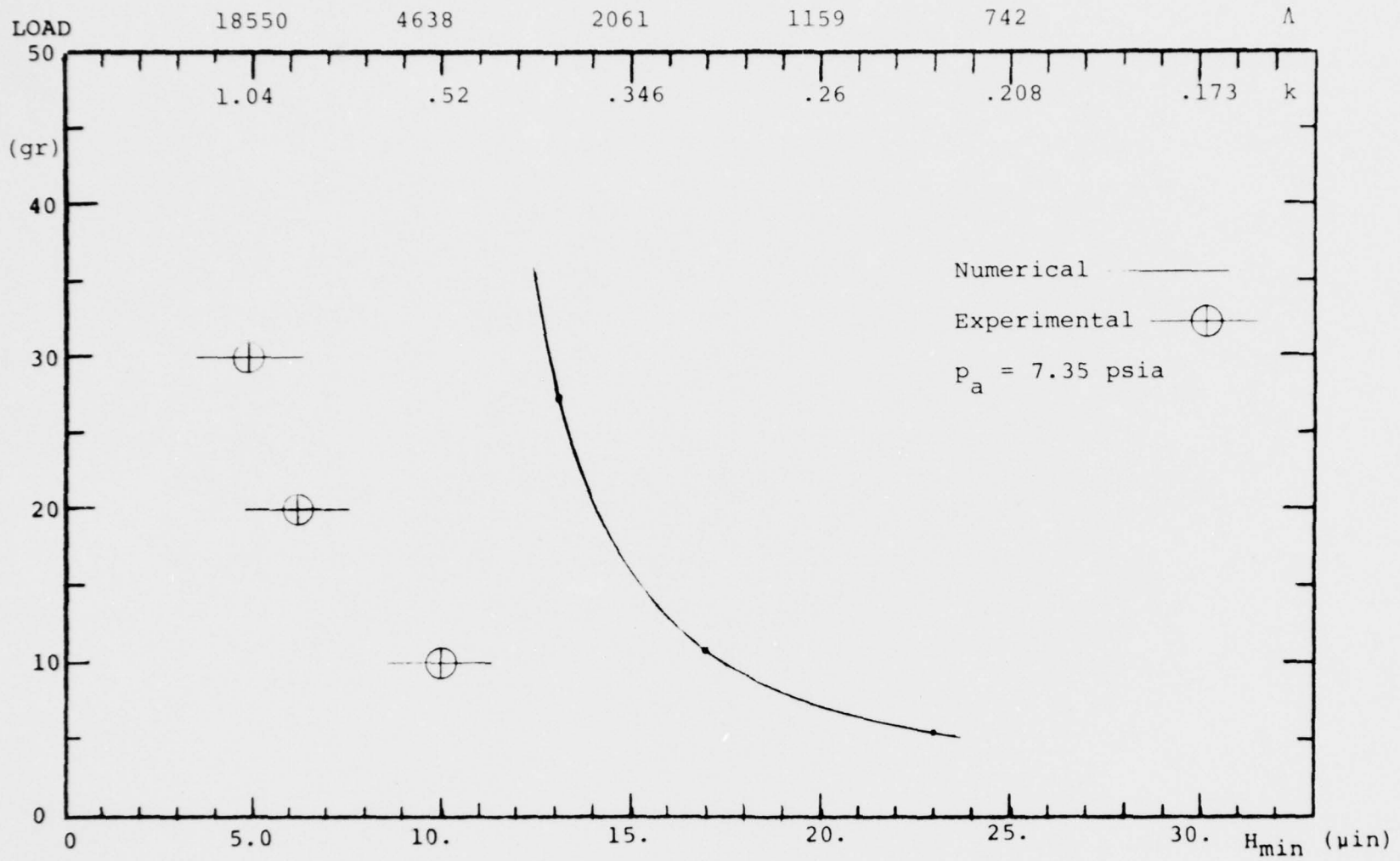

Figure 23 Load vs Minimum Clearance, U = 1000 in/sec

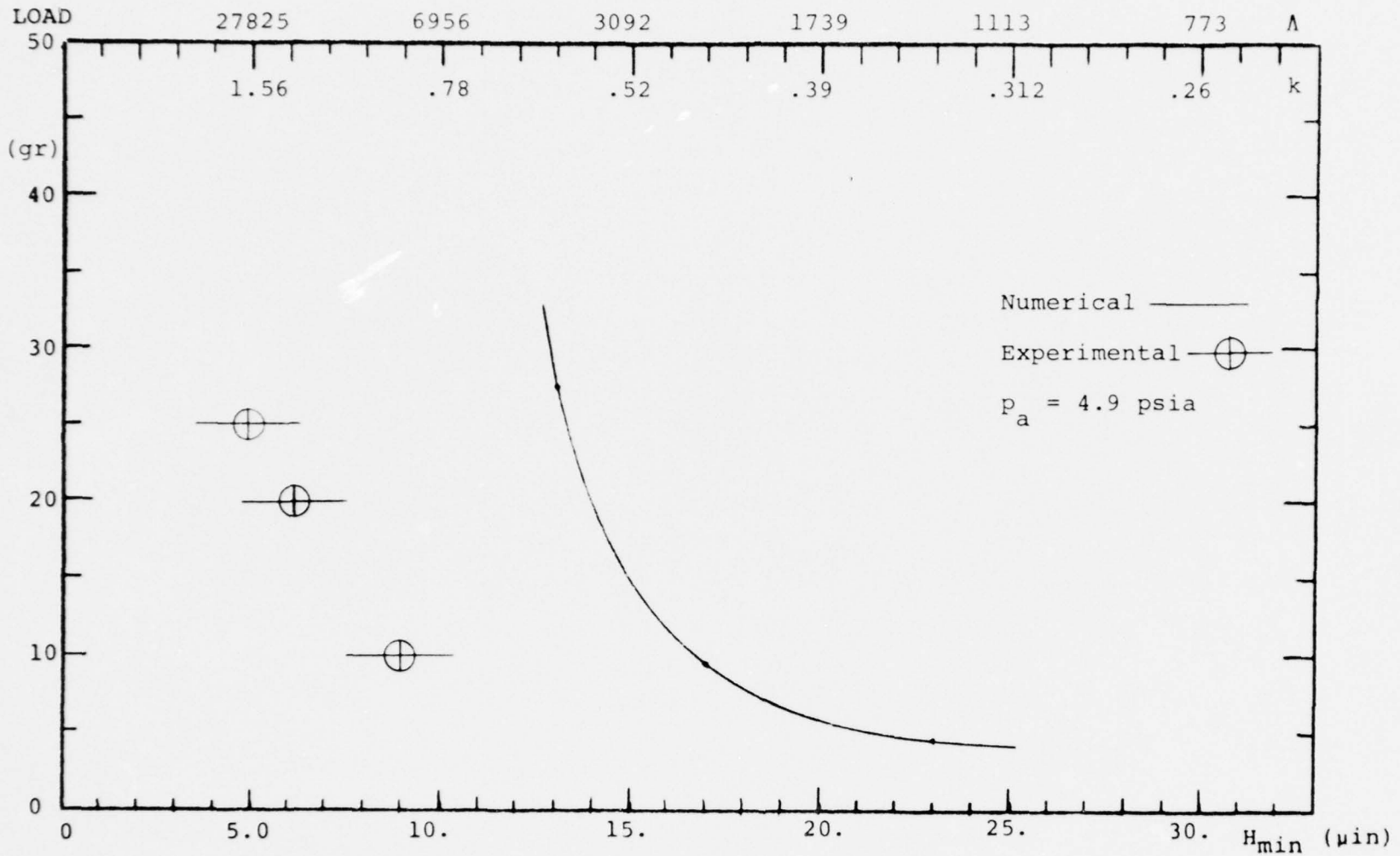

Figure 24 Load vs Minimum Clearance, U = 1000 in/sec

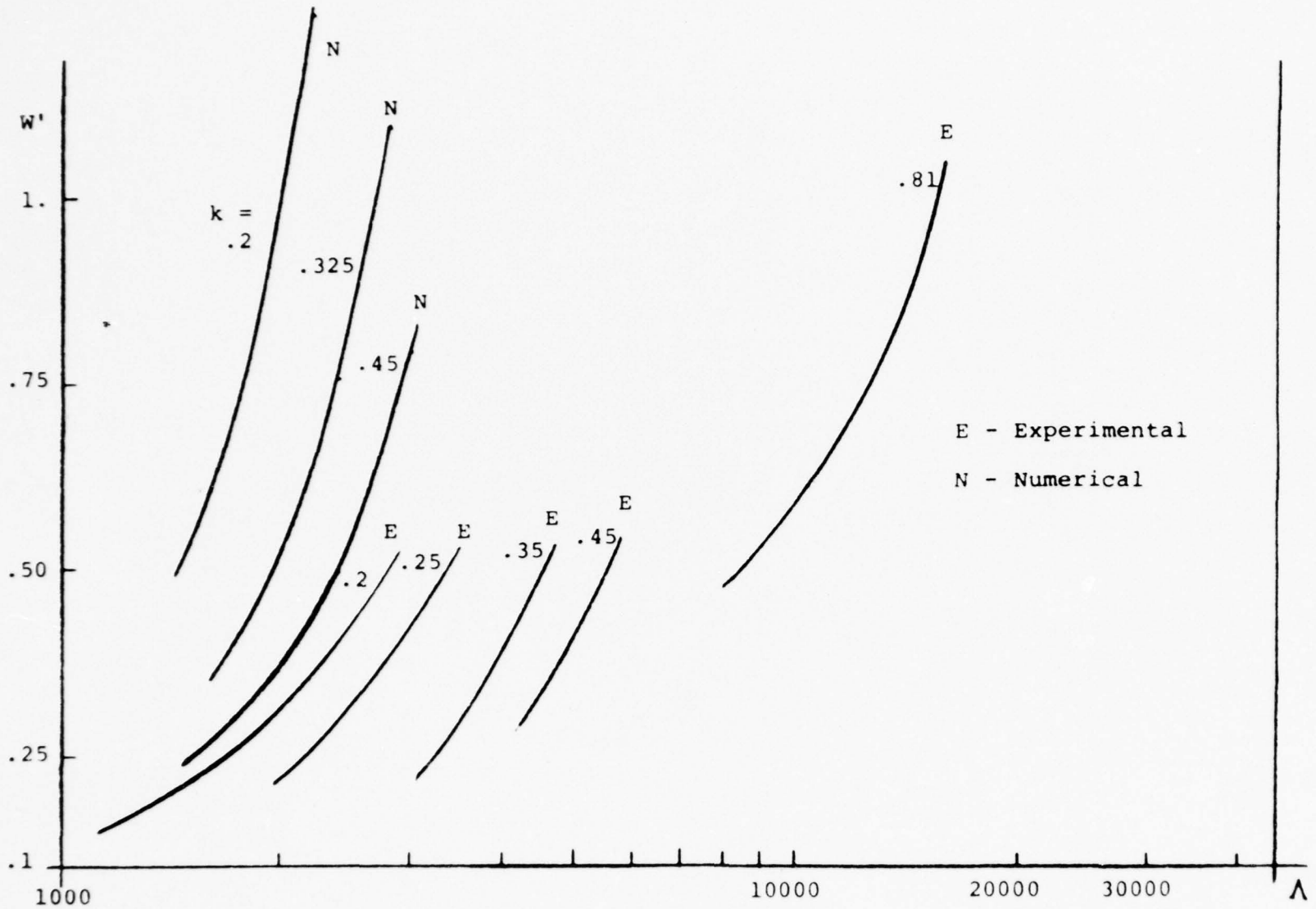

Figure 25 Load vs Bearing Number for Various Knudsen Numbers

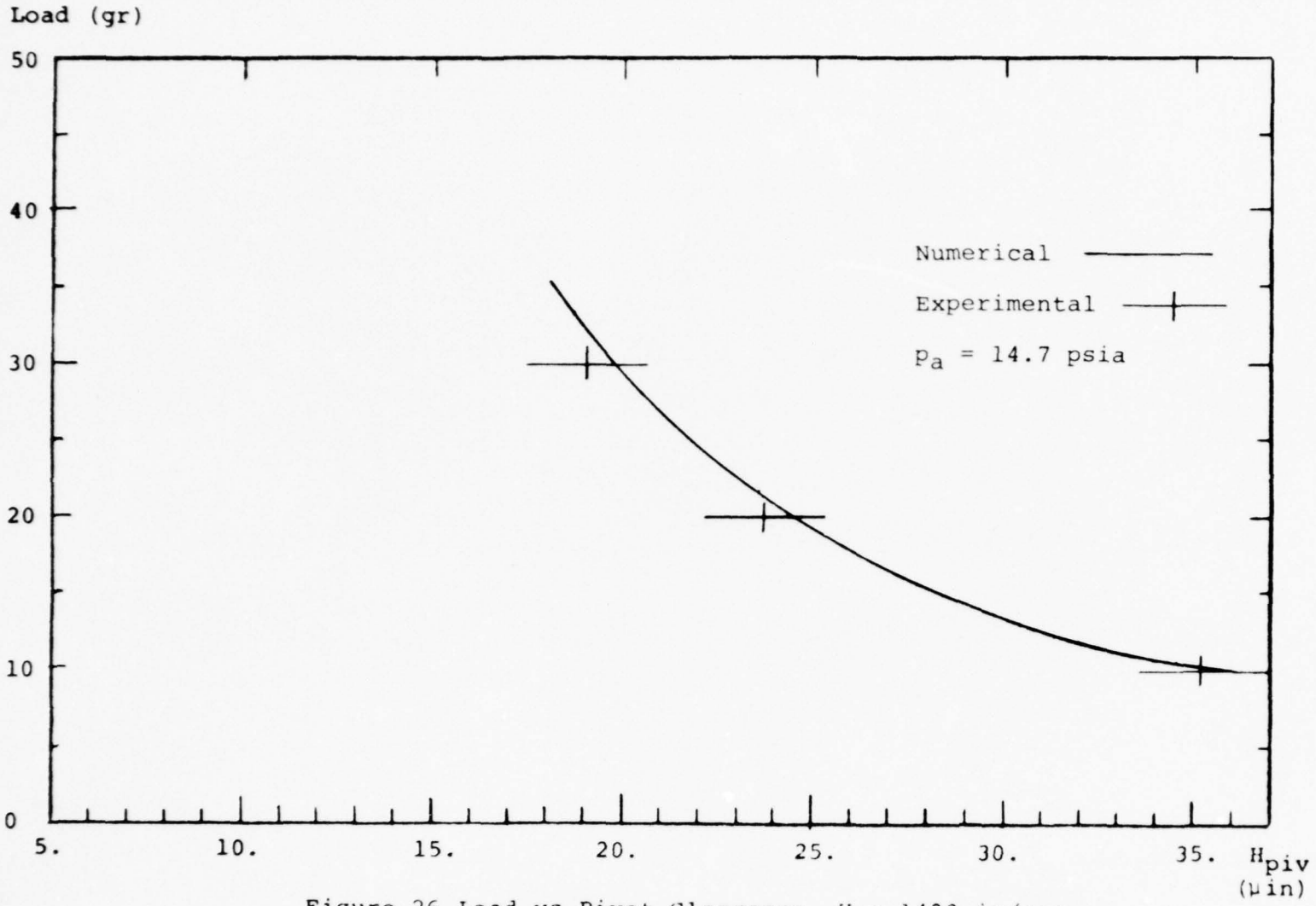

Figure 26 Load vs Pivot Clearance, U = 1490 in/sec

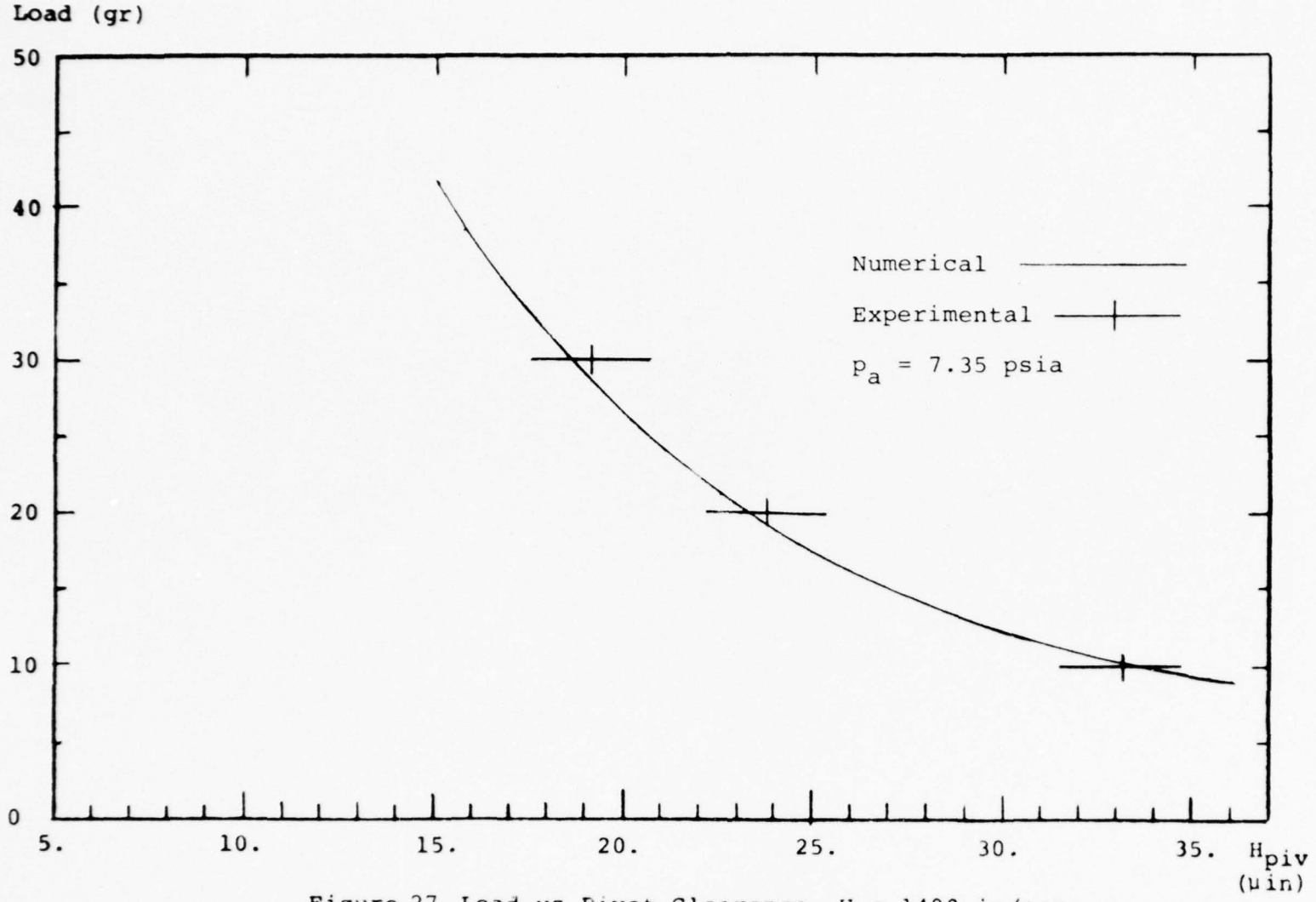

Figure 27 Load vs Pivot Clearance, U = 1490 in/sec

V. Remarks and Recommendations

The design of precise gas bearings to support today's recording heads with core clearances of 20 microinches has been greatly aided by rather accurate theoretical predictions. To design the next generation of heads flying with clearances down to 5 microinches, the theoretical models must be modified. The following recommendations are given to outline some of the additional highly needed research for the modelling and design of ultra-thin gas bearings:

* developing ways to check the accuracy of side leakage obtained by the currently available numerical methods;

* developing theoretical modification for the governing lubrication equation to be applicable in the transition regime of gas dynamics;

* improving and further developing the numerical methods in solving Reynolds equation for both narrow and wide bearings for cases with bearing numbers reaching 10,000;

* performing a theoretical study on gas bearings with

both slip and surface roughness effects included to observe regions of domination;

* bearing surface roughness characterization which provides surface data adequate for the theoretical modeling of roughness effects on bearing performance.

In conclusion, the author believes that this investigation has contributed toward improved experimental methods and has provided the first set of experimental data on low-load low-flight slider bearings. It is hoped that this experimental analysis may serve as the first link in future theoretical, numerical, and experimental work in the design and development of ultra-thin gas bearings.

VI. APPENDICES

APPENDIX A

Numerical Solution of Reynolds Equation with Slip Boundary Condition for Cases of Large Bearing Number ($\Lambda > 300$)

The numerical solution of the governing steady state lubrication equation that has been applied to obtain the theoretical results is described in this Appendix. In order to compare the experimental results with the theoretical predictions, an accurate solution of Reynolds equation with slip boundary conditions was needed.

Numerical solution methods that are described in a review paper by Castelli and Pirvics [9] were applied to the modified Reynolds equation for slider bearings with large bearing number. The numerical methods described here will point out ways to overcome major difficulties caused by large bearing number, $\Lambda > 300$, and because of large discontinuities in clearance slope of a slider bearing. It should be noted that in this investigation, the effort to obtain an accurate numerical solution was carried beyond the accuracy needed from the designer point of view.

Generally, there are two distinct methods of discretization applied to Reynolds equation (3)

$$\nabla \cdot [\, Q \, \nabla \, Q \,] \;=\; 0$$

differential discretization

$$\left(\frac{d\,Q}{d\,X} \right)_i^2 \;+\; Q \left(\frac{d^2 Q}{d\,X^2} \right)_i \;=\; 0$$

$$\left. \frac{d\,Q}{d\,X} \right)_i \;=\; \frac{Q_{i+1} \;-\; Q_{i-1}}{2\,\Delta x}$$

$$\left. \frac{d^2 Q}{d\,X^2} \right)_i \;=\; \frac{Q_{i+1} \;-\; 2\,Q_i \;+\; Q_{i-1}}{(\Delta x)^2}$$

integral discretization

$$Q \left. \frac{d\,Q}{d\,X} \right)_{i-\frac{1}{2}} \;=\; Q \left. \frac{d\,Q}{d\,X} \right)_{i+\frac{1}{2}}$$

$$Q_{i\pm\frac{1}{2}} \;=\; \frac{Q_{i\pm1} \;+\; Q_i}{2}$$

$$\left. \frac{d\,Q}{d\,X} \right)_{i\pm\frac{1}{2}} \;=\; \frac{\pm\, Q_{i\pm1} \;\mp\; Q_i}{\Delta\, x}$$

Figure 1A Differential vs Integral Discretization

differential discretization and integral discretization. Each method applied to a differential equation of the form resembling Reynolds equation is described in Fig. 1A. The integral discretization is obtained after integrating the Reynolds equation over the shaded area in Fig. 2A and then applying the Gauss theorem. The differential discretization is the method to be used when the differential equation is written in a finite difference form in a straightforward fashion.

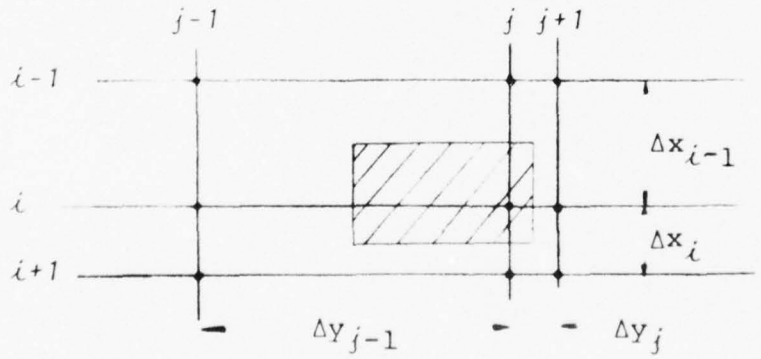

Fig. 2A

The governing lubrication equation one step before applying the differential discretization is given in Eq. (1A).

$$\nabla^2 Q - \nabla Q \cdot \nabla \text{Log} H - \frac{2Q}{H}\nabla^2 H - \frac{6k}{\sqrt{Q}+6k} \frac{\{\nabla Q \cdot \nabla Q - 2Q\nabla Q \cdot \nabla \text{Log}(H)\}}{2Q}$$

$$= \frac{\vec{\Lambda} \cdot \nabla Q}{\sqrt{Q}+6k} \frac{1}{H} \qquad (1A)$$

where $Q = (PH)^2$, $\vec{\Lambda} = 6\mu\vec{U}\ell/(P_a h^2_{min})$, $\vec{U} = U_x\hat{X}+U_y\hat{Y}$

and $k = \lambda_a/h_{min}$

Discretization of Eq. (1A) requires finite difference approximations of the first and second derivatives of Q and H. At this point, one can already note that the differential discretization will have some deficiencies in handling cases where significant discontinuities of clearance and clearance-slope appear.

The integral approach approximates Reynolds equation in the following way

$$\left(-\frac{1}{2}(1 + \frac{6k}{\sqrt{Q}})(H\frac{\partial Q}{\partial Y} - 2Q\frac{\partial H}{\partial Y}) + \Lambda_Y\frac{Q}{\sqrt{Q}}\right)_{i,j-\frac{1}{2}} +$$

$$\left(\frac{1}{2}(1 + \frac{6k}{\sqrt{Q}})(H\frac{\partial Q}{\partial Y} - 2Q\frac{\partial H}{\partial Y}) - \Lambda_Y\frac{Q}{\sqrt{Q}}\right)_{i,j+\frac{1}{2}} +$$

$$\left(-\frac{1}{2}(1 + \frac{6k}{\sqrt{Q}})(H\frac{\partial Q}{\partial X} - 2Q\frac{\partial H}{\partial X}) + \Lambda_X\frac{Q}{\sqrt{Q}}\right)_{i-\frac{1}{2},j} +$$

$$\left(\frac{1}{2}(1 + \frac{6k}{\sqrt{Q}})(H\frac{\partial Q}{\partial X} - 2Q\frac{\partial H}{\partial X}) - \Lambda_X\frac{Q}{\sqrt{Q}}\right)_{i+\frac{1}{2},j} = 0 \qquad (2A)$$

where $\Lambda_Y = 6\mu U_Y \ell/(p_a h^2_{min})$

$\Lambda_X = 6\mu U_X \ell/(p_a h^2_{min})$

With this method of discretization, only first order derivatives of Q and H are needed, and here, at the mid-points of the grid lines. It seems that the integral discretization approximates the Reynolds equation in a way such that it provides the needed conservation of mass.

After the linearization of equations (1A) and (2A) each method provides a system of linear equations that is solved by the so-called Column Method. Both the linearization and the solution of the linear system is described in Ref. [9].

The rules that were followed during the distribution of grid points and the variable grid spacings are outlined in Fig. 3A. To achieve convergence and to eliminate numerical instabilities a sufficient number of grid points were needed to handle sharp pressure changes in boundary layers. In addition, since discontinuities of clearance slope exist in the bearing tested, it was found to be important to position grid lines at those points.

The two different numerical approximations, the differential and the integral discretization, were first applied to a tapered slider bearing and the pressure profile resulting from each method agreed with each other to the third significant figure. Further testing of these numerical methods, applying them to the bearing under test, showed the expected superiority of the

A) Grid Lines Should Fall on all Boundaries

B) Grid Lines Should Fall on all Discontinuities of Clearance

C) Grid Lines Should Fall on all Discontinuities of Clearance-Slope

D) Sufficient Number of Grid Points Needed where Large Changes of Pressure Expected (bdry layers)

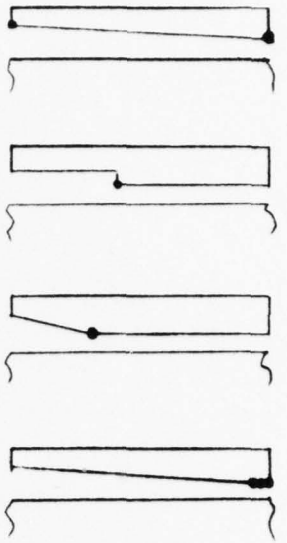

Figure 3A Grid-Points for the Numerical Solution of Reynolds Equation with Large Bearing Number

($\Lambda > 300$)

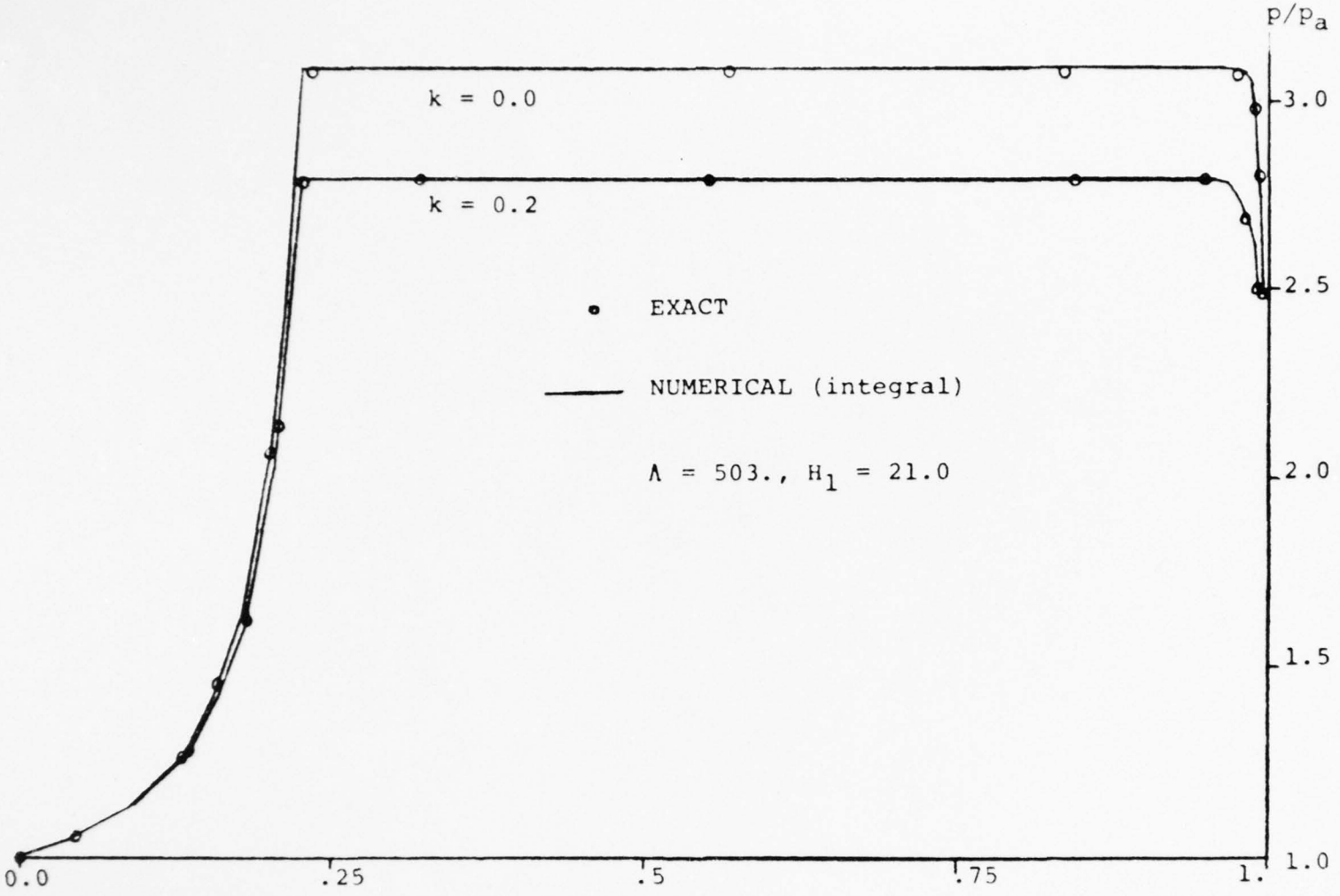

Figure 4A Pressure Profile for ∞ - Wide Tapered Flat Slider Bearing,

Exact versus Numerical

integral over the differential discretization. Results for this comparison, given in Table 1A, indicate a much stronger grid-size dependence on convergence for the differential approach.

At this point, a final testing of the numerical procedures was required. The exact, closed-form solution for the infinite-wide tapered, tapered-flat, and tapered-tapered slider bearing with slip boundary condition was obtained. This analytical solution, outlined in Appendix B, was found to be essential in order to verify the accuracy of the numerical solution. Having this exact solution facilitated a comparison between the two numerical methods and the exact solution. Results giving values of maximum pressure obtained are given in Tables 2A, and 3A. Fig. 4A describes the pressure profile obtained using the exact solution against results obtained using the numerical procedure for a bearing with similar dimensions to those used in the experimental work. Fig. 4A also verifies the numerical solution for handling both boundary layers and slip boundary conditions.

	Grid Size	Load (gr)
Diff.	9 x 25	30.69
	9 x 31	23.90
	9 x 61	20.50
Int.	9 x 25	19.23
	15 x 31	19.06
	15 x 41	18.91

Table 1A Numerical Results for Tapered Slider Bearing, $\ell/w = 11$, $\Lambda = 2000.0$, $k = 0.26$

	p_{max}
Exact	3.570
Int.	3.571
Diff.	3.638

Table 2A Exact vs Numerical for Tapered-Flat

∞ - Wide Slider Bearing

$H_1 = 4.0, \Lambda = 223, k = 0.0$

k		p_{max}
0.0	Exact	3.076
	Int.	3.095
	Diff.	No Convergence
0.2	Exact	2.798
	Int.	2.803
	Diff.	3.800

Table 3A Exact vs Numerical for Tapered-Flat

∞ - Wide Slider Bearing, $H_1 = 21., \Lambda = 503$

APPENDIX B

Exact Solution of the 1-D Reynolds Equation with Slip Boundary Condition for Tapered, Tapered-Flat, and Tapered-Tapered Slider Bearings

The solution for the modified Reynolds equation for a tapered, infinitely wide slider bearing was partially given by Burgdorfer [10]. Because of some errors in the solution in Ref. [10], the solution is repeated here. Slider bearings, for which the solution is outlined, can have any combination of tapered and/or flat surfaces. Separate solutions for tapered and flat sliders are given and the conditions of pressure and mass flow for a combined bearing are shown. With the solutions described here, one can obtain the bearing performance for any bearing that has a combination of tapered and flat surfaces.

The non-dimensional Reynolds equation with slip boundary condition for a slider bearing is given as

$$\frac{d}{dX}\left(\frac{H^3 P}{\Lambda}\frac{dP}{dX}\left(1 + \frac{6k}{PH}\right) - PH\right) = 0 \qquad (1B)$$

where $Y = x/\ell$, $H = h/h_1$, $k = \lambda_a/h_1$

A. Solution for a Tapered Bearing - Fig. 1B

Integrating equation (1B) gives

$$PH^3\frac{dP}{dX}\left(1 + \frac{6k}{PH}\right) - \Lambda PH = -K_1\Lambda \tag{2B}$$

changing variables from X to H and integrating again gives an equation in the form

$$\theta^2 - (\Lambda^* - 6k)\theta + \Lambda^* K_1 = K_2 H^2 \Psi(\theta) \tag{3B}$$

in which K_1 and C are the two constants of integration and $\Psi(\theta)$ assumes the following values:

$$\Psi_1(\theta) = \text{EXP}\left\{-\frac{\Lambda^* + 6k}{\sqrt{K}/2}\ tg^{-1}\left(\frac{\theta - (\Lambda^*/2 - 3k)}{\sqrt{K}/2}\right)\right\} \tag{4B}$$

for $K > 0$

$$\Psi_2(\theta) = \text{EXP}\left(\frac{\Lambda^* + 3k}{\theta - \Lambda^*/2 + 3k}\right) \tag{5B}$$

for $K = 0$

$$\Psi_3(\theta) = \left|\frac{\theta - \Lambda^*/2 + 3k + \sqrt{-K}/2}{\theta - \Lambda^*/2 + 3k - \sqrt{-K}/2}\right|^{\frac{\Lambda^* + 6k}{\sqrt{-K}}} \tag{6B}$$

for $K < 0$

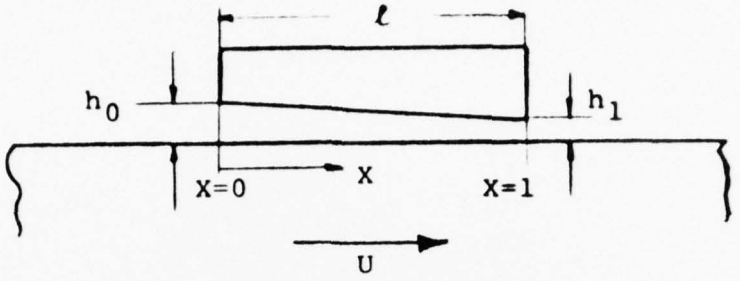

Figure 1B Tapered Slider Bearing

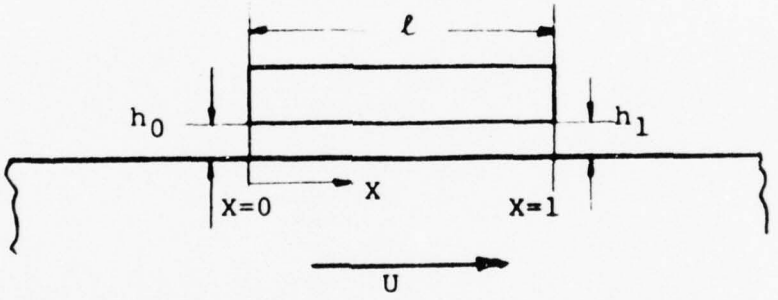

Figure 2B Flat Slider Bearing

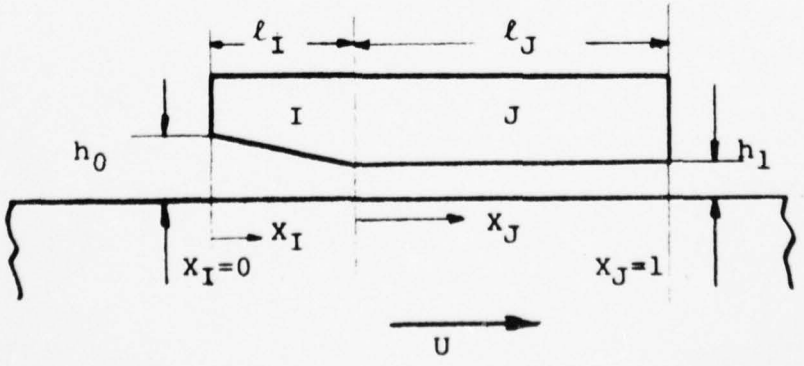

Figure 3B Tapered Flat Slider Bearing

where $K = 4\Lambda^* K_1 - (\Lambda^* - 6k)^2$

$\Lambda^* = \Lambda/(H_0 - 1)$

$\theta = PH$

and $H_0 = h_0/h_1$

B. Solution for a flat slider bearing - Fig. 2B

Equation (1B) for a flat slider bearing takes the following form

$$\frac{d}{dX}\left(P\left(1 + \frac{6k}{P}\right)\frac{dP}{dX} - \Lambda P\right) = 0 \qquad (7B)$$

Integration of Eq. (7B) gives

$$P(1 + 6k/P)\frac{dP}{dX} - \Lambda P = -C_1/\Lambda \qquad (8B)$$

Integration of Eq. (8B) gives

$$P + (C_1/\Lambda^2 + 6k)\,\mathrm{Log}(P - C_1/\Lambda^2) = \Lambda X + C_2 \qquad (9B)$$

where c_1 and c_2 are the integration constants.

C. Solution for a Tapered-Flat Slider Bearing - Fig. 3B

This solution for the tapered-flat slider bearing will demonstrate how to combine the solutions for the tapered bearing and the solution for a flat bearing. The bearing in Fig. 3B is divided into two regions indicated by subscript I and J. Solutions for the pressure in these regions were given in the two previous sections. Eqs. (3B) and (9B) together indicate the pressure. These equations carry constants C_1, C_2, K_1, and K_2, to be satisfied by boundary conditions at the leading and trailing edge of the bearing and by conditions on pressure continuity and conservation of mass between sections one and two of the bearing.

The condition on mass flow gives

$$\left(P_I H^3 (1 + \frac{6k}{P_I H}) \frac{dP_I}{dX_I} - \frac{6\mu U}{h_2^2 P_a} P_I H\right)_{x_1=\ell_I} = 0$$

$$\left(P_J (1 + \frac{6k}{P_J}) \frac{dP_J}{dX_J} - \frac{6\mu U}{h_2^2 P_a} P_J\right)_{x_2=0} = 0 \qquad (10B)$$

Using the condition on pressure

$$P_I(x_I=\ell_I) = P_J(x_J=0) \qquad (11B)$$

reduces Eq. (10B) to the following

$$K_1 = C_1/\Lambda_J^2 \tag{12B}$$

Finally, the four conditions needed to solve for the four constants in Eqs. (3B) and (9B) are given

$$\begin{aligned} P_I(x_I=0) &= p_a \\ P_J(x_J=\ell_J) &= p_a \\ P_I(x_I=\ell_I) &= P_J(x_J=0) \\ K_1 &= C_1/\Lambda_J^2 \end{aligned} \tag{13B}$$

The set of algebraic equations obtained using Eqs. (3B), (9B) and (13B) are transcendental. Careful observation and study of these equations avoids numerical round-off type errors that can alter solutions significantly. Listing of a computer program that solves Eqs. (3B) and (6B) are given in Appendix C.

APPENDIX C

Listing of Computer Program Solving the Exact 1-D Reynolds Equation with Slip Boundary Condition

```
C                    TAPERED SLIDER BEARING  (K.LT.0.0)
C         OUTPUT PROVICES K1,K2,P
C               ********************************
C                    INPUT FLOW CHART
C               ********************************
C       READ/DATA/H1,XL,M1,P
C               ********************************
C               ********************************
C       H1=(LEADING EDGE CLEARANCE)/(TRALING EDGE CLEARANCE)
C       M1=(MOLECULAR MEAN FREE PATH AT AMB. P)/(CLEARANCE AT
C           TRAILING EDGE)
C       P=(PRESSURE AT TRAILING EDGE)/(AMBIEN PRESSURE)
C       XL=6.*NU*U*L/(PA*HTR*HTR)
C       PA= AMBIENT PRESSURE (PSIA)
C       NU=FLUID VISCOSITY (LB*SEC/(IN*IN))
C       U= VELOCITY (IN/SEC)
C       L= BEARING LENGTH
C       HTR= CLEARANCE AT TRAILING EDGE (IN)
C     ************************************************************
      IMPLICIT REAL*8 (A-H,O-Z)
      REAL*8 M1
      REAL*8 X(2)
      REAL*4 ZREAL1,ZREAL2,UERTST
      EXTERNAL F
      COMMON H1,C1,XL,M1,P,ZETA,Q,C11,C22
      NAMELIST/DATA/H1,XL,M1,P,X,C1,C11,C22
      ID2=1
      STEPS=20.0D0
      NSTEPS=21
    1 READ(5,DATA,END=9999)
      C1=XL/(H1-1.D0)
      EPS2=0.001D0
      ETA=0.01D0
      NSIG=12
      N=1
      DMAX=(H1*H1+6.DC*H1*M1)/C1
      EP=C1/4.D0+9.DC*M1*M1/C1+H1*H1/C1+6.D0*M1*H1/C1-3.D0*
     1 M1-H1
   20 X(1)=(DMAX+EP)/2.D0
      X(2)=(DMAX+EP)/2.D0
      ITMAX=200
      WRITE(6,DATA)
```

AD-A043 917 COLUMBIA UNIV NEW YORK LUBRICATION RESEARCH LAB F/G 13/9
EXPERIMENTAL INVESTIGATION OF GAS BEARINGS WITH ULTRA-THIN FILM--ETC(U)
JUN 77 A SERENY, V CASTELLI N00014-75-C-0552
UNCLASSIFIED 26 NL

2 OF 2
AD
A043917

END
DATE
FILMED
9 -77
DDC

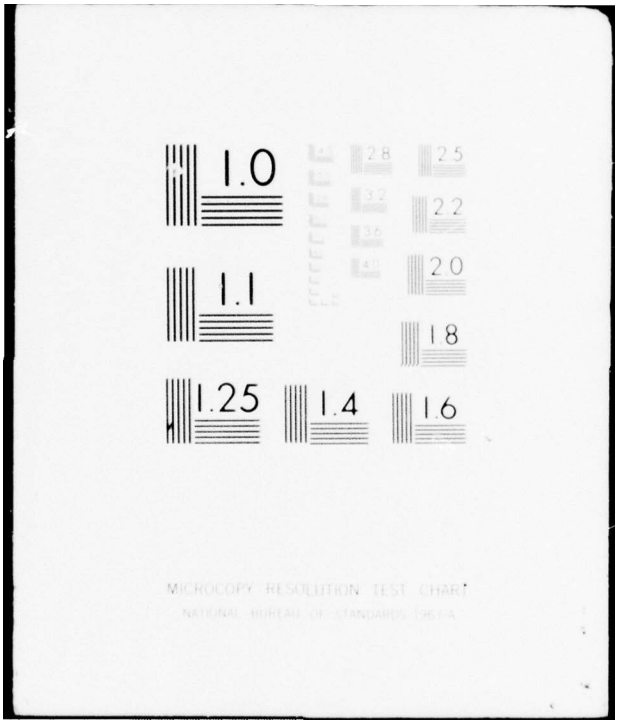
1.0
1.1
1.25
1.4
1.6
2.8
3.2
3.6
4
2.5
2.2
2.0
1.8
MICROCOPY RESOLUTION TEST CHART
NATIONAL BUREAU OF STANDARDS 1963-A

```
      CALL ZREAL1(F,EPS,EPS2,ETA,NSIG,N,X,ITMAX,IER,ID)
      IF(ID.EQ.1) GO TO 2
      XK1=H1-DMAX+X(1)
      WRITE(6,110) DMAX,XK1,P
      DEM=XK1-P
      IF(DABS(DEM).LE..1D-3) GO TO 10
      IF(I.EQ.2) GO TO 30
      IF(ID2.EQ.1) GO TO 10
      P2=P
      P=P*1.01D0
      XK2=XK1
      I=2
      GO TO 20
   30 PTEMP=P
      P=(P*(XK2-XK1)+XK1*(P-P2))/((P-P2)+(XK2-XK1))
      P2=PTEMP
      XK2=XK1
      GO TO 20
   10 WRITE(6,110) DMAX,XK1,P
  110 FORMAT(' ','DMAX=',D15.6,'K1=',D15.6, 20X,' P =',
     1 D15.6,/)
      D3=H1
      D=(H1-P)/STEPS
      EP=X(1)
      DO 90 I=1,NSTEPS
      H=(C1*((H1-D3)+EP)+6.D0*M1*(D3-H1)+(D3-H1)*(D3+H1))/
     1     (C22*FIH(D3))
      H=DSQRT(H)
      XX=(H-H1)/(1.0D0-H1)
      PRESS=D3/H
      WRITE(6,120) PRESS,H,XX,D3
  120 FORMAT(' ',7D17.7)
      D3=D3-D
   90 CONTINUE
    2 WRITE(6,DATA)
      GO TO 1
 9999 STOP
      END
      FUNCTION F(EPS,ID)
      IMPLICIT REAL*8 (A-H,O-Z)
      REAL*8 M1
      COMMON H1,C1,XL,M1,P,ZETA,Q,C11,C22
      ZETA=(4.D0*H1/C1+12.D0*M1/C1-(36.DC*M1*M1+4.D0*H1*H1+
     1    24.D0*M1*H1)/(C1*C1))+4.D0*EPS/C1
      A=ZETA-1.D0
      ID=0
      IF(A.LE.0.0D0) GO TO 10
      A=DABS(A)
      Q=       DSQRT(A)
      H=H1
```

```
      FI1=FIH(H)
      FI2=FIH(P)
      C11=C1*EPS/(H1*H1*FI1)
      C22=((H1-P)*(C1-P-H1-6.D0*M1)+C1*EPS)/FI2
      F=C11-C22
C      WRITE(6,100) F,EPS,ZETA,Q,C11,C22,FI1,FI2
      RETURN
   10 WRITE(6,100) EPS,ZETA,EPS
  100 FORMAT(' ',8D15.7)
      ID=1
      RETURN
      END
      FUNCTION FIH(THETA)
      IMPLICIT REAL*8 (A-H,O-Z)
      REAL*8 M1
      COMMON H1,C1,XL,M1,P,ZETA,Q,C11,C22
      A=2.D0*THETA/Q/C1
      B=-C1/Q/C1
      C=6.D0*M1/Q/C1
      A=DATAN((A+B)+C)
      FIH=DEXP(-(C1+6.D0*M1)*2.0D0/C1/Q*A)
      RETURN
      END
C     FUNCTION  - ZREAL1 FINDS REAL ZEROS OF A REAL FUNCTION
C        IER    - ERROR PARAMETER (OUTPUT)
C                 WARNING ERROR = 32 + N
C                 N = 1 INDICATES THAT CONVERGENCE WAS NOT
C                 OBTAINED FOR AT LEAST ONE INITIAL GUESS
C                 (WITHIN ITMAX ITERATIONS).
C                 X(I) IS SET TO 111111. FOR THE I'S WHERE
C                 CONVERGENCE IS NOT OBTAINED. NOTE THAT
C                 THE ROUTINE IS DESIGNED SO THAT A MULTIPLE
C                 ROOT WILL NOT APPEAR IN THE OUTPUT
C                 VECTOR X.
      SUBROUTINE ZREAL1(F,EPS,EPS2,ETA,NSIG,N,X,ITMAX,IER,ID)
      DIMENSION           X(1)
      REAL*8 P,P1,P2,X0,X1,X2,RT,FRT,FPRT,D,DD,DI,H,BI,DEN,
     *  DN,DM,TEM,X,F,EPS,EPS2,ETA,DIGT,TEN,ONE,ZERO,
     *  P9,P11,HALF,PP1,F4
      DATA TEN,ONE,ZERO,P9,P11,HALF,PP1,F4/10.D0,1.D0,
     *  0.D0,.9D0,1.1D0,.5D0,.1D0,4.D0/
C      DATA TEN,ONE,ZERO,P9,P11,HALF,PP1,F4/10.0,1.0,0.0,
      IER = 0
      DIGT = TEN**(-NSIG)
      P = -ONE
      P1 = ONE
      P2 = ZERO
      H = ZERO
      DO 95 L = 1,N
      JK = 0
```

```
      IF (X(L) .EQ. ZERO) GO TO 5
      P = P9*X(L)
      P1 = P11*X(L)
      P2 = X(L)
    5 RT = P
      GO TO 65
   10 IF (JK .NE. 1) GO TO 15
      RT = P1
      X0 = FPRT
      GO TO 65
   15 IF (JK .NE. 2) GO TO 20
      RT = P2
      X1 = FPRT
      GO TO 65
   20 IF (JK .NE. 3) GO TO 55
      X2 = FPRT
      D = -HALF
         IF (X(L) .EQ. ZERO) GO TO 25
      H =-PP1*X(L)
         GO TO 30
   25    H = -ONE
   30    DD = ONE+D
         BI = X0*D**2-X1*DD**2+X2*(DD+D)
         DEN = BI**2 -F4*X2*D*DD*(X0*D-(X1*DD)+X2)
         IF (DEN .LE. ZERO) GO TO 35
         DEN = DSQRT(DEN)
         GO TO 40
   35    DEN = ZERO
   40    DN = BI + DEN
         DM = BI - DEN
         IF (DABS(DN) .LE. DABS(DM)) GO TO 45
         DEN = DN
      GO TO 50
   45    DEN = DM
   50    IF (DEN .EQ. ZERO) DEN = ONE
         DI=-DD*(X2+X2)/DEN
         H = DI * H
         RT = RT + H
         IF (DABS(H) .LT. DABS(RT)*DIGT) GO TO 90
         GO TO 65
   55    IF (DABS(FPRT) .GE. DABS(X2*10.D0)) GO TO 60
      X0=X1
      X1=X2
      X2=FPRT
      D=DI
      GO TO 30
   60    DI = DI * HALF
         H = H * HALF
         RT = RT - H
   65    JK = JK + 1
```

```
      IF (JK .LT. ITMAX)  GO TO 75
      IER=33
      X(L)=111111.00
     GO TO 95
  75 FRT=F(RT,IC)
      FPRT = FRT
      IF (L .LT. 2) GO TO 81
      DO 80 I = 2,L
         TEM = RT - X(I-1)
         IF (DABS(TEM) .LT. EPS2) GO TO 85
         FPRT = FPRT/TEM
  80  CONTINUE
  81  CONTINUE
      IF((DABS(FRT).LT.EPS).AND.(DABS(FPRT).LT.EPS))
     1 GO TO 90
    GO TO 10
  85  RT = RT + ETA
      JK = JK - 1
    GO TO 65
  90  X(L) = RT
  95 CONTINUE
    ITMAX = JK
    IF(IER.EQ.0) GO TO 9005
9000 CONTINUE
    CALL UERTST (IER,6HZREAL1)
9005 RETURN
    END
    SUBROUTINE UERTST(IER,NAME)
    INTEGER*2  NAME(3)
    INTEGER  WARN,WARF,TERM,PRINTR
    DIMENSION ITYP(5,4),IBIT(4)
    EQUIVALENCE (IBIT(1),WARN),(IBIT(2),WARF),(IBIT(3),TERM)
    DATA ITYP      /'WARN','ING ','    ','    ','
   *       'WARN','ING(','WITH',' FIX',')   ',
   *       'TERM','INAL','    ','    ','    ',
   *       'NON-','DEFI','NED ','    ','    '/,
   *          IBIT      / 32,64,128,0/
    DATA     PRINTR    / 6/
    IER2=IER
    IF (IER2 .GE. WARN) GO TO 5
    IER1=4
    GO TO 20
  5 IF (IER2 .LT. TERM) GO TO 10
    IER1=3
    GO TO 20
 10 IF (IER2 .LT. WARF) GO TO 15
    IER1=2
    GO TO 20
 15 IER1=1
 20 IER2=IER2-IBIT(IER1)
```

```
      WRITE (PRINTR,25) (ITYP(I,IER1),I=1,5),NAME,IER2,IER
   25 FORMAT(' *** I M S L(UERTST) ***  ',5A4,4X,3A2,4X,I2,
     *    ' (IER = ',I3,')')
      RETURN
      END
```

APPENDIX D

Perturbation Solution for the 1-D Reynolds Equation with Slip Boundary Condition

1D. Introduction

The modified Reynolds equation describing the behavior of gas bearings in the "slip flow regime" was first introduced by Burgdorfer [10]. For bearings where the clearance is on the order of a few mean free paths this modified equation predicts a reduction in load carrying capacity. Slip can occur because of either extremely thin bearing films or low ambient pressure conditions. The use of singular perturbation techniques for bearings operating with large bearing numbers and including the molecular mean free path effects is here developed. Numerous previous studies, by Gross and Zachmanoglou [24], DiPrima [25], and Schmitt and DiPrima [26] are concerned with behavior of Reynolds equation with large bearing numbers. Elrod and McCabe [27] solved for the asymptotic behavior by linearization outside the boundary layer and by using the exact Harrison solution for a linear film thickness inside the boundary layer. None of these studies attempt to investigate the asymptotic behavior

of bearings with large bearing numbers while including the molecular mean free path terms.

The matched asymptotic expansion technique laid out by DiPrima [25] is followed in this analysis. The solution obtained in Sec. 2D, with the Knudsen number k set to zero, is similar to DiPrima's development; the outer expansion and the combined inner and outer solution are correct in the outer region to terms of $0(1/\Lambda^2)$ and in the boundary layer to terms of $0(1/\Lambda)$.

The solutions obtained in Sec. 2D, are applied first to a tapered slider and then to a parabolic one. The solutions for the tapered slider are compared with the exact analytical solution obtained by Burgdorfer [10]. The solution for the parabolic slider is compared with a numerical solution. In the latter case, it was worthwhile to use the asymptotic solution as the starting solution for the iterative numerical scheme.

2D. The Asymptotic Expansion

The use of the modified Reynolds equation to account for slip at the boundary for a slider bearing, as described in Fig. 1D, was first introduced by Burgdorfer. In one dimension, Burgdorfer obtained the following nondimensional nonlinear ordinary differential equation

$$\frac{d}{dX}\left[H^3P\left(1 + \frac{6k}{PH}\right)\frac{dP}{dX}\right] = \Lambda\frac{dPH}{dX} \qquad (1D)$$

where the pressure made nondimensional with respect to the ambient pressure p_a, H is the continuously differentiable height nondimensionalized with respect to the minimum clearance h_m and X is the spatial variable in the direction of motion of the running surface nondimensionalized with respect to bearing length ℓ. In equation (1D) $\Lambda = 6\mu U\ell/(p_a h_1^2)$ is the bearing number and $k = \lambda_a/h_1$ is the Knudsen number.

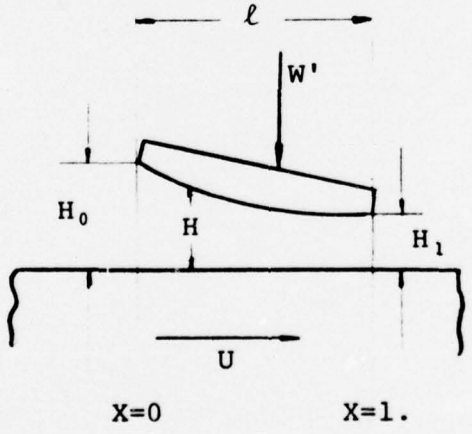

Fig. 1D

The following boundary conditions for Eq. (1D) satisfy the physical requirement of continuity of pressure

$$P(X=0) = 1.0$$

$$P(X=1) = 1.0 \qquad (2D)$$

For large speeds and small minimum clearances, i.e. for large compressibility numbers, Λ, P is assumed to have an expansion of the form

$$P^0(X;k,\Lambda) = P_0^0 + \frac{1}{\Lambda}P_1^0 + \frac{1}{\Lambda^2}P_2^0 + \ldots \qquad (3D)$$

where the superscript ^{0} is used to indicate the pressure solution out of the boundary layer with thickness of order $1/\Lambda$. Substitute (3D) into (1D) and get

$$\frac{d}{dX}[H^3(P_0^0+\frac{1}{\Lambda}P_1^0+\ldots)\frac{d}{dX}(P_0^0+\frac{1}{\Lambda}P_1^0+\ldots)+H^2 6k\frac{d}{dX}(P_0^0+\frac{1}{\Lambda}P_1^0+\ldots)]$$

$$= \Lambda\frac{d}{dX}(HP_0^0+H\frac{1}{\Lambda}P_1^0+H\frac{1}{\Lambda^2}P_2^0+\ldots) \qquad (4D)$$

Eq. (4D) describes the pressure behavior in the region outside the boundary layer at X = 1.0 for large bearing numbers. Hence, the appropriate bounday condition for P^0 is

$$P^0(X=0.0) = 1.0 \qquad (5D)$$

Now, Eq. (4D) is separated into equations having terms of

equal order with respect to $1/\Lambda$ and it becomes a set of equations of the form,

$$0 = \frac{dHP_0^0}{dX} \tag{6Da}$$

$$\frac{d}{dX}\left(H^3 P_0^0 \frac{dP_0^0}{dX} + H^2 6k \frac{dP_0^0}{dX}\right) = \frac{dHP_1^0}{dX} \tag{6Db}$$

$$\frac{d}{dX}\left(H^3 P_0^0 \frac{dP_1^0}{dX} + H^3 P_1^0 \frac{dP_0^0}{dX} + H^2 6k \frac{dP_1^0}{dX}\right) = \frac{d(HP_2^0)}{dX} \tag{6Dc}$$

Here the boundary conditions (5D) are satisfied by the zeroth order term of the pressure, i.e. $P_0^0(X = 0) = 1.0$, and for the higher order terms we apply $P_n^0(X = 0) = 0.0$ with n being larger than or equal to 1. With those boundary conditions in mind, solving equations (6Da), (6Db), and (6Dc), we get

$$P_0^0 = \frac{H_0}{H} \tag{7Da}$$

$$P_1^0 = \frac{H_0^2}{H}(H_0' - H') + \frac{6kH_0}{H}(H_0' - H') \tag{7Db}$$

$$P_2^0 = \frac{H_0}{H}(H_0 + 6k)\left[(H_0 + 6k)(H'^2 + H_0''H_0 - H''H - H'H_0') - H_0H'(H_0' - H')\right] \tag{7Dc}$$

where $H_0 = \frac{h_0}{h_1}$ is the nondimensional bearing clearance at the leading edge.

These equations, representing the solution for the pressure away from the boundary layer show the effect of the slip boundary condition to be on the order of $1/\Lambda$.

For the solution of Eq. (1D), valid in the trailing edge boundary layer, the stretched coordinate $\xi = \Lambda(1-X)$ is introduced. This change of variable follows the argument by DiPrima [25]. Eq. (1D) with the stretched coordinate ξ takes the form

$$\frac{d}{d\xi}[(H^3P^i + H^2 6k)\frac{dP^i}{d\xi}] = -\frac{d(P^iH)}{d\xi} \tag{8D}$$

where the superscript i indicates the pressure inside the boundary layer.

Taylor series of $H(1-\frac{\xi}{\Lambda})$ about $\xi = 0$ $(X = 1)$ gives

$$H(1-\frac{\xi}{\Lambda}) = H_1 - \frac{\xi}{\Lambda}H_1' + \frac{1}{2!}(\xi/\Lambda)^2 H_1'' + \ldots \tag{9D}$$

and the pressure expansion gives

$$P^i = P_0^i + \frac{1}{\Lambda}P_1^i + \frac{1}{\Lambda^2}P_2^i + \ldots \tag{10D}$$

Substituting expansions for H and P^i into eq. (8D) results in

$$\frac{d}{d\xi}[H_1^3P_1^i\frac{dP_0^i}{d\xi} + H_1^2 6k\frac{dP_0^i}{d\xi}] = -\frac{dP_0^iH_1}{d\xi} \tag{11Da}$$

$$\frac{d}{d\xi}[H_1^3P_1^i\frac{dP_0^i}{d\xi} + H_1^3P_0^i\frac{dP_1^i}{d\xi} - 3H_1^2\xi H_1'P_0^i\frac{dP_0^i}{d\xi} +$$

$$6k\left(H_1^2\frac{dP_1^i}{d\xi} - 2\xi H_1 H_1' 6k\frac{dP_0^i}{d\xi}\right)] = \frac{d}{d\xi}[P_0^i \xi H_1' - P_1^i H_1] \qquad (11Db)$$

where Eqs. (11Da) and (11Db) are the zeroth and the first order terms with respect to $1/\Lambda$. According to Eq. (2D) one of the two needed boundary conditions for Eqs. (11Da) and (11Db) take the following form

$$\begin{aligned} P_0^i(\xi=0) &= 1.0 \\ P_n^i(\xi=0) &= 0.0 \qquad n = 1,2,\ldots \end{aligned} \qquad (12D)$$

The secondary boundary condition needed for those second order differential equations is obtained by matching this boundary layer solution with the outer solution.

The solution of the second order differential equation (11Da) for the zeroth order inner expansion satisfying the boundary condition (12D), gives

$$P_0^i - 1 + (c + 6k)\,\mathrm{Log}\frac{c - P_0^i}{c - 1} = -\xi \qquad (13D)$$

where c is the second condition to be obtained by ordinary matching between the outer solution, P_0^0 and the inner solution, P_0^i. Following the matching principle outlined in Chaprters IV and V in [28] the limit of P_0^i as $x \to 1$

is set equal to the limit of P_0^i as $\xi \to \infty$. Hence, the missing condition is supplied by matching the two expansions. This matching gives

$$c = H_0 \tag{14D}$$

To obtain a composite expansion, the method of additive composition is used. The sum of the inner and outer expansions is corrected by subtracting the part that the two expansions have in common. The composite representation of the two terms of the outer expansion is given by

$$P = \frac{H_0}{H} + [P_0^i(\xi) - H_0] + \frac{H_0}{\Lambda H}(H_0 + 6k)(H_0' - H') \tag{15D}$$

where the expression for $P_0^i(\xi)$ is given by Eqs. (13D) and (14D)*. This composite expansion has at least the accuracy of each of its constituents.

Thus, expression (15D) is in error by no more than $0(1/\Lambda^2)$ away from the boundary layer and $0(1/\Lambda)$ near the boundary layer. Although the pressure P_0^i appears implicitly in (13Db), the pressure evaluation using (15D) is

---

* see [25] and [28] for a more complete discussion on expansions and matching.

straightforward. After observing that P_0^i approaches exponential behavior with increasing ξ, this behavior can be applied to obtain X explicitly for any P_0^i. Hence Eq. (15D) can be solved explicitly by choosing a P_0^i between 1 and H_0, obtaining X from (13D) using these values in (15D). Using Eq. (15D) we obtain the following form for the nondimensional load

$$W'(a,\varepsilon,k,\Lambda) = \int_0^1 (P-1)dX =$$

$$\int_0^1 \left(\frac{H_0}{H} - 1\right)dX - \int_0^1 [H_0 - P_0^i(\xi)]dX + \frac{H_0(H_0+6k)}{\Lambda}\int_0^1 \frac{H'-H'_0}{H}dX \qquad (16D)$$

It is useful to subdivide the load W' in a way similar to that of DiPrima [25]; this subdivision allows direct comparison between the expansion for k equal to zero [25] and k different from zero. Hence,

$$W' = W'_\infty - \frac{1}{\Lambda}W'_B + \frac{1}{\Lambda}W'_E \qquad (17D)$$

where W'_∞, the first term in Eq. (16D), is the limiting nondimensional load as $\Lambda \to \infty$. W'_E, the last term in Eq. (16D), is the value of the load correction outside of the boundary layer due to terms on the order of $1/\Lambda$ and W'_B, the second integral in (16D), is the correction to W'_∞ due to the boundary layer.

Using the fact that this solution is valid for a large bearing number, it can be shown for a parabolic slider that*

$$W'_B = \Lambda \int_0^1 [H_0 - P_0^i(\xi)]dX = \varepsilon + \frac{\varepsilon^2}{2} + 6k\varepsilon + 0(e^{-\frac{\Lambda}{H_0}}) \qquad (18D)$$

where the nondimensional bearing clearance H has the form

$$H = 1 + \varepsilon[aX^2 - (1 + a)X + 1] \qquad (19D)$$

Eqs. (13D), (15D) and (16D) are easily computed by programmable hand calculator or by a simple computer program. Two simple examples are given here in Sec. 3D.

---

* Follow Appendix B of [25] with some modification

3D. Examples

a. Tapered slider

For this bearing, the analytical solution given by Burgdorfer [10] was used to check the expansion solution. For this case, since $H_1' = H_0' = H'$, the solution of (15D) and (16D) is significantly simplified. The comparison for the pressure profile given in Figs. 2D and 3D for different bearing numbers shows a good correlation with the analytical solution. In Fig. 4D, also a solution for tapered sliders, it is shown that the reduction in pressure due to slip vanishes with increasing bearing numbers.

b. Parabolic slider

A slider with parabolic film thickness H of the form given in Eq. (19D) was investigated. Sample calculations for various values of a, k, and the bearing number Λ with $\varepsilon = 2$ are given in Table 1D. A more detailed description of the calculations are given by DiPrima [26] for the case of $k = 0.0$. The additional terms due to mean free path effects present in Eqs. (15D) and (16D) did not make the calculations any more difficult. The load carrying

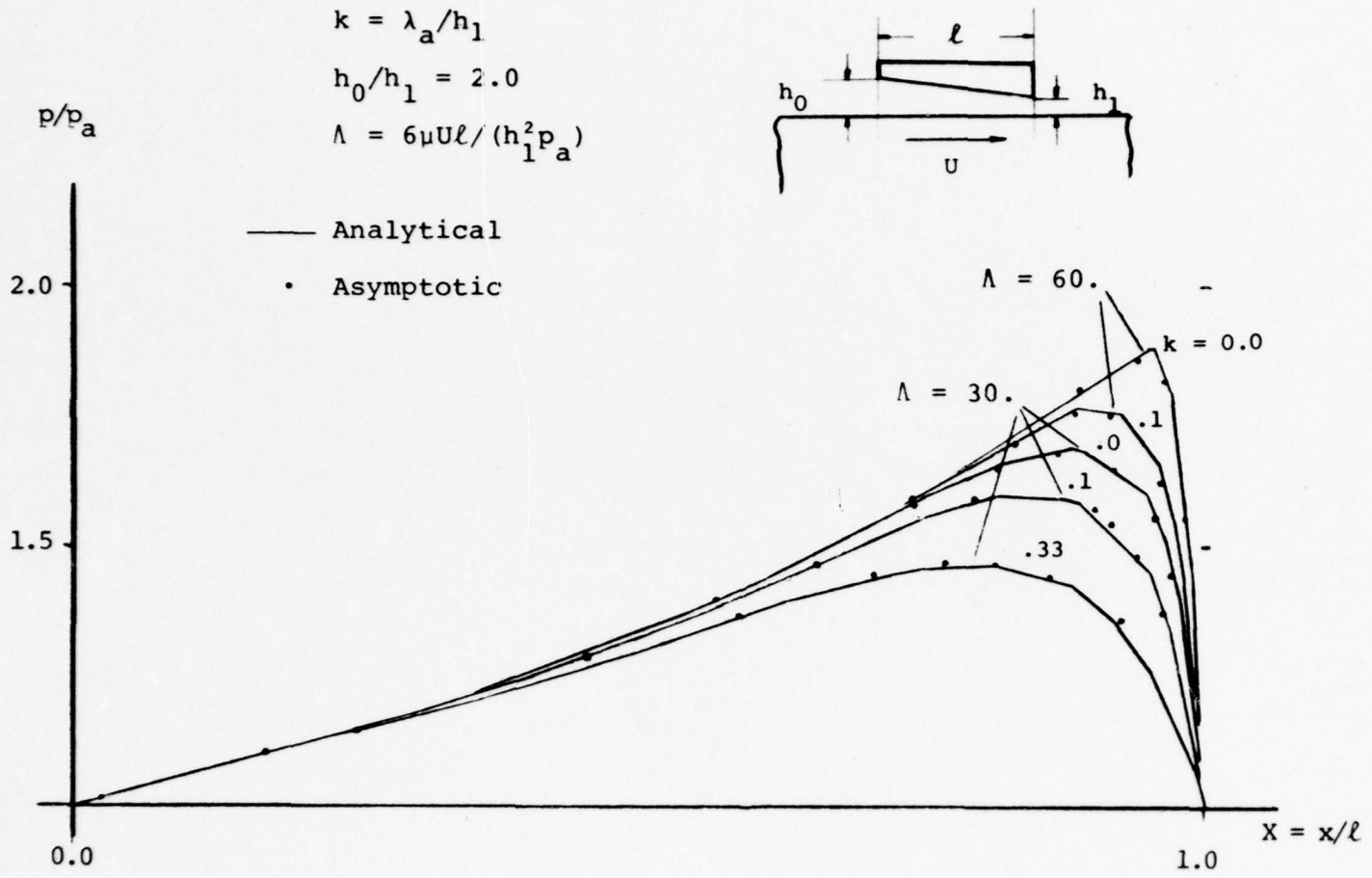

Figure 2D Pressure Distribution, Analytical vs Asymptotic

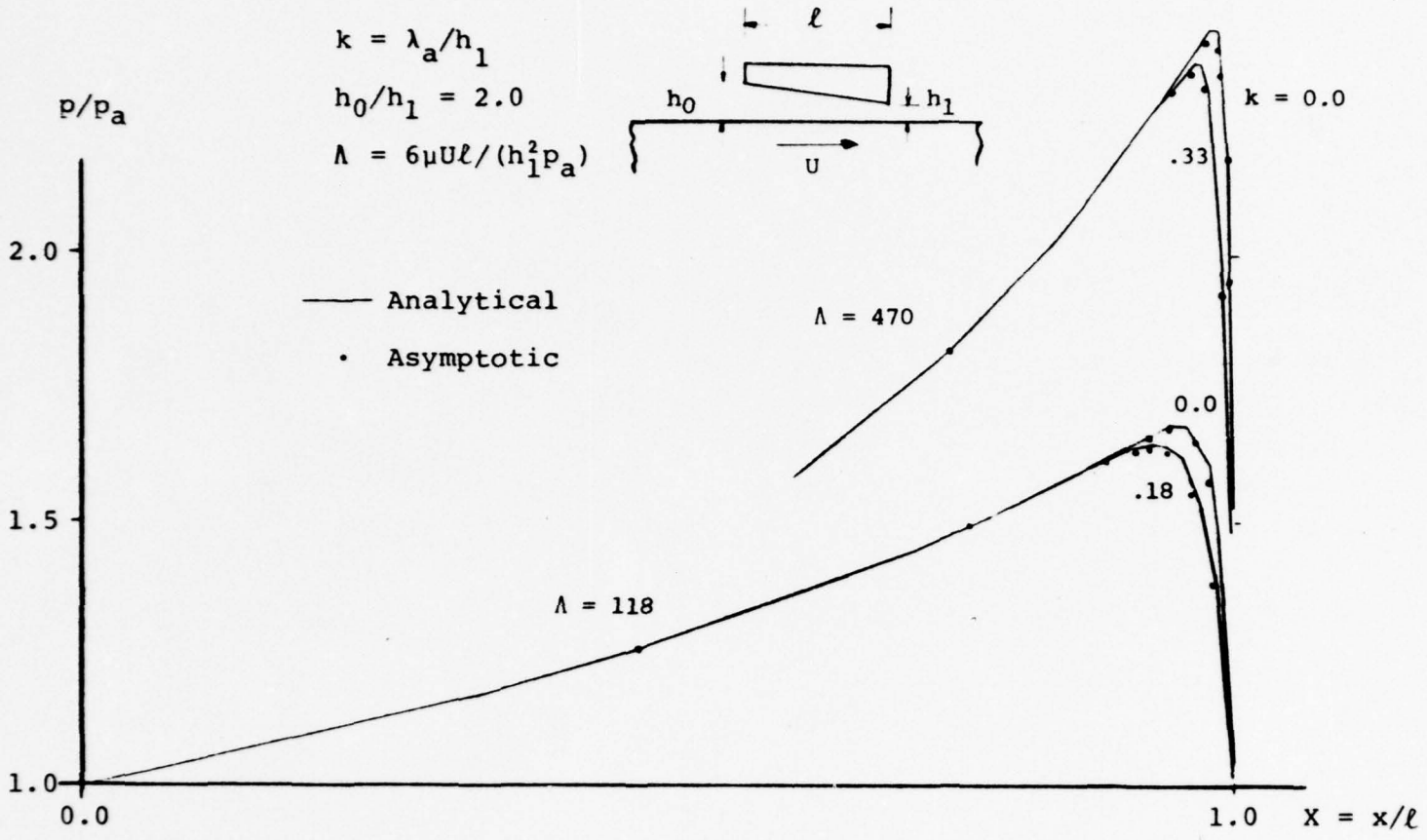

Figure 3D Pressure Distribution, Analytical vs Asymptotic

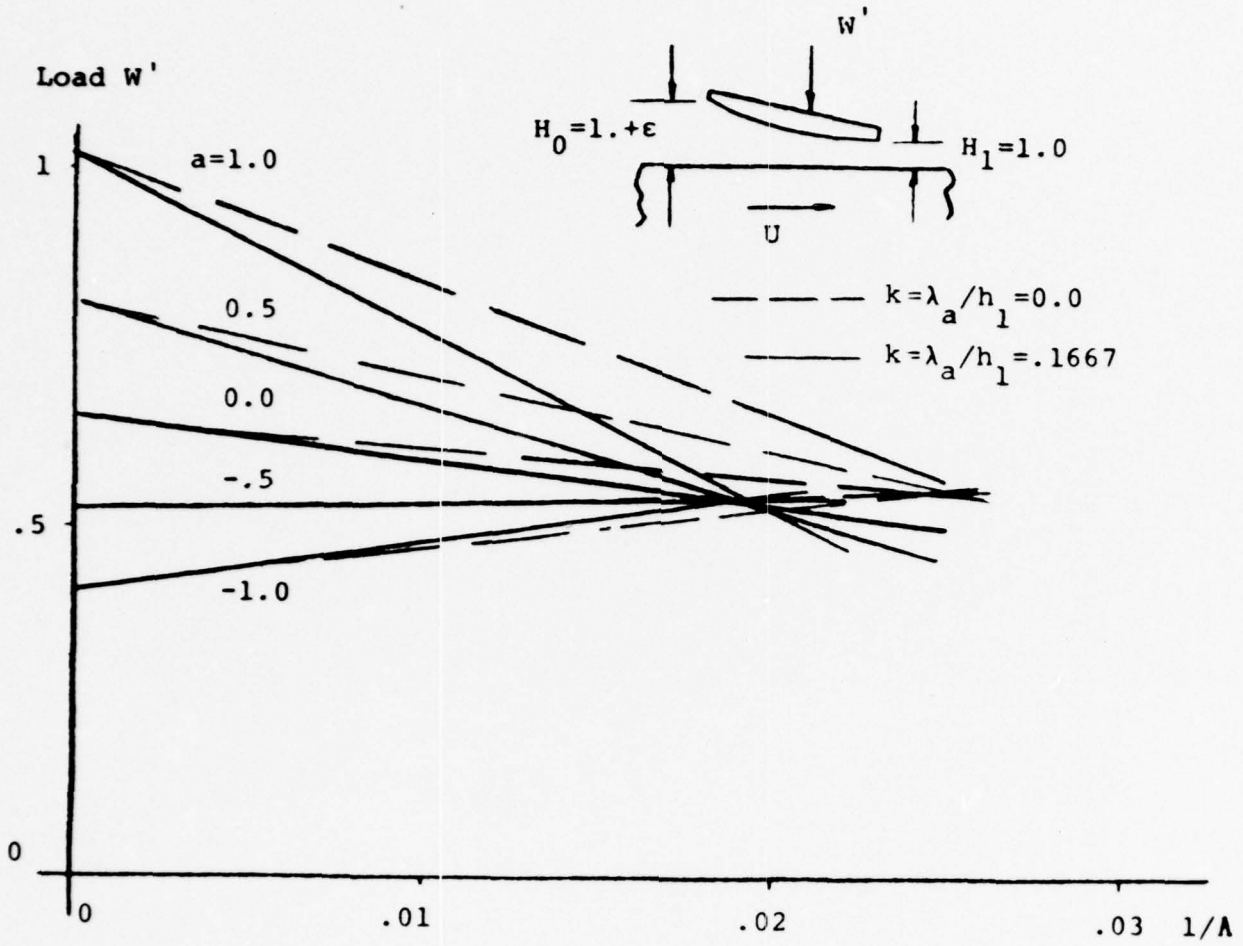

Figure 4D Load vs. Bearing Number for ε=2.0 and Various Values of a

	W'	Λ = 50	100	200	1000000
k=.0 ε=2.	a = 1.0	.6580	.8422	.9344	1.0265
	0.5	.6051	.7095	.7617	.8139
	0.0	.5681	.6081	.6281	.6481
	-.5	.5414	.5279	.5212	.5145
	-1.	.5220	.4631	.4336	.4042
k=1/6 ε=2.	a = 1.0	.5217	.7741	.9003	1.0265
	0.5	.5222	.6681	.7410	.8139
	0.0	.5281	.5881	.6181	.6481
	-.5	.5370	.5258	.5201	.5145
	-1.	.5479	.4760	.4401	.4042

Table 1D Sample Calculations of W' for Various Values of a and Λ (k=0.,1/6)

capacity does not vary while changing the parameter "a" of the parabolic bearing profile. This behavior can be applied in an optimal design for constant loading of a flat slider bearing where manufacturing tolerances cause some crown to exist.

4D. Conclusion

A simple asymptotic solution for a complicated nonlinear differential equation has many uses. The most involved numerical solution of a nonlinear differential equation can be easily checked when there exists some knowledge of its asymptotic behavior. Here, such an asymptotic solution was presented. For an infinite slider bearing, this solution predicts the limiting load carrying capacity with molecular mean free path effects included.

The systematic application of the asymptotic expansion arrives at expressions such as Eqs. (13D), (15D), and (16D), which are easily solved with a hand-held programmable calculator.

The only restriction to this asymptotic solution, exact within $0(1/\Lambda)$, is the existence of the first derivative of the bearing clearance. Following Schmitt and DiPrima's work [26] and the development that was

given in this paper, the asymptotic method with mean free path effects could be expanded to be applicable to bearings with a discontinuity in the film profile.

It should also be noted that no check of this asymptotic solution was made for values of k greater than 1/3. Although, purely from the mathematical point of view, k could have any value, the actual physics of the flow dictate that the modified Reynolds equation (1D) is only valid for small values of k.

VII. NOMENCLATURE

a = crown parameter for parabolic profile slider

c = matching constant

C_1, C_2 = integration constants

h = bearing clearance

h_0 = bearing clearance at leading edge

h_1, h_{min} = bearing clearance at trailing edge

h_r = ramp height; (Fig. 9)

h_c = crown height of bearing skate; (Fig. 9)

H, H_0, H_1 = nondimensional bearing clearance; ($H=h/h_1$, $H_0=h_0/h_1$, $H_1=h_1/h_1$)

k = ambient Knudsen number; ($k=\lambda_a/h_1$)

K = $4\Lambda^* K_1 - (\Lambda^*-6k)^2$

K_1, K_2 = integration constants

ℓ = total length of slider

ℓ_t = tapered length

ℓ_p = distance from trailing edge to pivot point; (Fig. 9)

P = nondimensional pressure with respect to the ambient pressure; ($P=p/p_a$)

p_a = ambient pressure

Q = $(PH)^2$

R = radial position of slider center

s_1, s_2 = width of skates; (Fig. 9)

U = linear velocity of disk under slider

U_x, U_y = linear velocity in the x and y directions

w = width of slider; (Fig. 9)

W' = nondimensional load, $W' = \text{load}/(p_a \ell w)$

$\hat{x}, \hat{y}$ = unit vectors in the x and y directions

X = nondimensional spatial coordinate in the direction of motion

Y = nondimensional spatial coordinate in the direction perpendicular to motion

Δx_i = grid spacing in the x direction between points i and i-1

Δy_j = grid spacing in the y direction between points j and j-1

ε = parameter for parabolic slider

θ = PH

λ = wave length of monochromatic light source

λ_a = molecular mean free path at ambient pressure

Λ = bearing number = $6\mu U\ell/(p_a h_1^2)$

Λ^* = $\Lambda/(H_0-1)$

Λ_x = bearing number = $6\mu U_x \ell/(p_a h_1^2)$

Λ_y = bearing number = $6\mu U_y \ell/(p_a h_1^2)$

μ = viscosity of lubricant

ξ = streched boundary layer coordinate

σ = surface accommodation coefficient

ψ_1, ψ_2, ψ_3 = transcendential function of θ

Differential Operator

$\nabla = \hat{x}\frac{\partial}{\partial x} + \hat{y}\frac{\partial}{\partial y}$

Superscripts

^{0} = refers to the outer solution

^{i} = refers to the inner solution

$'$ = d/dX

Subscripts

a = ambient conditions

$_{0,1,2}$ = order of perturbation

$_{i,j}$ = x-y index of grid points

I = refers to values for the tapered region of the tapered-flat slider bearing

J = refers to values for the flat region of the tapered-flat slider bearing

VIII. References

1. D.D. Fuller, Theory and Practice of Lubrication for Engineers, J. Wiley, 1956.

2. R.B. Mulvany, "Engineering Design of a Disk Storage Facility with Data Modules", I.B.M. J. Res. Develop., Nov. 1974.

3. C. Lin, "Techniques for the Measurement of Air-Bearing Separation - A Review", I.E.E.E. Trans. on Magnetics, Dec. 1973.

4. R.K. Brunner, J.M. Harker, K.E. Haughton, A.G. Osterlund, "A Gas Film Lubrication Study Part III Experimental Investigation of Pivoted Slider Bearings", I.B.M. J. Res. Develop., July 1959.

5. C. Lin, R.F. Sullivan, "An Application of White Light Interferometry in Thin Film Measurements", I.B.M. J. Res. Develop., May 1972.

6. G.R. Briggs, P.G. Herkart, "Unshielded Capacitor Probe Technique for Determining Disk Memory Ceramic Slider Flying Characteristics", I.E.E.E. Trans. on Magnetics, Sept. 1971.

7. G.D. Galvin, D.W. Morecroft, A.G. Patterson, "Developments in Supercleaning and Boundary Lubrication for Gas-Bearing Gyros Related to Surface Phenomena", A.S.M.E. Trans., J. Lub. Tech., Oct. 1968.

8. C.B. Pear, Jr., Editor, Magnetic Recording in Science and Industry, Reinhold Publishing Corporation, New York, 1967.

9. V. Castelli, J. Pirvics, "Review of Numerical Methods in Gas Bearing Film Analysis", A.S.M.E. Trans. J. Lub. Tech., Oct. 1968.

10. A. Burgdorfer, "The Influence of the Molecular Mean Free Path on the Performance of Hydrodynamic Gas Lubricated Bearings", A.S.M.E. Trans., J. Lub. Tech., March 1959.

11. A.S. Hoagland, Digital Magnetic Recording, John Wiley and Sons, New York 1963.

12. T. Tang, "Dynamics of Air-Lubricated Slider Bearings for Noncontact Magnetic Recording", A.S.M.E. Trans., J. Lub. Tech., April 1971.

13. R.C. Tseng, "Rarefaction Effects of Gas-Lubricated Bearings in a Magnetic Recording Disk File", A.S.M.E. Trans., J. Lub. Tech., Oct. 1975.

14. H.G. Elrod, "Lubrication Theory for Newtonian Fluids with Striated Roughness or Grooving", Lub. Research Lab., Columbia University, Aug. 1972.

15. S.K. Rhow, H.G. Elrod, "Effects of Surface Roughness or Grooving on Thin, Laminar Lubricating Films", Columbia University Lub. Res. Lab., Report No. 23, Nov. 1973.

16. L.D. Lipschutz, "Dynamic Measurements of Small Separations by a Light Interference Method", Inst. of E.E., Proc. of the International Conference on Magnetic Recording, July 1964.

17. J. Harper, P. Levenglick, J. Wilczynski, "An Interferometric Method of Determining the Separation Between Two Moving Surfaces", I.B.M. Res. Report, RC-1189, May 1964.

18. W.A. Gross, Gas Film Lubrication, Wiley, New York, 1962.

19. F.C. Hsing, S.B. Malanoski, "Mean Free Path Effect in Spiral Grooved Thrust Bearings", A.S.M.E. Paper No. 68-LubS-17, July 1968.

20. S.T. Tzeng, E. Saibel, "Surface Roughness Effects on Slider Bearing Lubrication", A.S.L.E. Trans., Oct. 1967.

21. H. Christensen, K. Tonder, "The Hydrodynamic Lubrication of Rough Surfaces", A.S.M.E. Trans., J. of Lub. Tech., 1971.

22. H. Christensen, "Stochastic Models for Hydrodynamic Lubrication of Rough Surfaces", Proc. Instn. Mech. Engrs., Vol. 184, Pt. 1, No. 55, 1969-70.

23. S.A. Schaaf, "Recent Progress in Rarefied Gas-dynamics", ARS J., Vol. 30, No. 5, p. 443, 1960.

24. W.A. Gross, E.C. Zachmanoglou, "Perturbation Solutions for Gas-Lubricated Films", A.S.M.E. Trans., J. of Basic Engr., pp. 139-144, 1961.

25. R.C. DiPrima, "Higher Order Approximations in the Asymptotic Solution of the Reynolds Equation for Slider Bearings at High Bearing Numbers", A.S.M.E. Trans., J. of Lub. Tech., Jan. 1969.

26. J.A. Schmitt, and R.C. DiPrima, "Asymptotic Methods for and Infinite Slider Bearing with a Discontinuity in Film Slope", A.S.M.E. Trans., J. of Lub. Tech., July 1976.

27. H.G. Elrod, Jr., J.T. McCabe, "Theory of Finite-Width High-Speed Self-Acting Gas-Lubricated Slider Bearings", A.S.M.E. Paper No. 68-LubS-15, 1968.

28. M. Van Dyke, Perturbation Methods in Fluid Mechanics, Academic Press, New York, 1964.

29. E.H. Kennard, Kinetic Theory of Gases, McGraw-Hill, New York, 1938.

30. H.G. Elrod, C. Cheng, Private communication, Columbia University, New York, 1976.

DISTRIBUTION LIST FOR UNCLASSIFIED
TECHNICAL REPORTS ISSUED UNDER

CONTRACT N00014-67-A-0108-0037 TASK NR 062-491

All addresses receive one copy unless otherwise specified

Defense Documentation Center
Cameron Station
Alexandria, VA 22314

Mr. Stanley L. Zedekar
Dept. 244-2, Bldg. 71
Autonetics
P. O. Box 4181
Anaheim, CA 92803

Library
Naval Academy
Annapolis, MD 21402

Air Force Office of Scientific
Research (SREM)
1400 Wilson Boulevard
Arlington, VA 22209

Air Force Office of Scientific
Research (SRHM)
1400 Wilson Boulevard
Arlington, VA 22209

Dr. Coda Pan
Shaker Research Corporation
Northway 10 Executive Park
Ballston Lake, N.Y. 12019

Director
Office of Naval Research Branch
Office
495 Summer Street
Boston, MA 02210

Commander
Puget Sound Naval Shipyard
Bremerton, WA 98314

Mr. Alvin S. Lieberman
Code SPY 934
Naval Strategic Systems
Navigation Facility
Flushing and Washington Aves.
Brooklyn, N.Y. 11251

Library
C.S. Draper Laboratory
68 Albany Street
Cambridge, MA 02139

Mr. M. L. Levene
Leader, Advanced Mechanics
Advanced Technology Laboratories,
Building 10-8
RCA Defense Electronic Products
Camden, N.J. 08102

Dr. Edgar J. Gunter, Jr.
University of Virginia
School of Engineering and Applied
Science
Charlottesville, VA 22903

Director
Office of Naval Research Branch
Office
536 South Clark Street
Chicago, IL 60605

Professor L. N. Tao
Illinois Institute of Technology
Chicago, IL 60616

Code 753
Naval Weapons Center
China Lake, CA 93555

Mr. W. J. Anderson
NASA Lewis Research Center
Cleveland, OH 44871

Acquisitions Branch (S-AD/DL)
NASA Scientific and Technical
Information Facility
P. O. Box 33
College Park, MD 20740

Mr. J. W. Kannel
Battelle Memorial Institute
505 King Avenue
Columbus, OH 43201

Mr. H. M. Anderson
Xerox Data Systems
701 South Aviation Boulevard
El Segundo, CA 90245

Professor Ralph Burton
Department of Mechanical Engrg.
and Astronautical Sciences
Northwestern University
Evanston, IL 60210

C. C. Moore, Manager
Reliability and Safety Engrg.
Gas Turbine Division
General Electric Company
Schenectady, NY 12345

Mr. L. R. Manoni
Manager, Advanced Programs
United Aircraft Corporation
Systems Center
1690 New Britain Avenue
Farmington, CT 06023

Research & Technology Division
Army Engineering Reactors Group
Fort Belvoir, VA 22060

Technical Documents Center
Building 315
Army Mobility Equipment Research
Center
Fort Belvoir, VA 22060

Mr. Richard P. Shevchenko
Pratt and Whitney Aircraft Corp.
East Hartford, CT 06108

Mr. P. H. Broussard, Jr.
Guidance and Control Division
National Aeronautics & Space
Administration
George C. Marshall Space Flight Ct.
Huntsville, AL 35812

Professor Willian K. Stair
Assistant Dean, Mechanical and
Aerospace Engineering
University of Tennessee
Knoxville, TN 37916

Professor J. Modrey
School of Mechanical Engineering
Purdue University
Lafayette, IN 47907

Mr. Otto Decker
Mechanical Technology, Incorporated
968 Albany-Shaker Road
Latham, NY 12110

Commander
Long Beach Naval Shipyard
Long Beach, CA 90801

Mr. K. Liebler, Supervisor
Head & Media Development
Control Data Corporation
Normandale Division
7801 Computer Avenue
Minneapolis, MN 55424

Professor Paul F. Pucci
Mechanical Engineering Department
Naval Postgraduate School
Monterey, CA 93940

Library
Naval Postgraduate School
Monterey, CA 93940

Office of Naval Research
New York Area Office
715 Broadway - 5th Floor
New York, NY 10003

Engineering Societies Library
345 East 47th Street
New York, NY 10017

Professor D. D. Fuller
Department of Mechanical Engineering
Columbia University
New York, NY 10027

Professor V. Castelli
Department of Mechanical Engineering
Columbia University
New York, New York 10027

Professor H. G. Elrod
Department of Mechanical Engineering
Columbia University
New York, NY 10027

Ralph F. DeAngelias
Norden Division of United Aircraft Corp.
Helen Street
Norwalk, CT 06852

Mr. E. L. Swainson
Precision Products Department
Nortronics
100 Morse Street
Norwood, MA 02062

Mr. R. G. Jordan
Oak Ridge Gaseous Diffusion Pl.
Union Carbide Corp. - Nuclear Div.
P. O. Box P
Oak Ridge, TN 37830

Mr. R. E. MacPherson
Oak Ridge National Laboratory
P. O. Box Y
Oak Ridge, TN 37831

Miss O. M. Leach, Librarian
Aeronautical Library
National Research Council
Montreal Road
Ottawa 7, Canada

Director
Office of Naval Research Branch
Office
1030 East Green Street
Pasadena, CA 91106

Technical Library
Philadelphia Naval Shipyard
Philadelphia, PA 19112

Mr. Wilbur Shapiro, Manager
Friction and Lubrication Lab.
The Franklin Institute Research Labs.
The Benjamin Franklin Parkway
Philadelphia, PA 19103

Dr. F. Osterle
Department of Mechanical Engrg.
Carnegie Institute of Technology
Pittsburgh, PA 15213

Technical Library
Naval Missile Center
Point Mugu, CA 93041

Commander
Norfolk Naval Shipyard
Portsmouth, VA 23709

Chief, Document Section
Redstone Scientific Information Center
Army Missile Command
Redstone Arsenal, AL 35809

Mr. M. Wildmann
Ampex Corporation
401 Broadway
Redwood City, CA 94063

U. S. Army Research Office
P. O. Box 12211
Research Triangle Park, NC 27709

Editor, Applied Mechanics Reviews
Southwest Research Institute
8500 Culebra Road
San Antonio, TX 78206

Office of Naval Research
San Francisco Area Office
760 Market Street - Room 447
San Francisco, CA 94102

Technical Library
Hunters Point Naval Shipyard
San Francisco, CA 94135

Fenton Kennedy Document Library
The Johns Hopkins University
Applied Physics Laboratory
8621 Georgia Avenue
Silver Spring, MD 20910

Mr. Graham Patterson
Admiralty Compass Observatory
Ditton Park
Slough, Bucks, England

Mr. Steve Rohrbough
Mail Station
Honeywell
13350 U.S. Highway 19
St. Petersburg, FL 33733

Mr. Roland Baldwin
Section Head - Inertial Components
Honeywell Inc., Aerospace Division
13350 U.S. Highway 19
St. Petersburg, FL 33733

Professor J. V. Foa
School of Engineering and
Applied Science
George Washington University
Washington, DC 20006

Walt Tucker
Nuclear Engineering Department
Brookhaven National Laboratory
Upton, Long Island, NY 11973

Technical Library
Mare Island Naval Shipyard
Vallejo, CA 94592

Mr. E. Roland Maki
Mechanical Development Dept.
General Motors Corporation
12 Mile and Mound Roads
Warren, MI 48090

Office of Naval Research
Code 438
800 N. Quincy Street
Arlington, VA 22217 3 copies

Office of Naval Research
Code 473
800 N. Quincy Street
Arlington, VA 22217

Office of Naval Research
Code 411
800 N. Quincy Street
Arlington, VA 22217

Code 2627
Naval Research Laboratory
Washington, D.C. 20375 6 copies

Code 2029, Library (ONRL)
Naval Research Laboratory
Washington, DC 20375 6 copies

Code 5230
Naval Research Laboratory
Washington, DC 20375

Code 0341
Naval Sea Systems Command
Washington, DC 20362

Library
Naval Sea Systems Command
Washington, DC 20362

Code 5641
Naval Ship Research and Dev. Center
Bethesda, MD 20084

Code 6140
Naval Ship Engineering Center
Center Building
Prince George's Center
Hyattsville, MD 20782

Code SP 230
Strategic Systems Projects
Department of the Navy
Washington, DC 20376

Code 03B
Naval Air Systems Command
Washington, DC 20361

Code 310
Naval Air Systems Command
Washington, DC 20361

ORD 03
Naval Sea Systems Command
Washington, DC 20360

Librarian Station 5-2
Coast Guard Headquarters
NASSIF Building
400 Seventh Street, S. W.
Washington, DC 20591

Chief of Research & Development
Office of Chief of Staff
Department of the Army
The Pentagon
Washington, DC 20310

AFDRD-AS/M
U. S. Air Force
The Pentagon
Washington, DC 20330

Headquarters Library
Research & Development Administration
Washington, DC 20545

Mr. Clarence E. Miller, Jr.
Division of Reactor Development and
Technology
Energy Research and Development
Administration
Washington, DC 20545

Mr. W. M. Crim
Energy Research and Development
Administration
Office of Coal Research
Washington, DC 20545

National Science Foundation
Engineering Division
1800 G. Street, N. W.
Washington, DC 20235

Science and Technology Division
Library of Congress
Washington, DC 20540

Defense Research and Development
Attache
Australian Embassy
1601 Massachusetts Avenue, N.W.
Washington, DC 20036

Librarian
Naval Surface Weapons Center
White Oak Laboratory
Silver Spring, MD 20910

Dr. L. Licht
123 N. El Camino Real, #18
San Mateo, CA 94401

Mr. Everett Lake (APFL)
AF Aero Propulsion Laboratory
Wright-Patterson AFB. OH 45433

Unclassified

Security Classification

DOCUMENT CONTROL DATA - R&D

(Security classification of title, body of abstract and indexing annotation must be entered when the overall report is classified)

1. ORIGINATING ACTIVITY *(Corporate author)*
Columbia University, Department of Mechanical and Nuclear Engineering, Lubrication Research Lab.

2a. REPORT SECURITY CLASSIFICATION
Unclassified

2b. GROUP

3. REPORT TITLE
Experimental Investigation of Gas Bearings with Ultra-thin Films

4. DESCRIPTIVE NOTES *(Type of report and inclusive dates)*
Technical Report

5. AUTHOR(S) *(Last name, first name, initial)*
Aron Sereny and Vittorio Castelli

6. REPORT DATE
June 7, 1977

7a. TOTAL NO. OF PAGES
14

7b. NO. OF REFS
30

8a. CONTRACT OR GRANT NO.
N00014-75-C-0552

b. PROJECT NO.
Task NR 062-491

c.

d.

9a. ORIGINATOR'S REPORT NUMBER(S)
No. 26 Lubrication Research Lab

9b. OTHER REPORT NO(S) *(Any other numbers that may be assigned this report)*

10. AVAILABILITY/LIMITATION NOTICES
This document has been approved for public release and sale; its distribution is unlimited.

11. SUPPLEMENTARY NOTES

12. SPONSORING MILITARY ACTIVITY
Office of Naval Research

13. ABSTRACT

The experimental investigation described here involves the highly accurate measurement of bearing clearances on the order of 10 microinches in self-acting pivoted narrow-slider gas bearings. The experimental measurements are based on light interferometry using a variable-wavelength pulsed dye laser and a CW HeNe laser as monochromatic sources. The light interference in the gas bearing is obtained by flying the slider on a very precise optically flat quartz disk through which the light beam is transmitted.

The combined effect of high Knudsen numbers and surface irregularities on the flying height of narrow gas bearings is observed by varying the load on the bearing and the ambient molecular mean free path. The experimentally measured bearing clearances are compared quantitatively with rather accurate theoretical predictions obtained by numerical solution of Reynolds differential equation for compressible fluids with slip boundary conditions.

The result of this study indicates that, as clearances in narrow gas bearings get progressively smaller, while the Knudsen number increases to values beyond 0.1, the theoretical model fails to predict the bearing behavior. It is also argued that this failure is because of the weakness of the continuum model.

DD FORM 1 JAN 64 1473

Unclassified

Security Classification

Security Classification

14. KEY WORDS	LINK A		LINK B		LINK C	
	ROLE	WT	ROLE	WT	ROLE	WT
Reynolds Equation						
Slip Boundary Condition						
Knudsen Number						
Surface Roughness						
Gas Lubricated Slider Bearing						
Ultra-thin Film						

INSTRUCTIONS

1. ORIGINATING ACTIVITY: Enter the name and address of the contractor, subcontractor, grantee, Department of Defense activity or other organization *(corporate author)* issuing the report.

2a. REPORT SECURITY CLASSIFICATION: Enter the overall security classification of the report. Indicate whether "Restricted Data" is included. Marking is to be in accordance with appropriate security regulations.

2b. GROUP: Automatic downgrading is specified in DoD Directive 5200.10 and Armed Forces Industrial Manual. Enter the group number. Also, when applicable, show that optional markings have been used for Group 3 and Group 4 as authorized.

3. REPORT TITLE: Enter the complete report title in all capital letters. Titles in all cases should be unclassified. If a meaningful title cannot be selected without classification, show title classification in all capitals in parenthesis immediately following the title.

4. DESCRIPTIVE NOTES: If appropriate, enter the type of report, e.g., interim, progress, summary, annual, or final. Give the inclusive dates when a specific reporting period is covered.

5. AUTHOR(S): Enter the name(s) of author(s) as shown on or in the report. Enter last name, first name, middle initial. If military, show rank and branch of service. The name of the principal author is an absolute minimum requirement.

6. REPORT DATE: Enter the date of the report as day, month, year, or month, year. If more than one date appears on the report, use date of publication.

7a. TOTAL NUMBER OF PAGES: The total page count should follow normal pagination procedures, i.e., enter the number of pages containing information.

7b. NUMBER OF REFERENCES: Enter the total number of references cited in the report.

8a. CONTRACT OR GRANT NUMBER: If appropriate, enter the applicable number of the contract or grant under which the report was written.

8b, 8c, & 8d. PROJECT NUMBER: Enter the appropriate military department identification, such as project number, subproject number, system numbers, task number, etc.

9a. ORIGINATOR'S REPORT NUMBER(S): Enter the official report number by which the document will be identified and controlled by the originating activity. This number must be unique to this report.

9b. OTHER REPORT NUMBER(S): If the report has been assigned any other report numbers *(either by the originator or by the sponsor)*, also enter this number(s).

10. AVAILABILITY/LIMITATION NOTICES: Enter any limitations on further dissemination of the report, other than those imposed by security classification, using standard statements such as:

(1) "*Qualified requesters may obtain copies of this report from DDC.*"

(2) "Foreign announcement and dissemination of this report by DDC is not authorized."

(3) "U. S. Government agencies may obtain copies of this report directly from DDC. Other qualified DDC users shall request through

_____."

(4) "U. S. military agencies may obtain copies of this report directly from DDC. Other qualified users shall request through

_____."

(5) "All distribution of this report is controlled. Qualified DDC users shall request through

_____."

If the report has been furnished to the Office of Technical Services, Department of Commerce, for sale to the public, indicate this fact and enter the price, if known.

11. SUPPLEMENTARY NOTES: Use for additional explanatory notes.

12. SPONSORING MILITARY ACTIVITY: Enter the name of the departmental project office or laboratory sponsoring *(paying for)* the research and development. Include address.

13. ABSTRACT: Enter an abstract giving a brief and factual summary of the document indicative of the report, even though it may also appear elsewhere in the body of the technical report. If additional space is required, a continuation sheet shall be attached.

It is highly desirable that the abstract of classified reports be unclassified. Each paragraph of the abstract shall end with an indication of the military security classification of the information in the paragraph, represented as *(TS)*, *(S)*, *(C)*, or *(U)*.

There is no limitation on the length of the abstract. However, the suggested length is from 150 to 225 words.

14. KEY WORDS: Key words are technically meaningful terms or short phrases that characterize a report and may be used as index entries for cataloging the report. Key words must be selected so that no security classification is required. Identifiers, such as equipment model designation, trade name, military project code name, geographic location, may be used as key words but will be followed by an indication of technical context. The assignment of links, roles, and weights is optional.

DD FORM 1 JAN 64 1473 (BACK)

Security Classification